Application of single-layer particle tracking for radiation field decomposition and interaction point reconstruction at MoEDAL

Declan Garvey, Benedikt Bergmann, Petr Mánek, Stanislav Pospíšil,
Petr Smolyanskiy,

On behalf of MoEDAL

Declan.Garvey@utef.cvut.cz

Timepix3: Radiation Imaging Detector

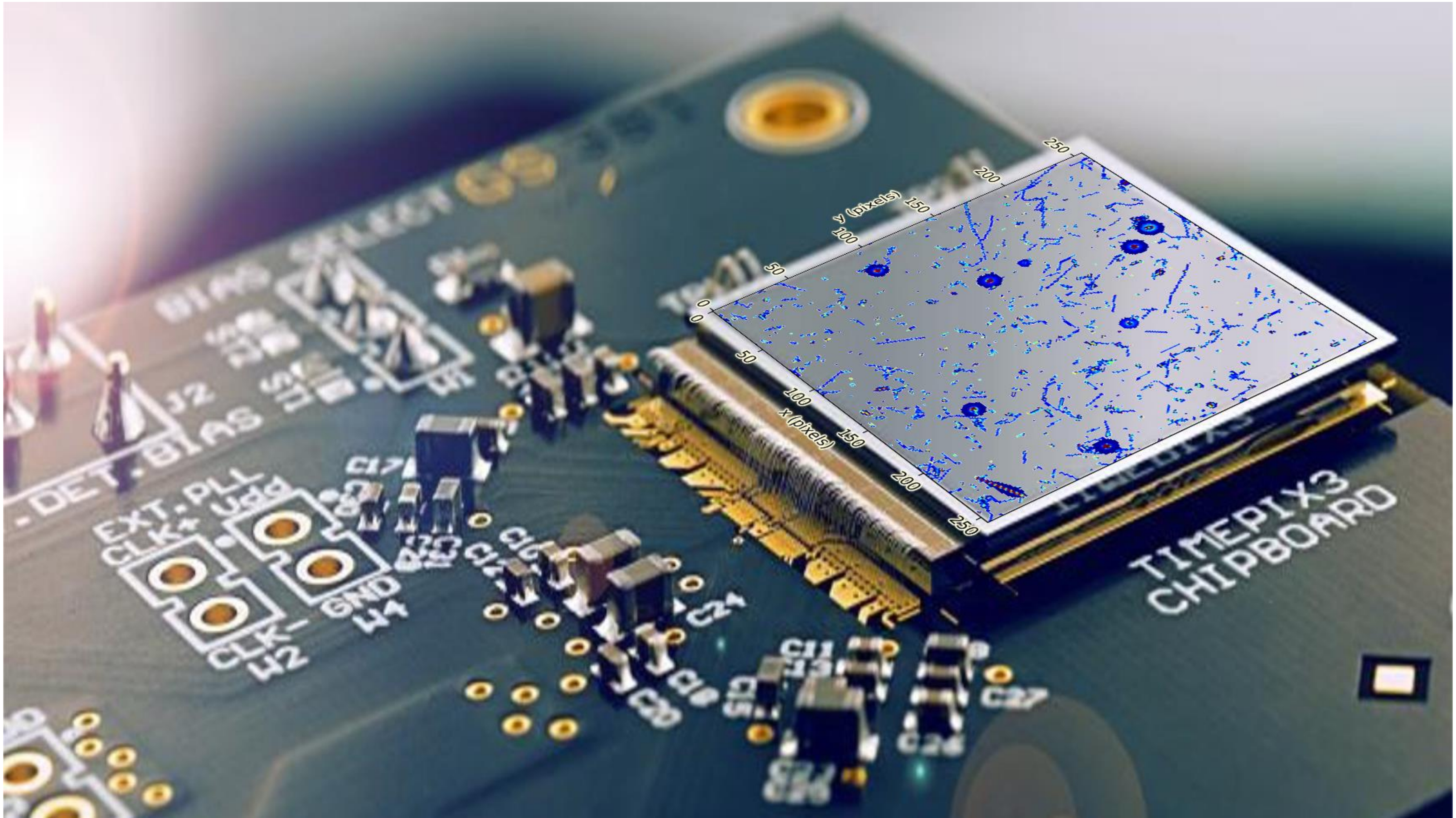

Timepix and Timepix3

- 256 x 256 pixels with 55 μm pitch (1.98 cm^2)
- Sensor layer (silicon, GaAs, CdTe, ...) flip-chip bump bonded to the ASIC

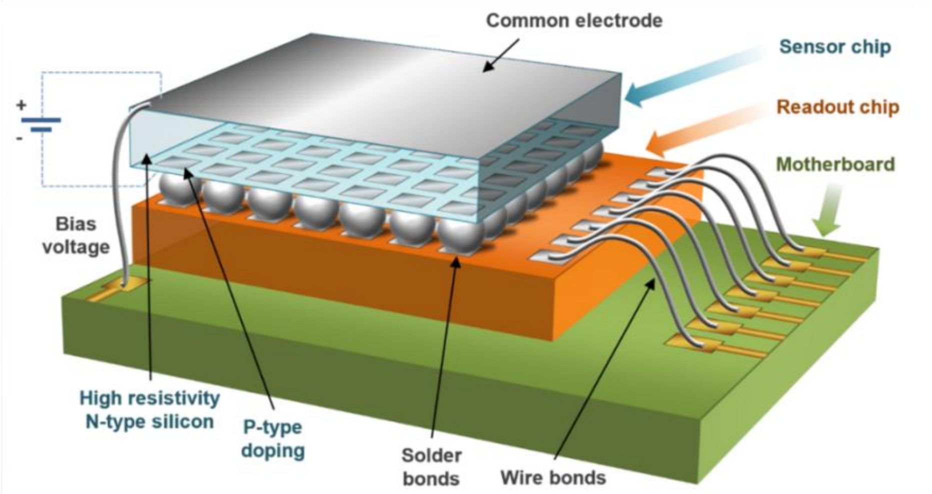

Timepix

- Frame-based readout (92 fps) – dead time > 11 ms
  - ⇨ Information is read out on a frame-by-frame basis
- Measurement of energy **or** time (Δt = 20.8 ns)
- Minimal detectable energy: ~ 3.5 keV

Timepix3

- Data-driven readout (max. count rate 40 Mpix/s)
  - ⇨ Pixels are continuously read out throughout the entire measurement
- Per pixel dead time: 475 ns
- Measurement of energy **and** time (Δt = 1.56 ns)
- Minimal detectable energy per pixel: 3 keV

Timepix3 with chipboard

Particle Tracking by Connecting the Dots

- Traditionally, particle tracking is performed using multiple layers of thin detectors
- Tracking information is then calculated by recording coincidence measurements in each detector and "connecting the dots"

So, the question is:

Can we achieve similar results using only a single-layer detector?

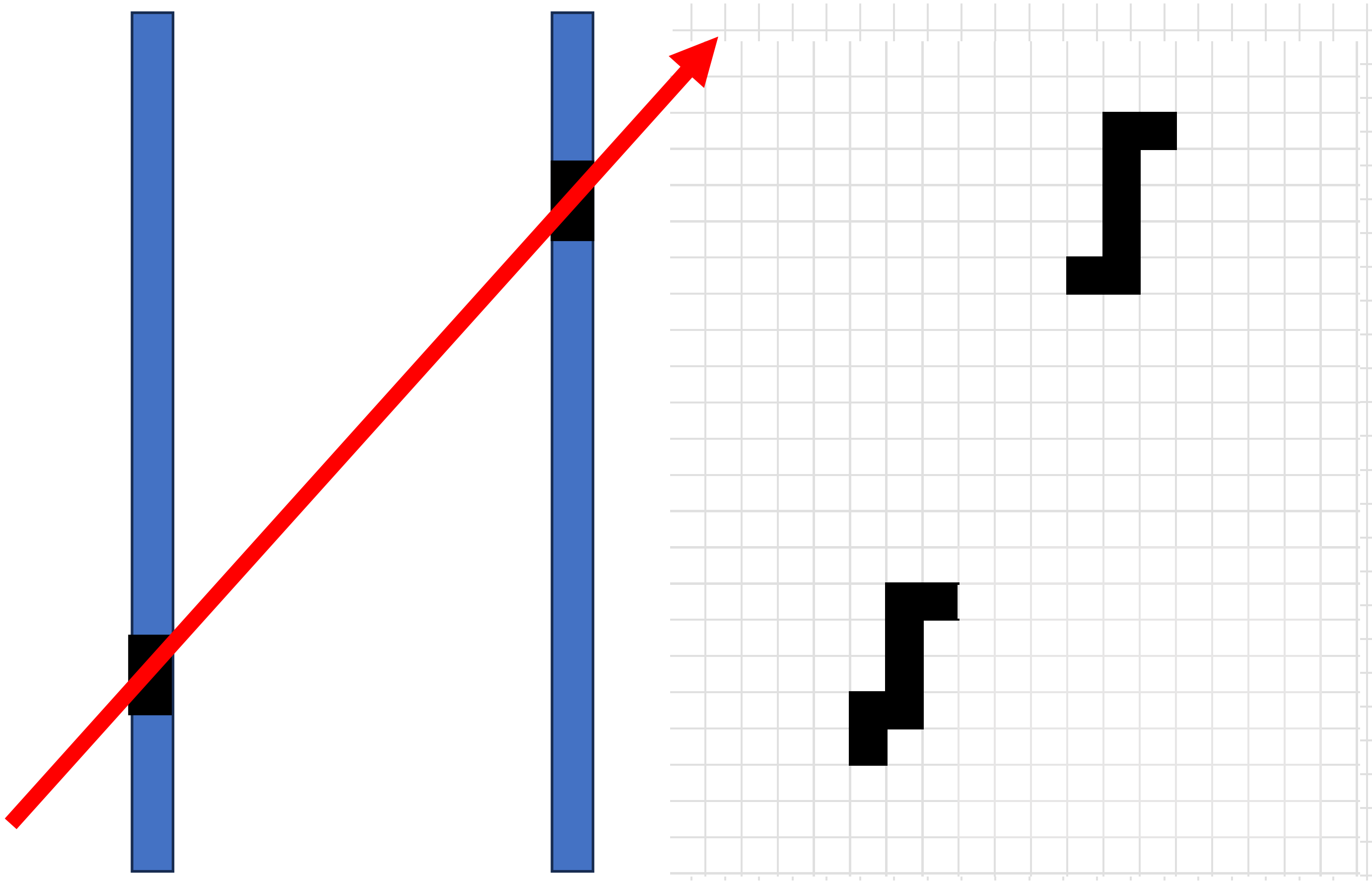

Particle Tracking by Connecting the Dots

- Traditionally, particle tracking is performed using multiple layers of thin detectors
- Tracking information is then calculated by recording coincidence measurements in each detector and "connecting the dots"

So, the question is:

Can we achieve similar results using only a single-layer detector?

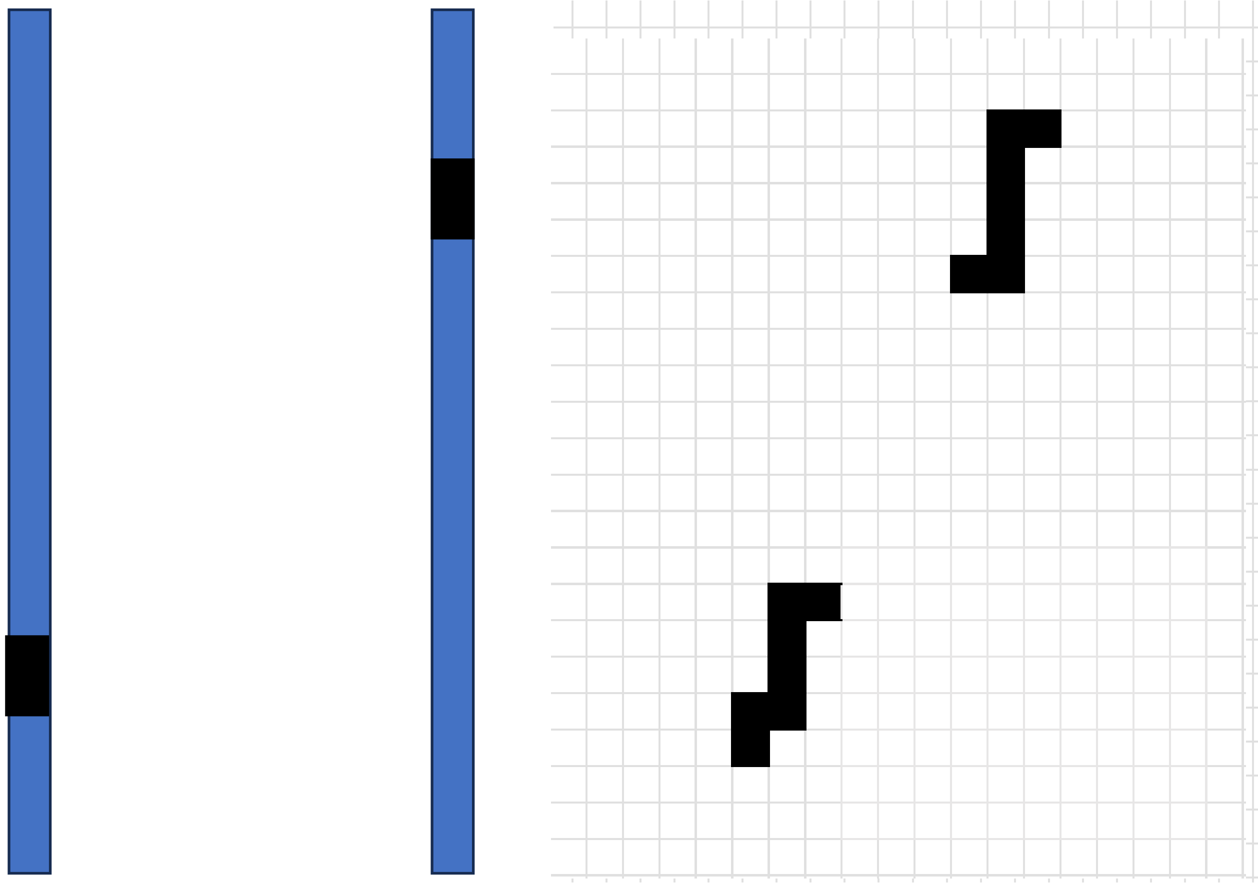

Particle Tracking by Connecting the Dots

- Traditionally, particle tracking is performed using multiple layers of thin detectors
- Tracking information is then calculated by recording coincidence measurements in each detector and "connecting the dots"

So, the question is:

Can we achieve similar results using only a single-layer detector?

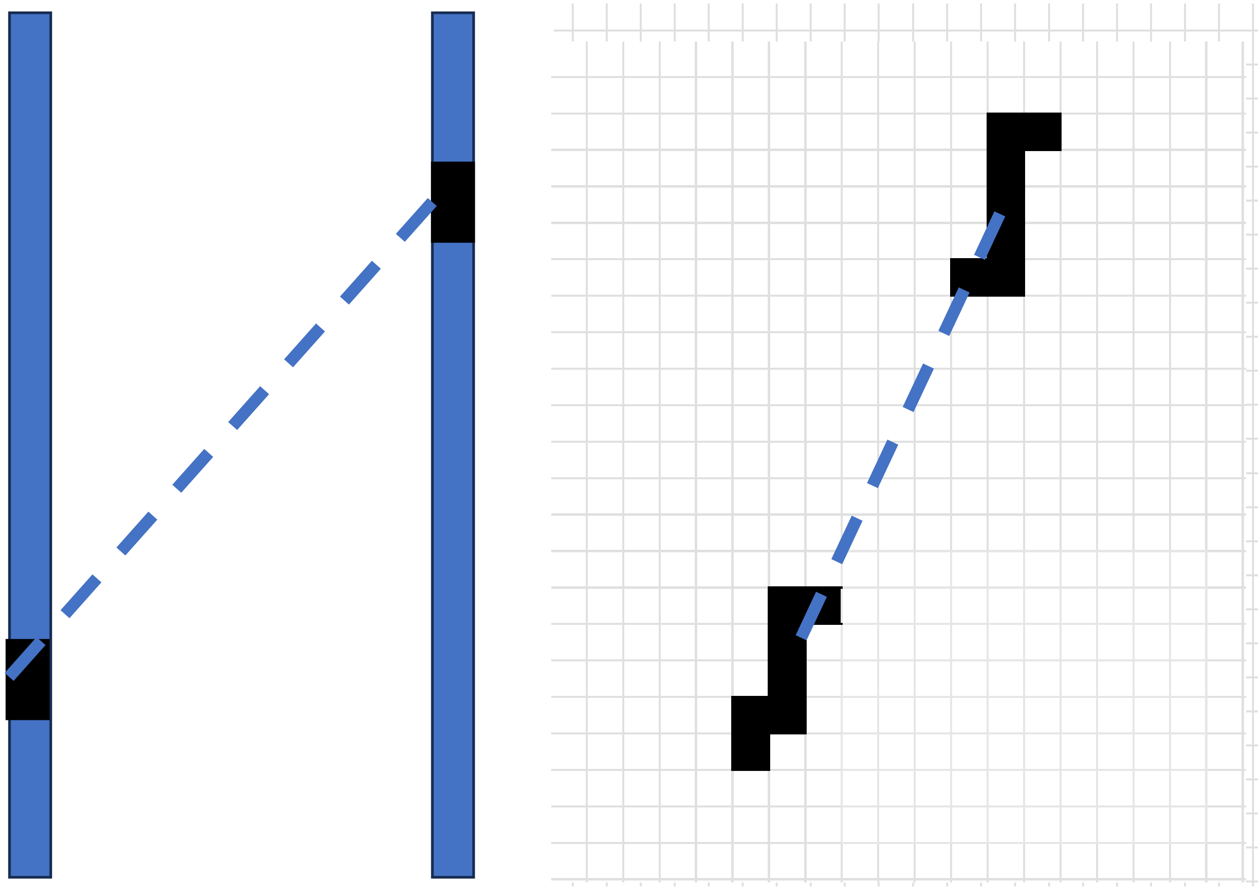

Solid-State Time-Projection Chamber:

3D Reconstruction of Particle Tracks

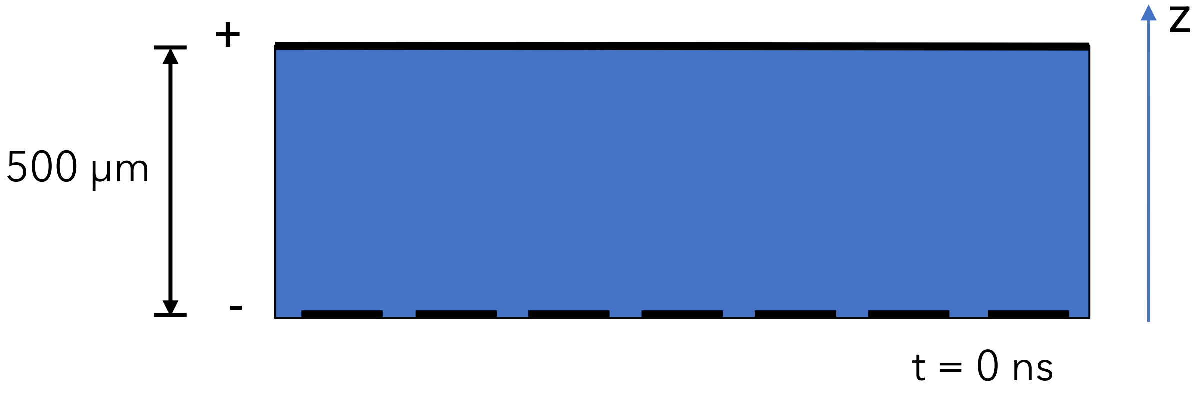

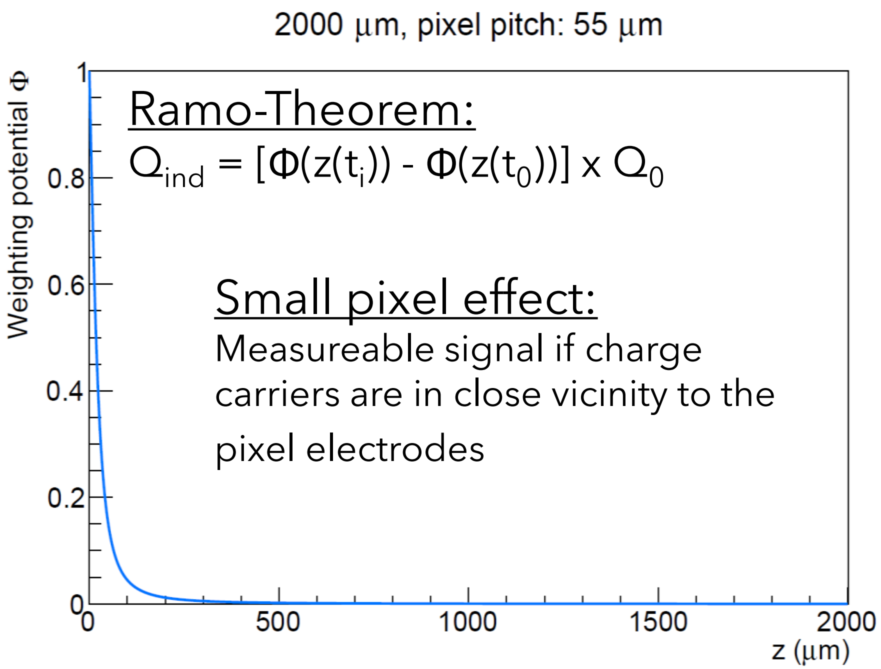

Ramo-Theorem:

$Q_{ind} = [\Phi(z(t_i)) - \Phi(z(t_0))] \times Q_0$

Small pixel effect:

Measureable signal if charge carriers are in close vicinity to the pixel electrodes

Charge carrier drift motion:

e^- and h^+ drift described by

$$v_e = -\mu_e \times E(z)$$
$$v_h = \mu_h \times E(z)$$

$\mu_{e/h}$: Mobility of e^-/h^+

Electric field parametrisation:

$$\text{Si:} \quad \vec{E}(z) = \frac{U_B}{d}\vec{e_z} + \frac{2U_{dep}}{d^2}\left(\frac{d}{2} - z\right)\vec{e_z} \,;$$

$$\text{CdTe:} \quad \vec{E}(z) = \frac{U_B}{d}\vec{e_z}$$

U_B: Bias voltage; U_{dep}: Depletion voltage; d: Sensor thickness

→ Look up table: $z(t_{meas.}, E_{meas.})$

Bergmann et al. Eur. Phys. J. C (2017) 77: 421. https://doi.org/10.1140/epjc/s10052-017-4993-4
Bergmann et al., Eur. Phys. J. C (2019) 79: 165. https://doi.org/10.1140/epjc/s10052-019-6673-z

Solid-State Time-Projection Chamber:

3D Reconstruction of Particle Tracks

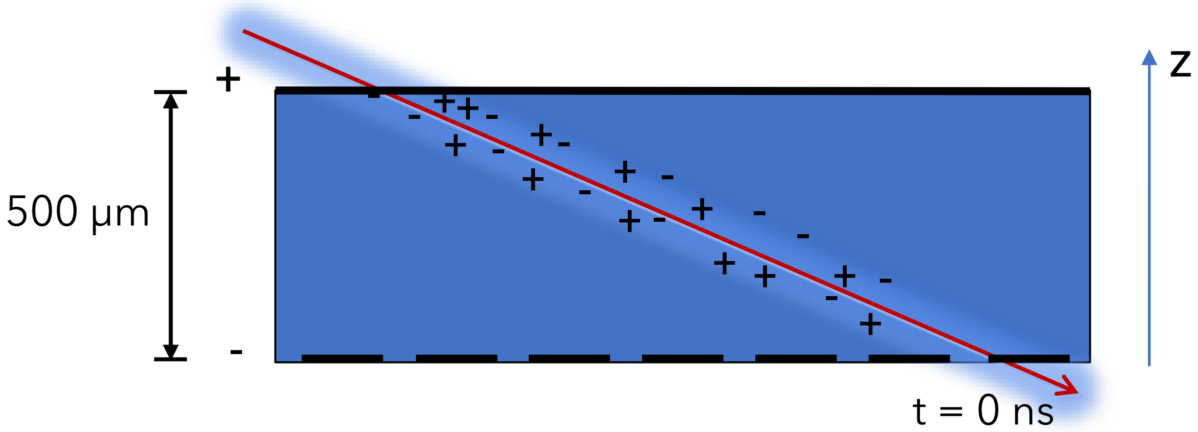

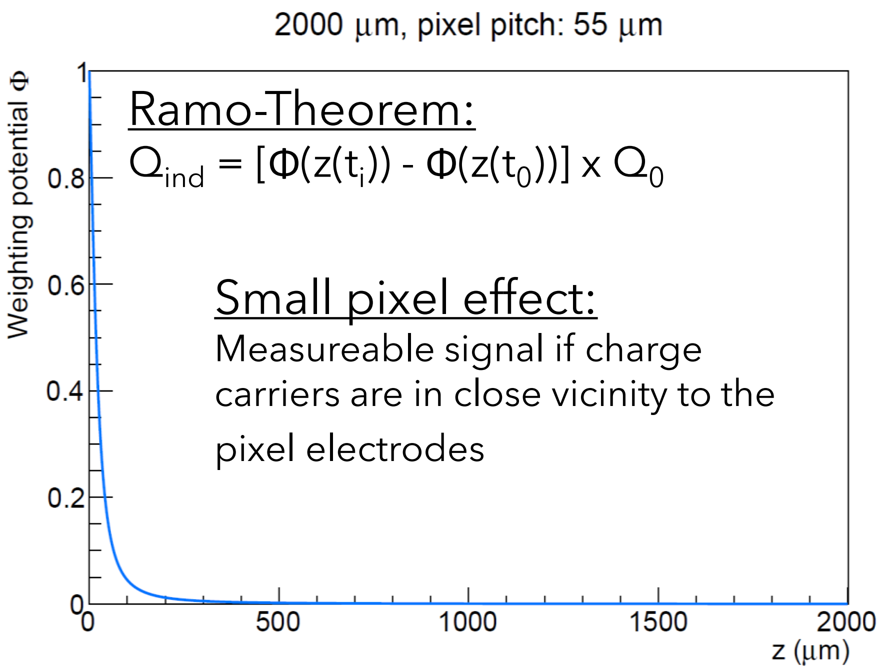

Ramo-Theorem:

$Q_{ind} = [\Phi(z(t_i)) - \Phi(z(t_0))] \times Q_0$

Small pixel effect:

Measureable signal if charge carriers are in close vicinity to the pixel electrodes

Charge carrier drift motion:

e^- and h^+ drift described by

$$v_e = -\mu_e \times E(z)$$
$$v_h = \mu_h \times E(z)$$

$\mu_{e/h}$: Mobility of e^-/h^+

Electric field parametrisation:

Si: $\vec{E}(z) = \frac{U_B}{d}\vec{e_z} + \frac{2U_{dep}}{d^2}\left(\frac{d}{2} - z\right)\vec{e_z}$;

CdTe: $\vec{E}(z) = \frac{U_B}{d}\vec{e_z}$

U_B: Bias voltage; U_{dep}: Depletion voltage; d: Sensor thickness

→ Look up table: $z(t_{meas.}, E_{meas.})$

Bergmann et al. Eur. Phys. J. C (2017) 77: 421. https://doi.org/10.1140/epjc/s10052-017-4993-4
Bergmann et al., Eur. Phys. J. C (2019) 79: 165. https://doi.org/10.1140/epjc/s10052-019-6673-z

Solid-State Time-Projection Chamber:
3D Reconstruction of Particle Tracks

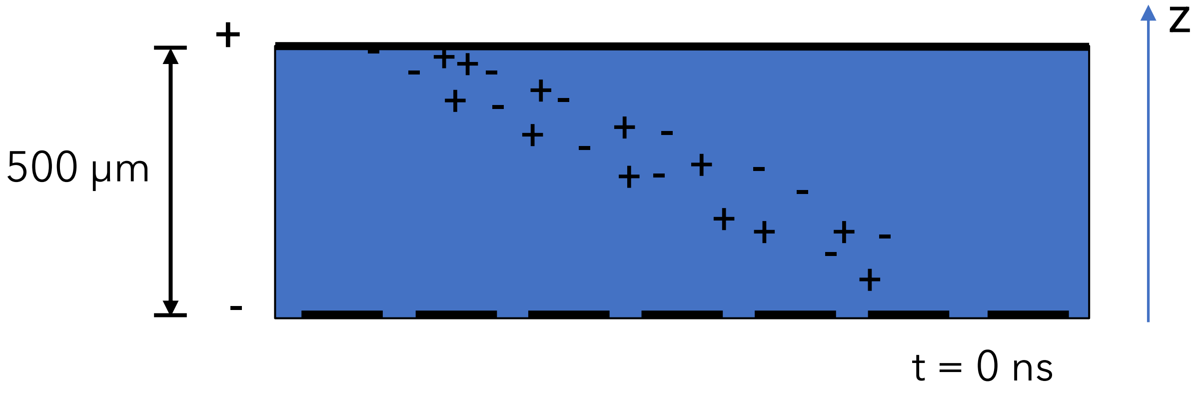

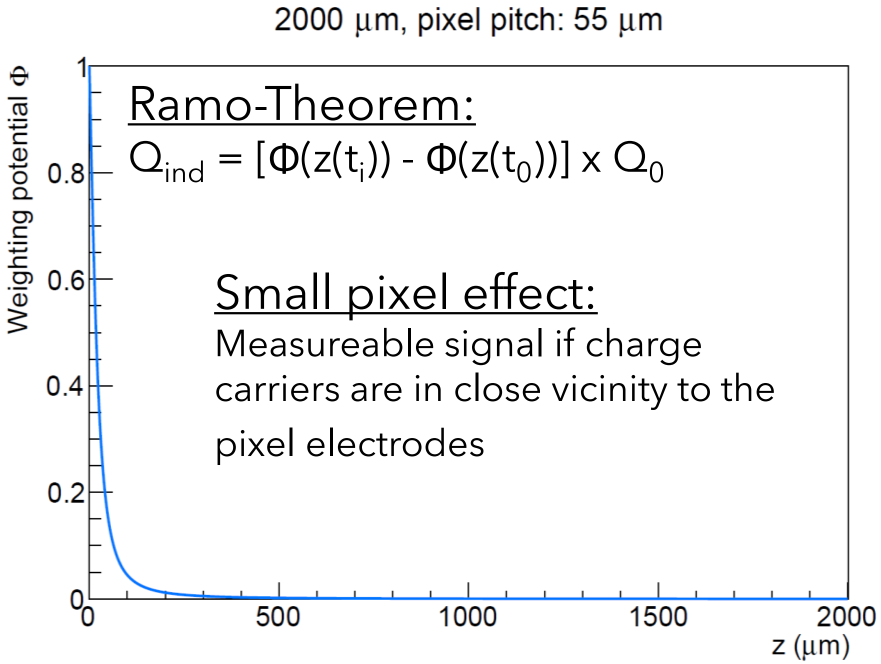

Charge carrier drift motion:

e^- and h^+ drift described by

$$v_e = -\mu_e \times E(z)$$
$$v_h = \mu_h \times E(z)$$

$\mu_{e/h}$: Mobility of e^-/h^+

Electric field parametrisation:

$$\text{Si:} \quad \vec{E}(z) = \frac{U_B}{d}\vec{e_z} + \frac{2U_{dep}}{d^2}\left(\frac{d}{2} - z\right)\vec{e_z}\,;$$

$$\text{CdTe:} \quad \vec{E}(z) = \frac{U_B}{d}\vec{e_z}$$

U_B: Bias voltage; U_{dep}: Depletion voltage; d: Sensor thickness

→ Look up table: $z(t_{meas.}, E_{meas.})$

Bergmann et al. Eur. Phys. J. C (2017) 77: 421. https://doi.org/10.1140/epjc/s10052-017-4993-4
Bergmann et al., Eur. Phys. J. C (2019) 79: 165. https://doi.org/10.1140/epjc/s10052-019-6673-z

Solid-State Time-Projection Chamber:

3D Reconstruction of Particle Tracks

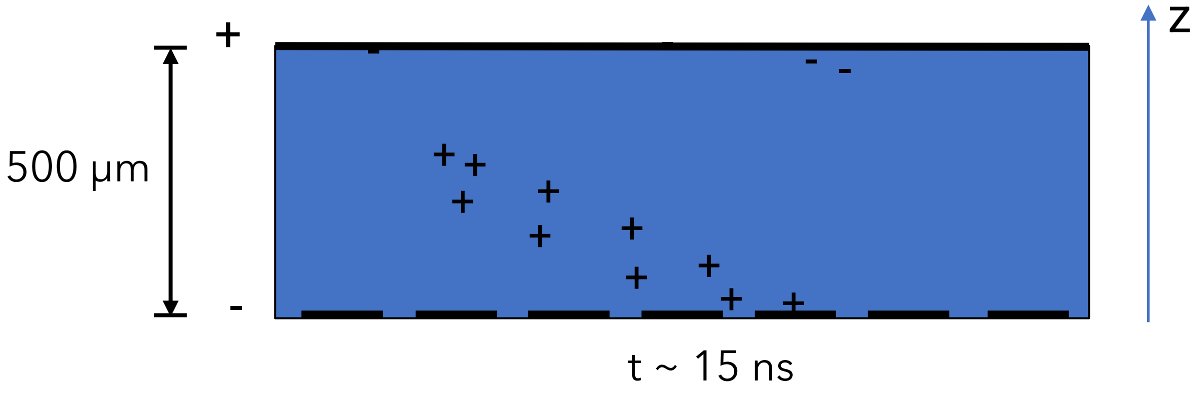

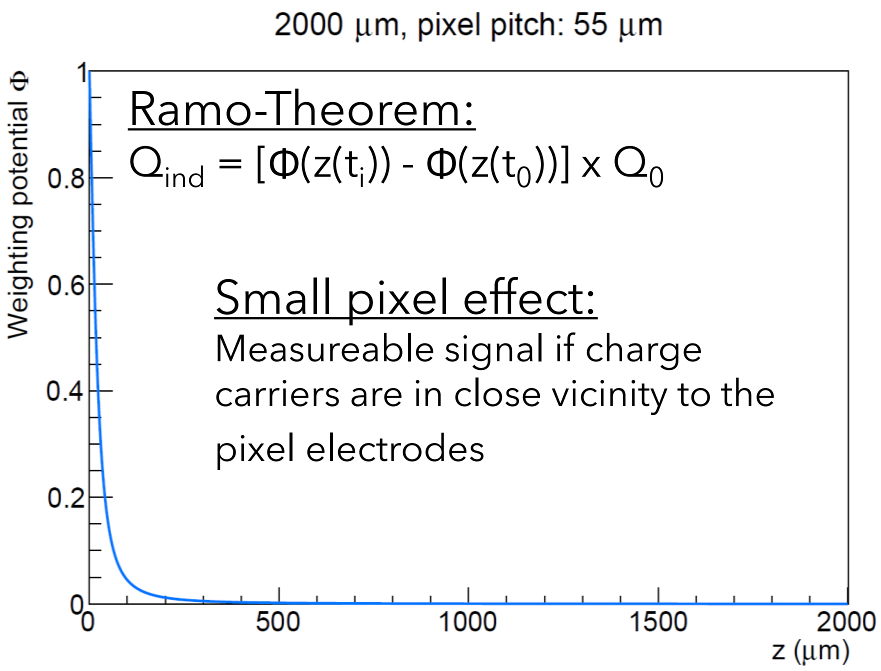

Charge carrier drift motion:

e^- and h^+ drift described by

$$v_e = -\mu_e \times E(z)$$
$$v_h = \mu_h \times E(z)$$

$\mu_{e/h}$: Mobility of e^-/h^+

Electric field parametrisation:

Si: $\vec{E}(z) = \frac{U_B}{d}\vec{e_z} + \frac{2U_{dep}}{d^2}\left(\frac{d}{2} - z\right)\vec{e_z}$;

CdTe: $\vec{E}(z) = \frac{U_B}{d}\vec{e_z}$

U_B: Bias voltage; U_{dep}: Depletion voltage; d: Sensor thickness

→ Look up table: $z(t_{meas.}, E_{meas.})$

Bergmann et al. Eur. Phys. J. C (2017) 77: 421. https://doi.org/10.1140/epjc/s10052-017-4993-4
Bergmann et al., Eur. Phys. J. C (2019) 79: 165. https://doi.org/10.1140/epjc/s10052-019-6673-z

Solid-State Time-Projection Chamber:

3D Reconstruction of Particle Tracks

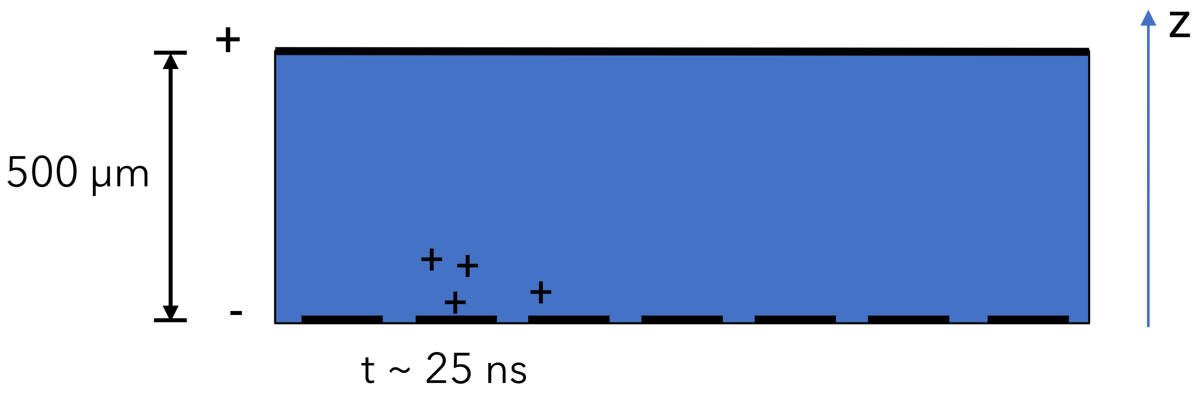

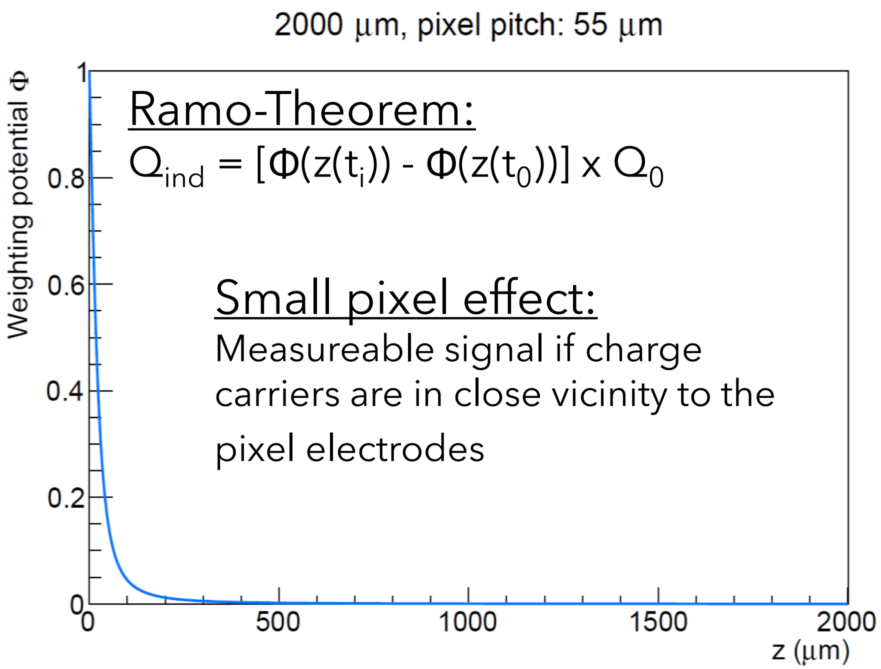

Ramo-Theorem:

$Q_{ind} = [\Phi(z(t_i)) - \Phi(z(t_0))] \times Q_0$

Small pixel effect:

Measureable signal if charge carriers are in close vicinity to the pixel electrodes

Charge carrier drift motion:

e^- and h^+ drift described by

$$v_e = -\mu_e \times E(z)$$
$$v_h = \mu_h \times E(z)$$

$\mu_{e/h}$: Mobility of e^-/h^+

Electric field parametrisation:

Si: $\vec{E}(z) = \frac{U_B}{d}\vec{e_z} + \frac{2U_{dep}}{d^2}\left(\frac{d}{2} - z\right)\vec{e_z}$;

CdTe: $\vec{E}(z) = \frac{U_B}{d}\vec{e_z}$

U_B: Bias voltage; U_{dep}: Depletion voltage; d: Sensor thickness

→ Look up table: $z(t_{meas.}, E_{meas.})$

Bergmann et al. Eur. Phys. J. C (2017) 77: 421. https://doi.org/10.1140/epjc/s10052-017-4993-4
Bergmann et al., Eur. Phys. J. C (2019) 79: 165. https://doi.org/10.1140/epjc/s10052-019-6673-z

3D Tracking in 500 µm Si Timepix3

120 GeV/c pion tracks accompanied by δ-rays measured at SPS:

z-resolution:
σ_z ~30 µm

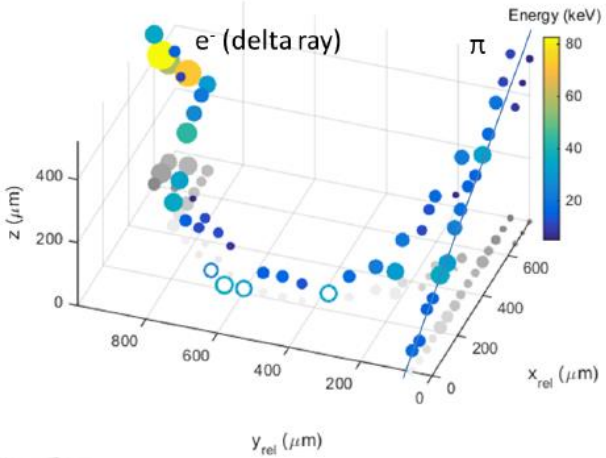

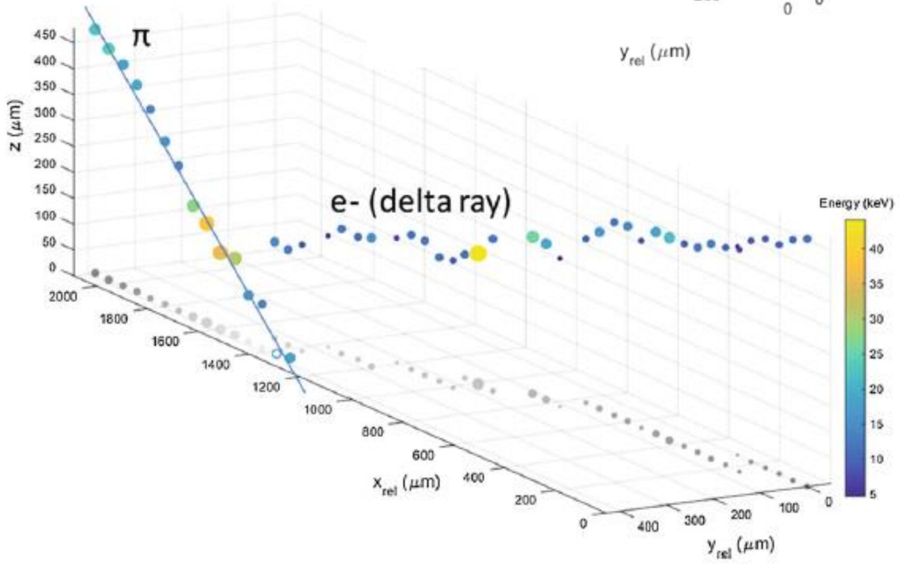

A cosmic µ measured in the Prague laboratory:

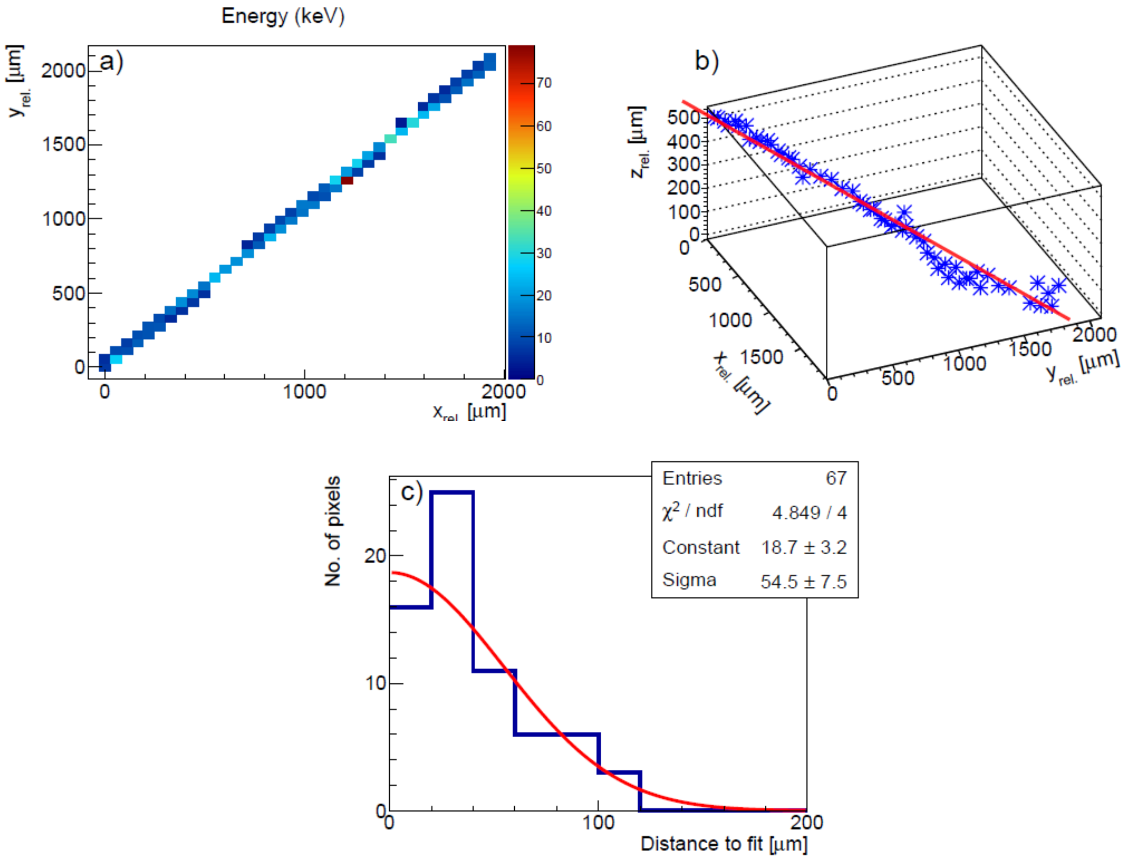

Bergmann et al. Eur. Phys. J. C (2017) 77: 421.
https://doi.org/10.1140/epjc/s10052-017-4993-4

Energy Deposition Spectra of Charged Energetic Particles

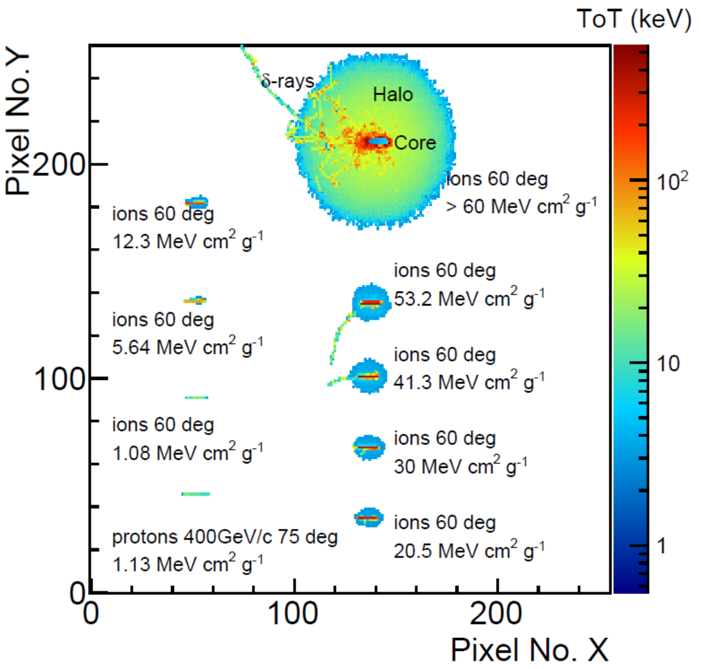

Different track shapes observed in a mixed relativistic ion beam 330 GeV/c Pb on target

Energy loss of energetic charged particles described by Landau-Vavilov distribution with Gaussian smearing

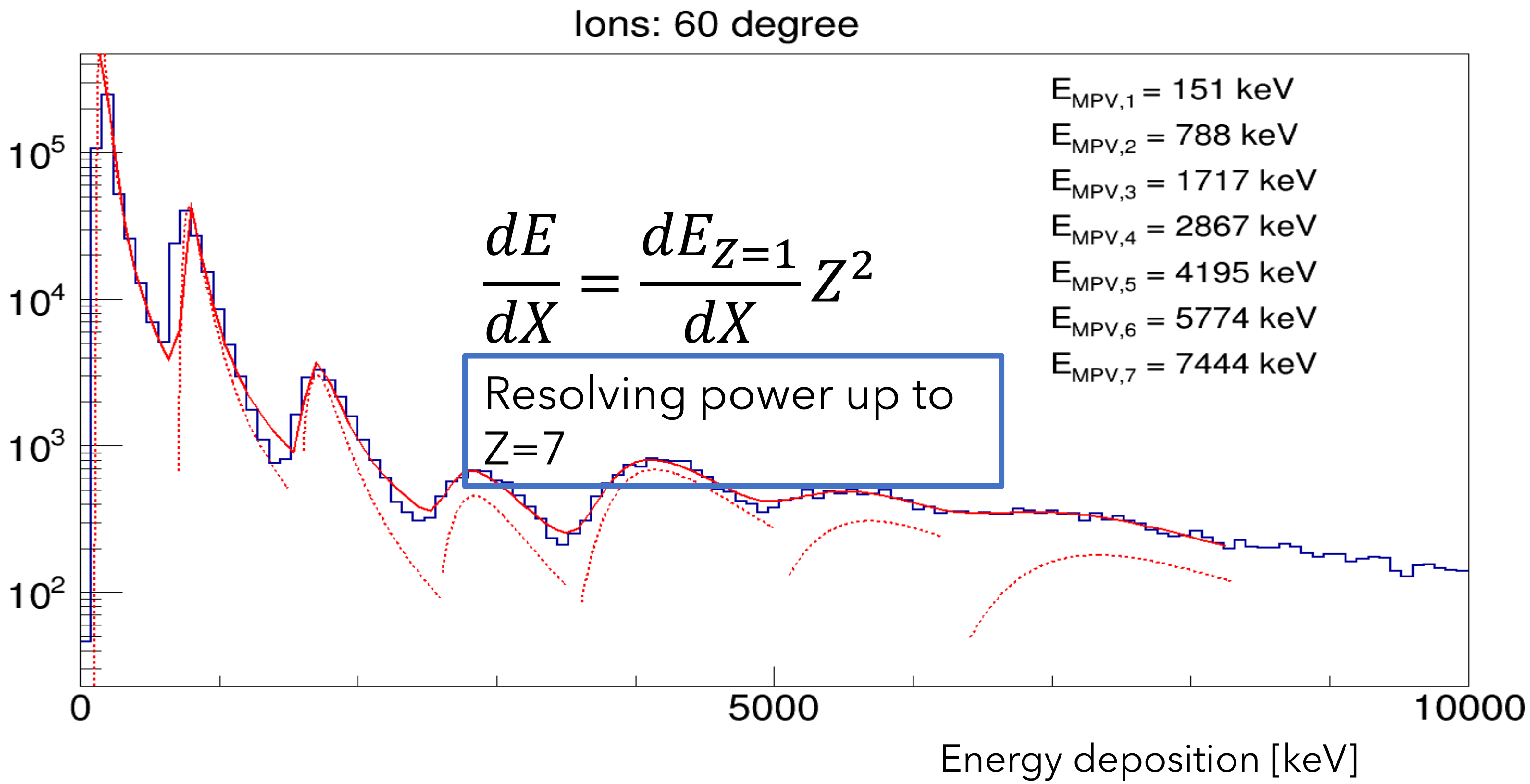

P. Smolyanskiy *et al.* *JINST* **16** P01022, 2021. https://dx.doi.org/10.1088/1748-0221/16/01/P01022

Single-Layer Particle Tracking in MoEDAL

Timepix3 in MoEDAL at Run 2 – Feasibility Study

Installation of two Timepix3 detectors in MoEDAL in **September 2018**. Timepix3 are placed at 1.1 m distance to IP8 with a relatively unobstructed view

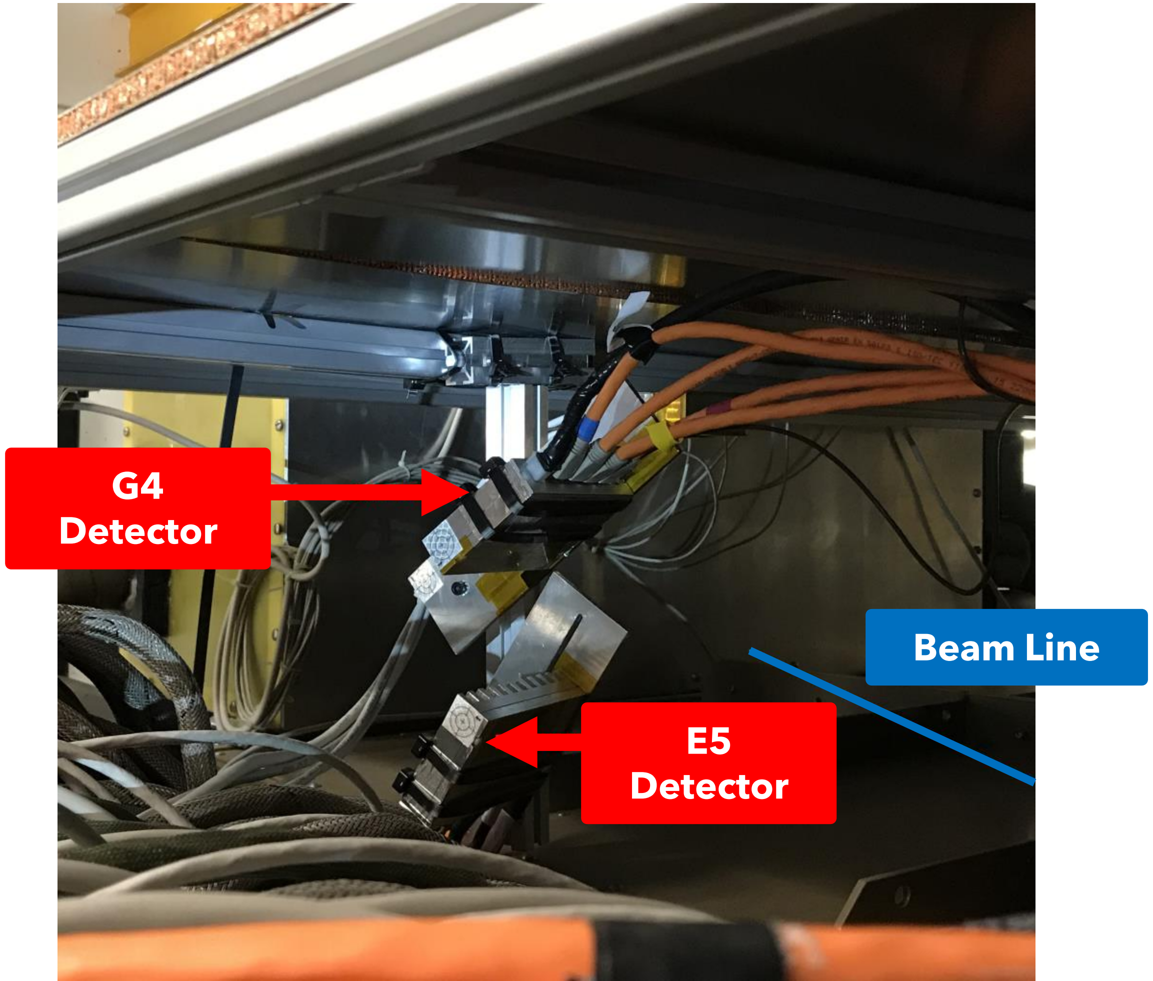

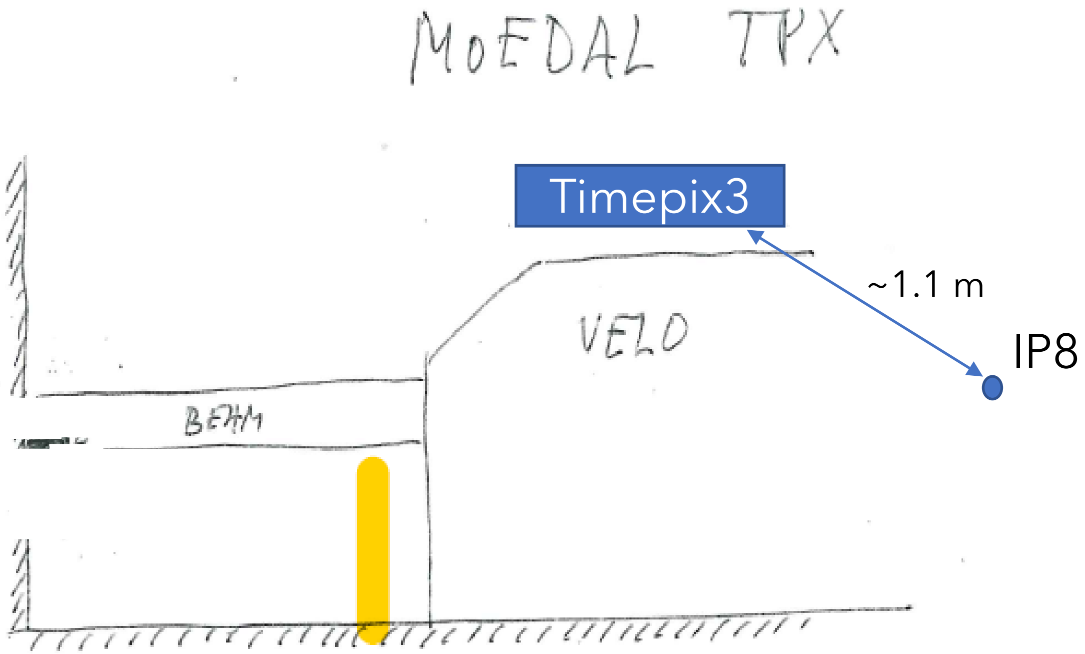

Continuous quasi dead-time free measurement (in real time) keeping a permanent record of **all particle traces**

- Tracking and identification of **all** particles
- Online outlier detection to search for exotics (highly ionising events)
- Bunch-by-bunch luminosity measurement
- Search for exotic signatures, e.g., "soup" events requiring timing information

Radiation Levels and Radiation Field

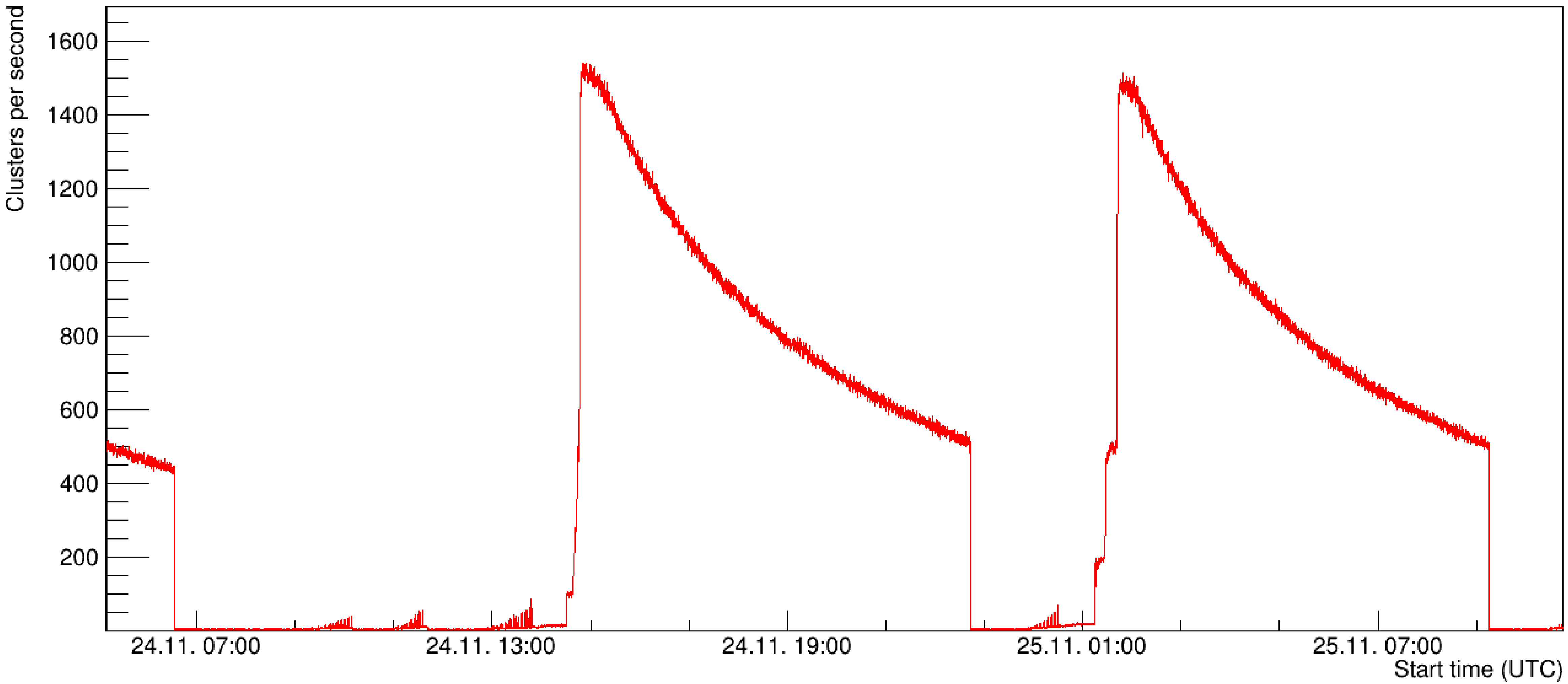

Radiation Levels and Radiation Field

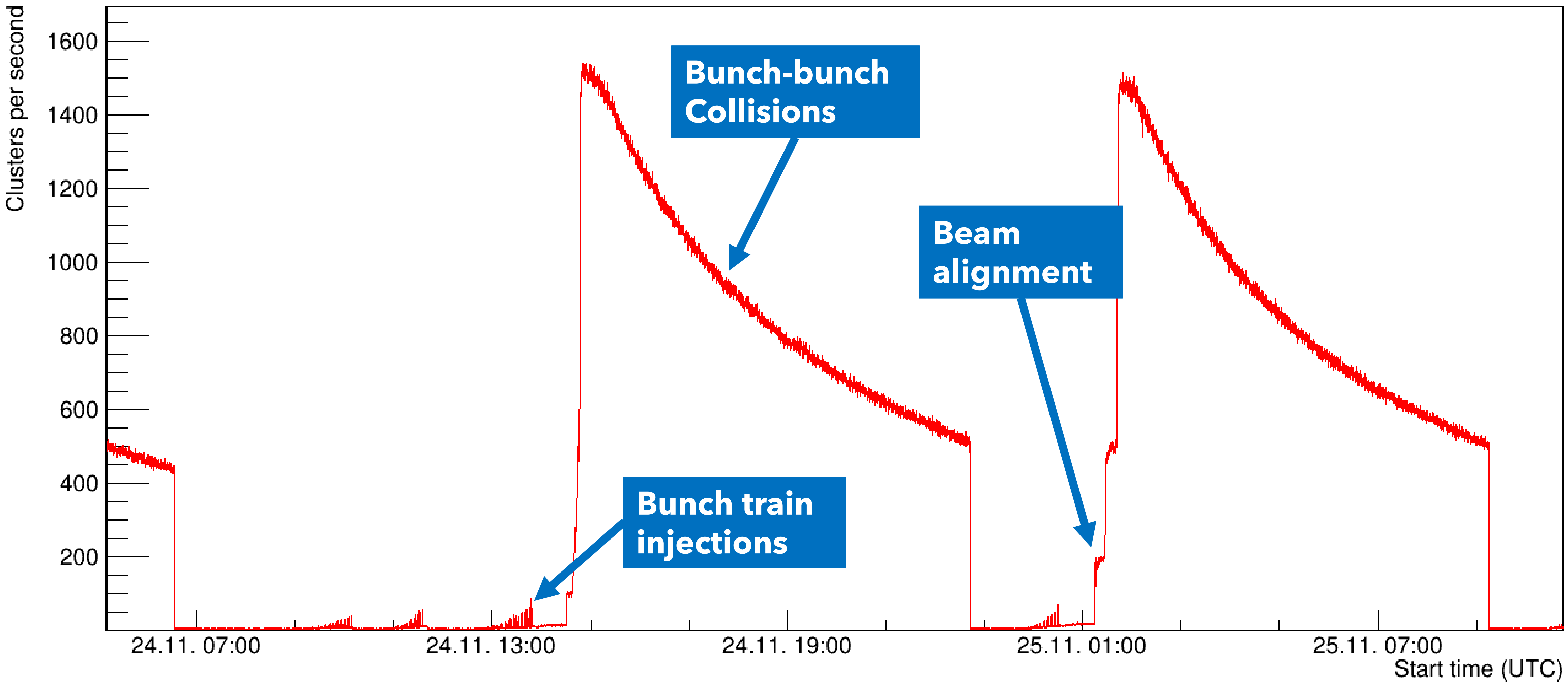

Radiation Levels and Radiation Field

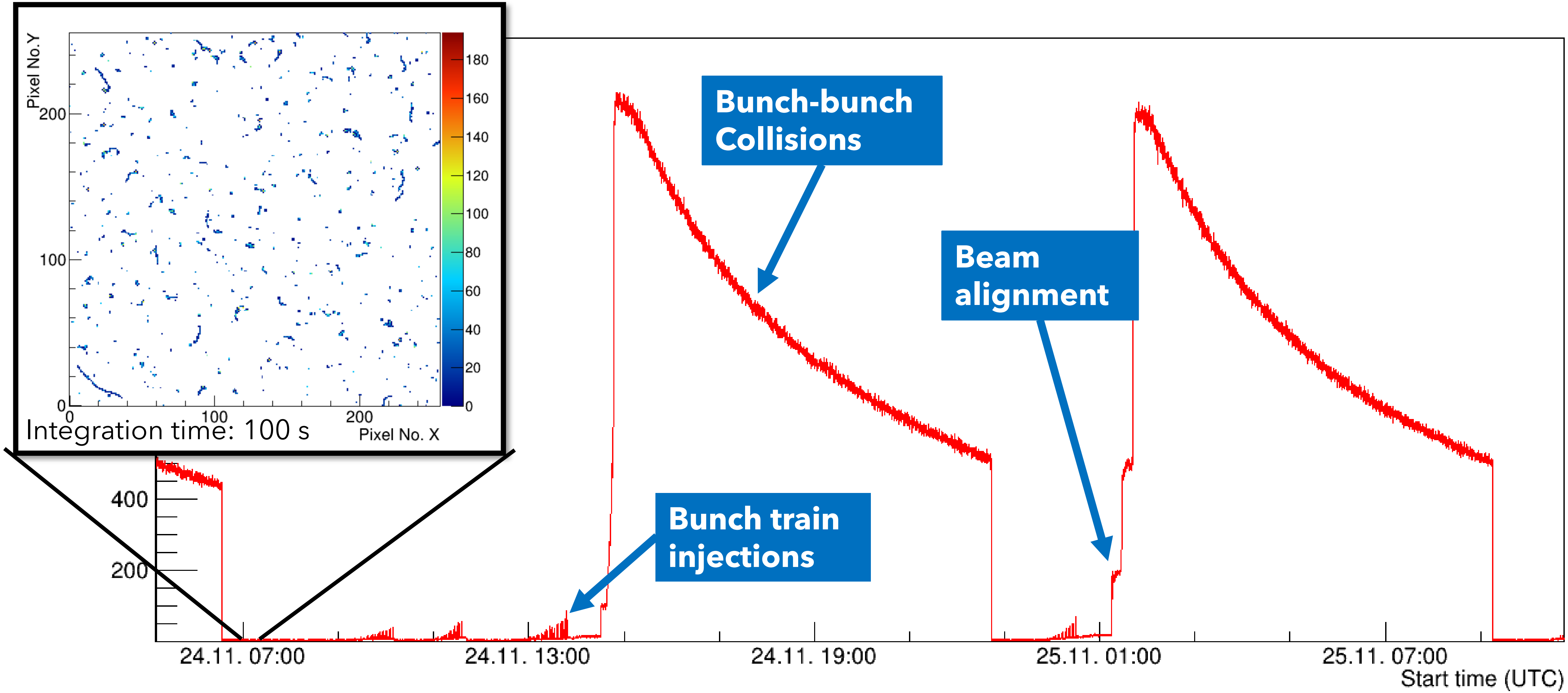

Radiation Levels and Radiation Field

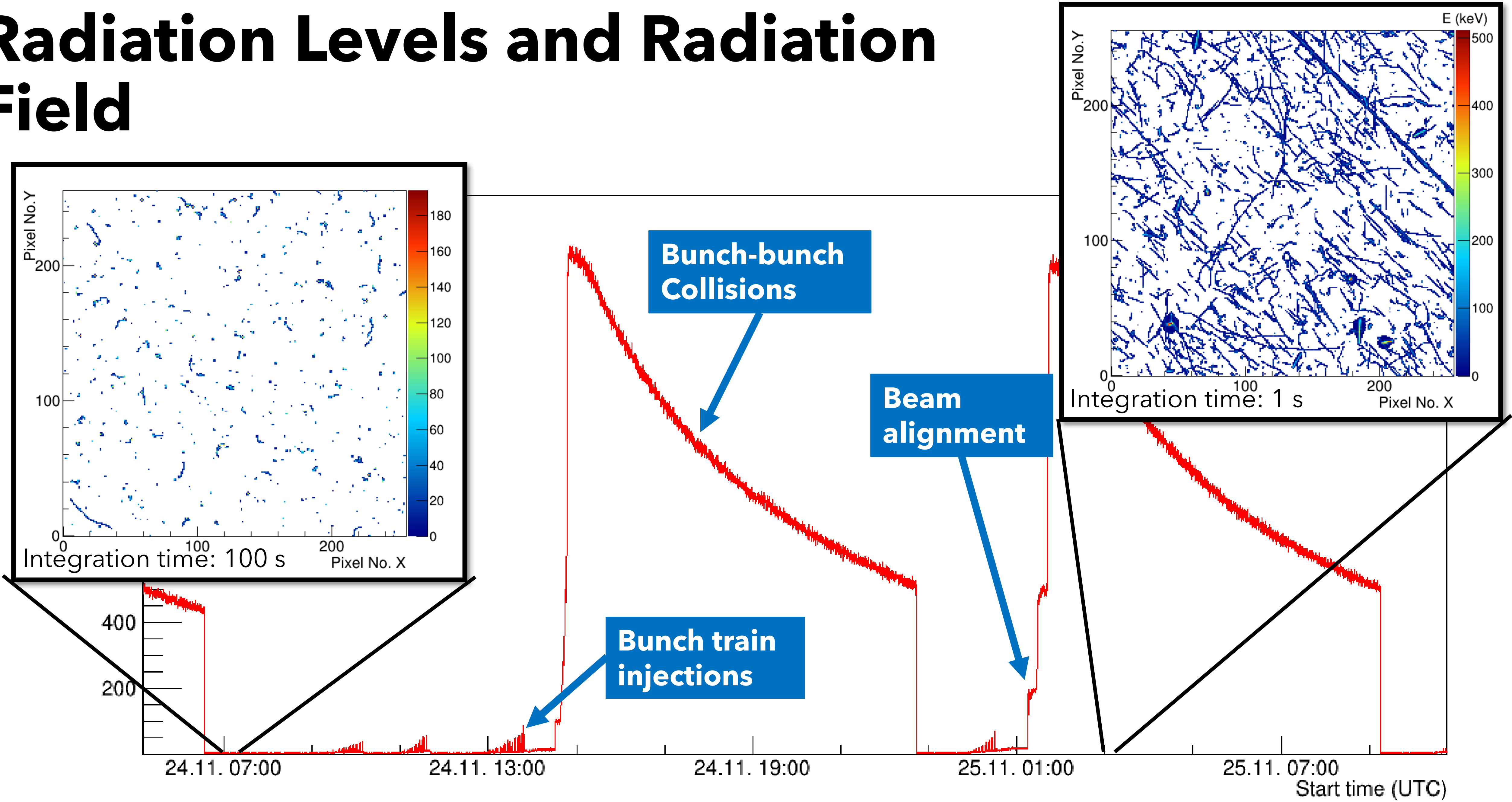

Theta Predictor Model

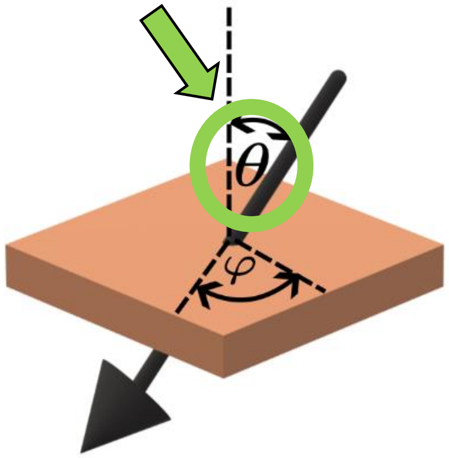

- To reduce the complexity of the problem, only the following two incidence angles are predicted: Azimuthal and perpendicular. Reducing it to regression problem
- **Datasets used for model development:**
  - ➪ 0.01-10 MeV electrons (curly tracks)
  - ➪ 10-500 MeV protons (thick, straight tracks)
  - ➪ 40 GeV pions (thin, straight tracks)
- It was found through an extensive study that a Random Forrest Regressor with a selection of input features produced optimal results

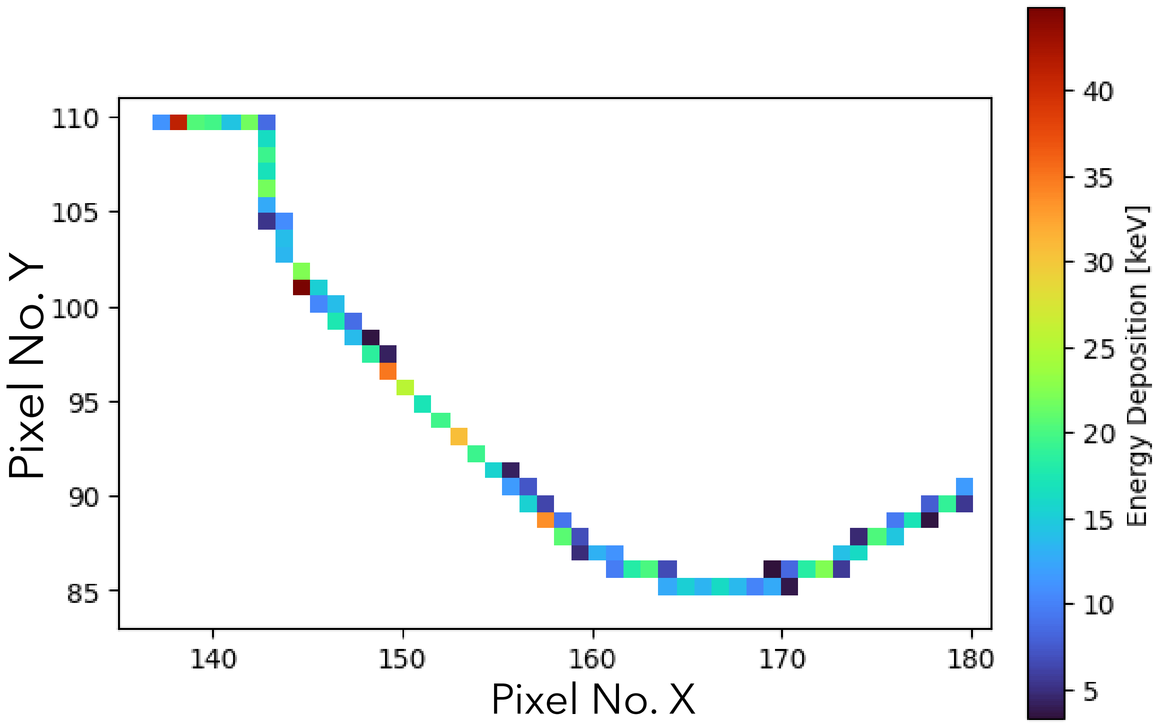

Input Features:

Theta Predictor Model

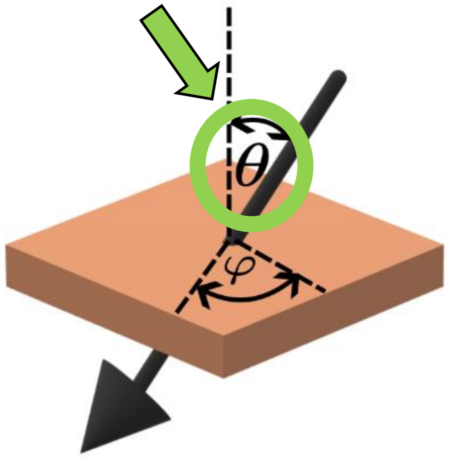

- To reduce the complexity of the problem, only the following two incidence angles are predicted: Azimuthal and perpendicular. Reducing it to regression problem
- **Datasets used for model development:**
  - ➯ 0.01-10 MeV electrons (curly tracks)
  - ➯ 10-500 MeV protons (thick, straight tracks)
  - ➯ 40 GeV pions (thin, straight tracks)
- It was found through an extensive study that a Random Forrest Regressor with a selection of input features produced optimal results

Input Features:

1. Size [no. of pixels]

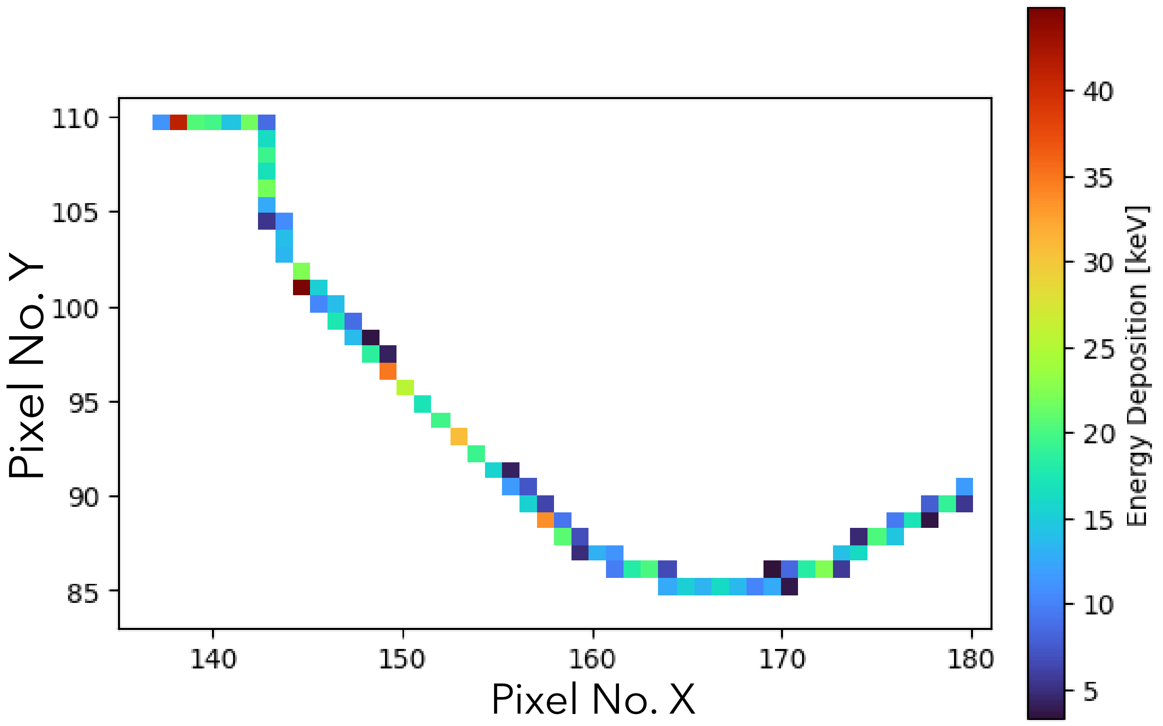

Theta Predictor Model

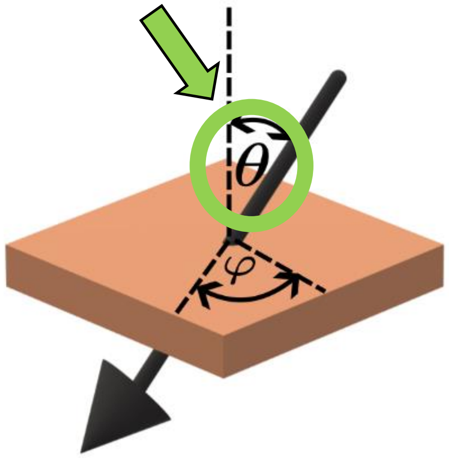

- To reduce the complexity of the problem, only the following two incidence angles are predicted: Azimuthal and perpendicular. Reducing it to regression problem
- **Datasets used for model development:**
  - ➯ 0.01-10 MeV electrons (curly tracks)
  - ➯ 10-500 MeV protons (thick, straight tracks)
  - ➯ 40 GeV pions (thin, straight tracks)
- It was found through an extensive study that a Random Forrest Regressor with a selection of input features produced optimal results

Input Features:

1. Size [no. of pixels]
2. Line standard deviation

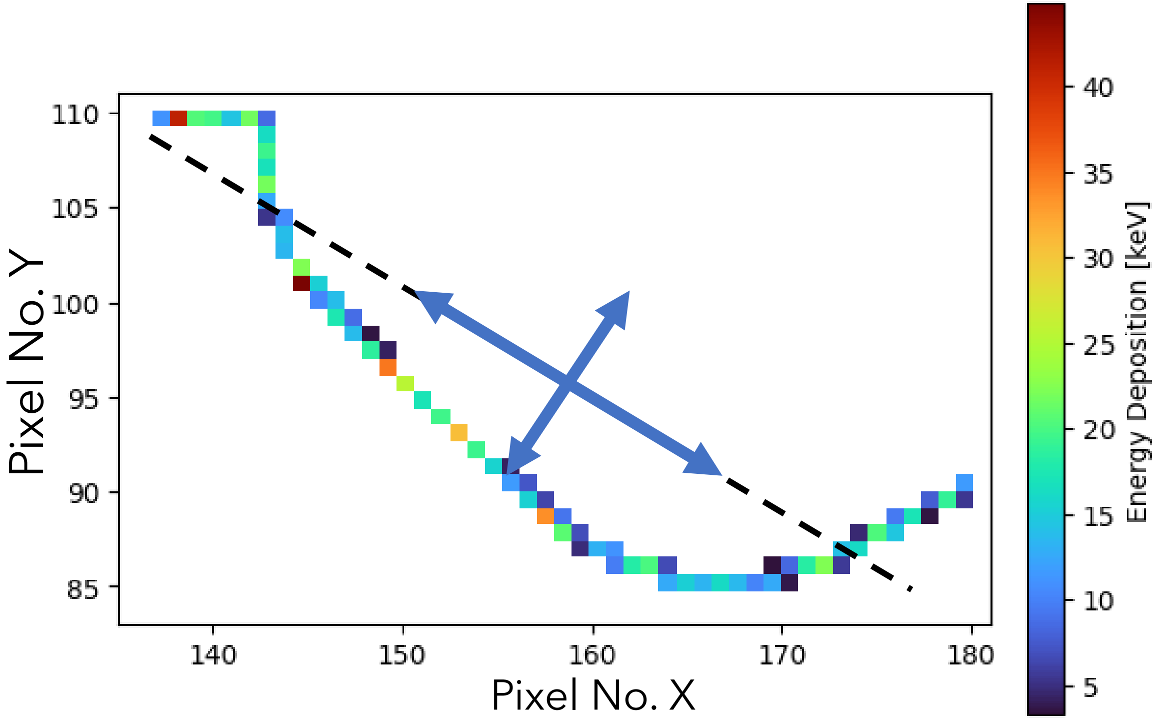

Theta Predictor Model

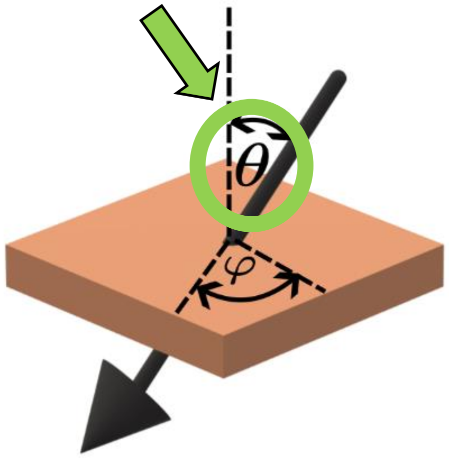

- To reduce the complexity of the problem, only the following two incidence angles are predicted: Azimuthal and perpendicular. Reducing it to regression problem
- **Datasets used for model development:**
  - ➪ 0.01-10 MeV electrons (curly tracks)
  - ➪ 10-500 MeV protons (thick, straight tracks)
  - ➪ 40 GeV pions (thin, straight tracks)
- It was found through an extensive study that a Random Forrest Regressor with a selection of input features produced optimal results

Input Features:

1. Size [no. of pixels]
2. Line standard deviation
3. Box dimensions

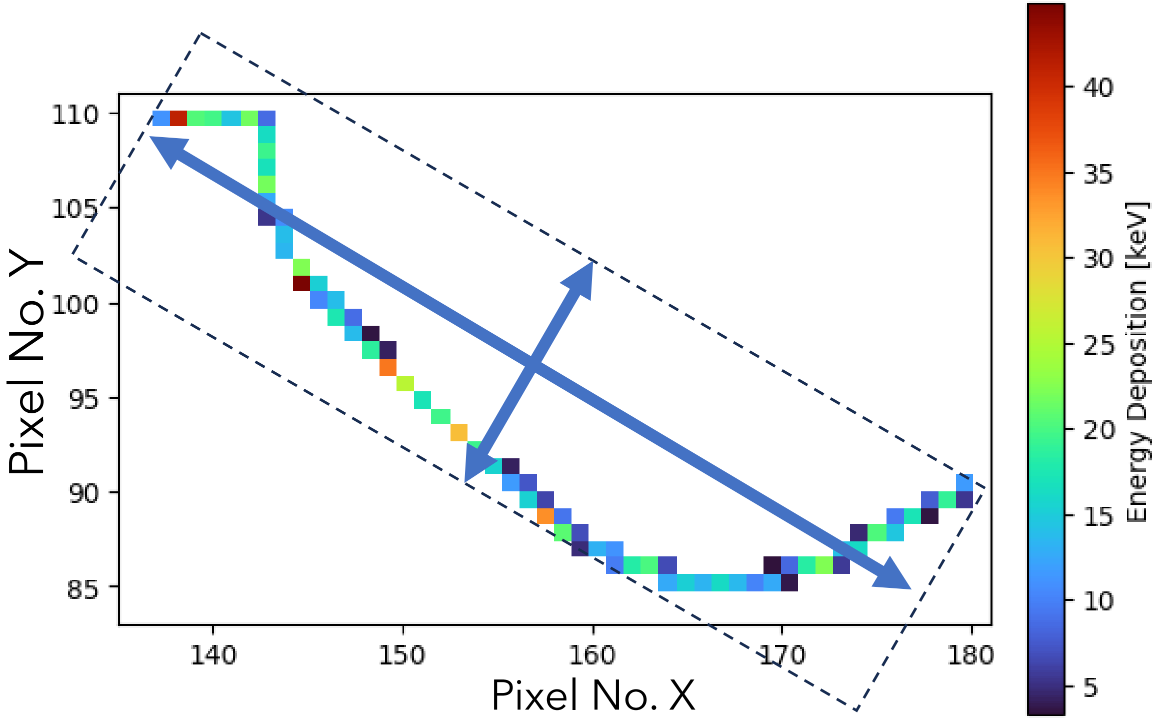

Theta Predictor Model

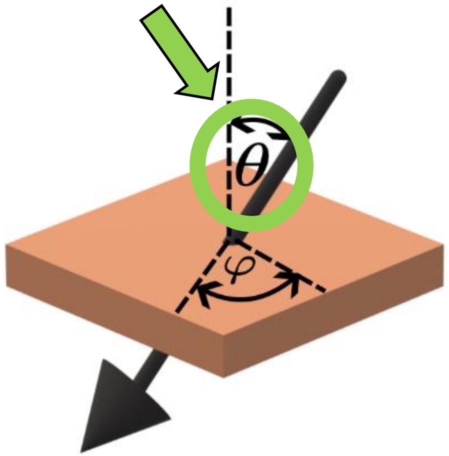

- To reduce the complexity of the problem, only the following two incidence angles are predicted: Azimuthal and perpendicular. Reducing it to regression problem
- **Datasets used for model development:**
  - ➯ 0.01-10 MeV electrons (curly tracks)
  - ➯ 10-500 MeV protons (thick, straight tracks)
  - ➯ 40 GeV pions (thin, straight tracks)
- It was found through an extensive study that a Random Forrest Regressor with a selection of input features produced optimal results

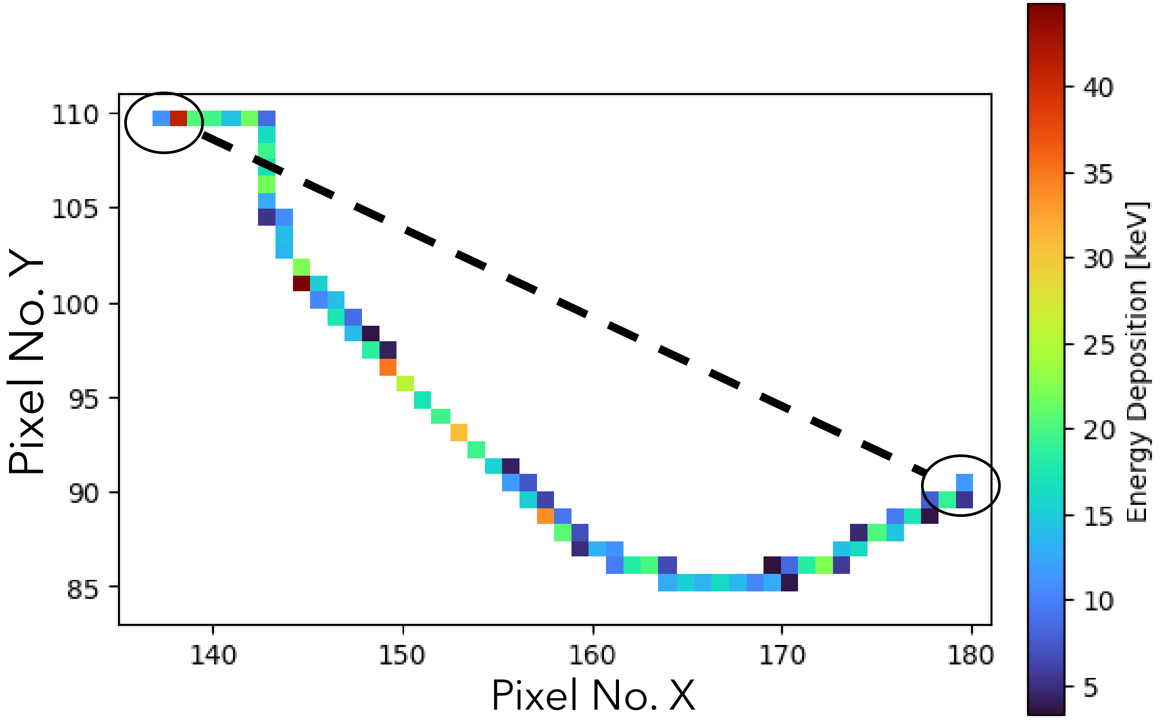

Input Features:

1. Size [no. of pixels]
2. Line standard deviation
3. Box dimensions
4. End point distance

Theta Prediction Results

For testing separate simulation datasets were created

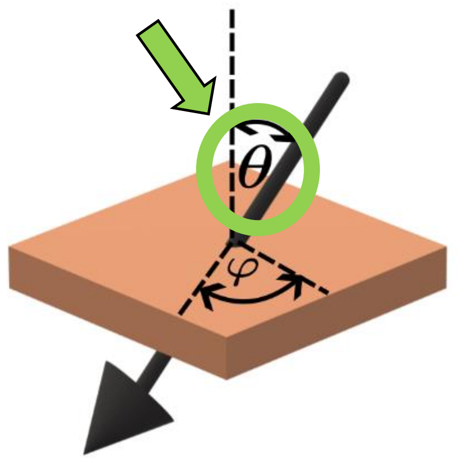

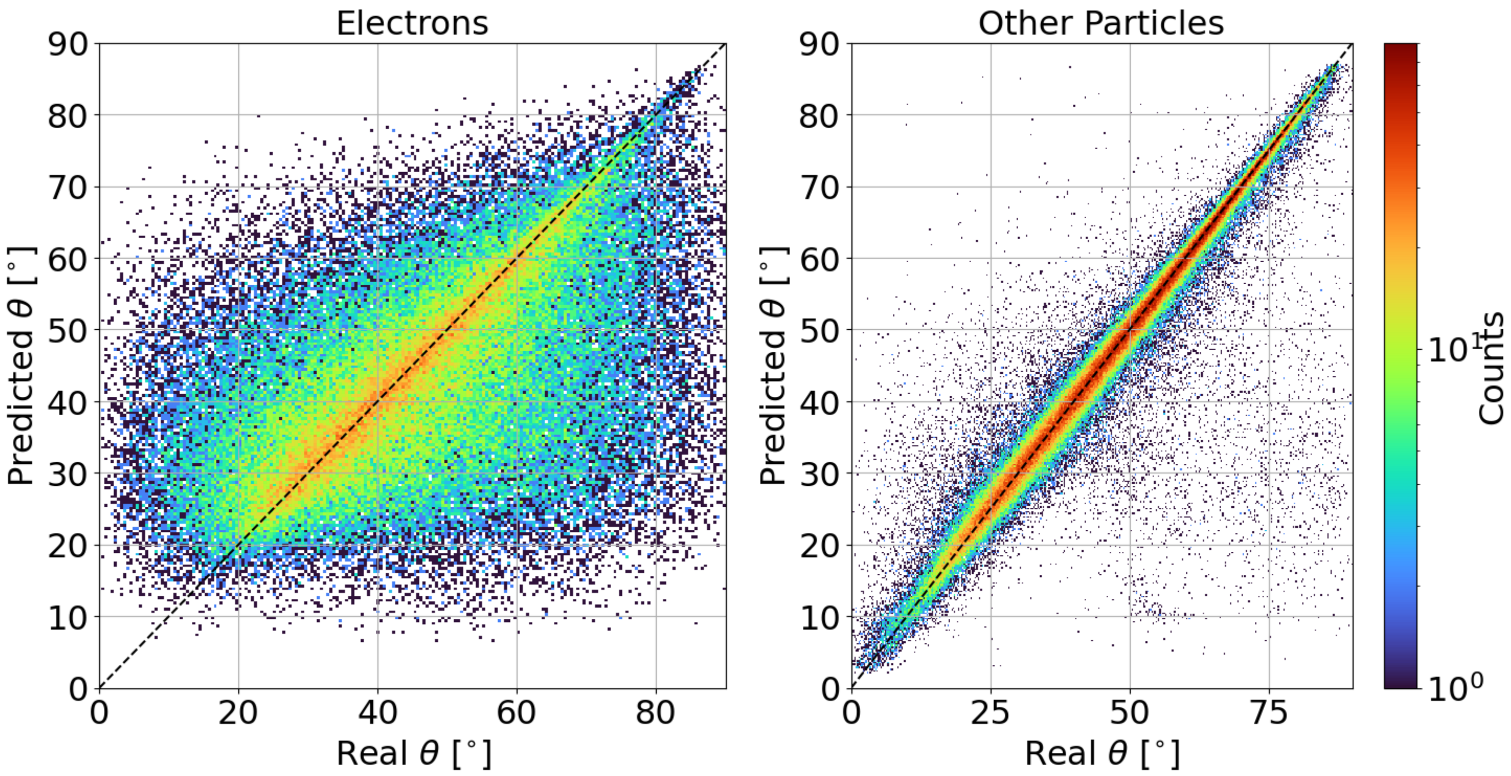

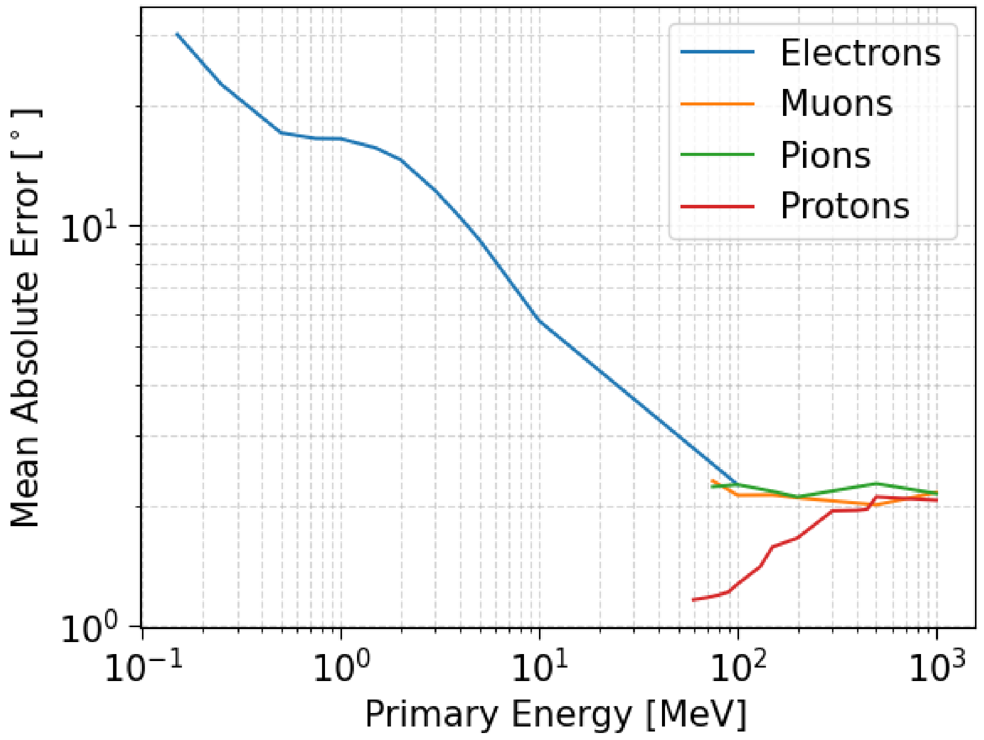

Phi Determination

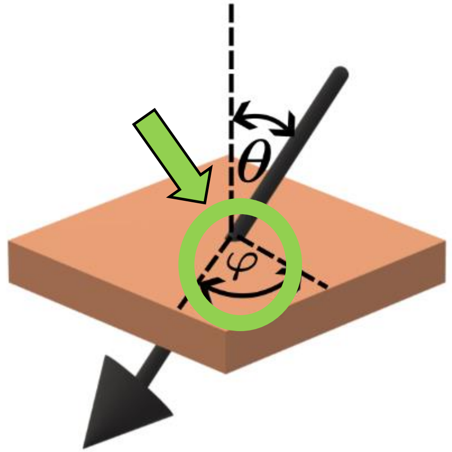

- An analytic approach was used as no improvement using machine learning algorithms was achieved
- Following an extensive study, Time of Arrival [ToA] weighted averaging was found to produce the most accurate results*
- In this method, we utilise the effect that drift time within the sensor has on ToA to approximate the “mean” entry and exit points

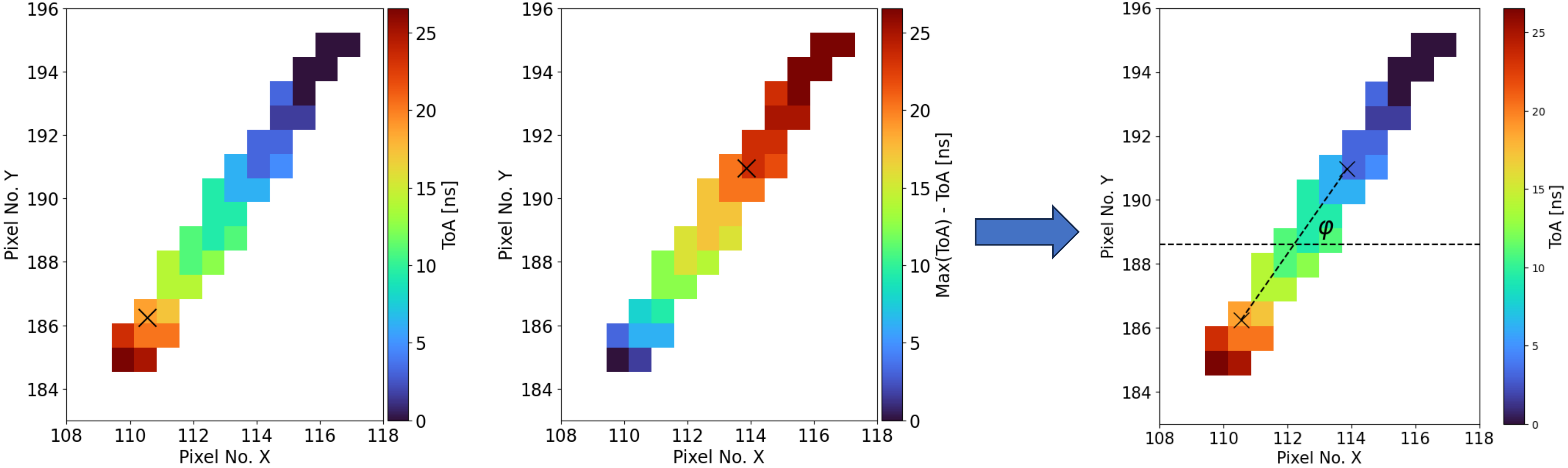

*P. Mánek et al. In: Journal of Instrumentation (2022), p. C01062. https://dx.doi.org/10.1088/1748-0221/17/01/C01062

Phi Model Results

For testing separate simulation datasets were created

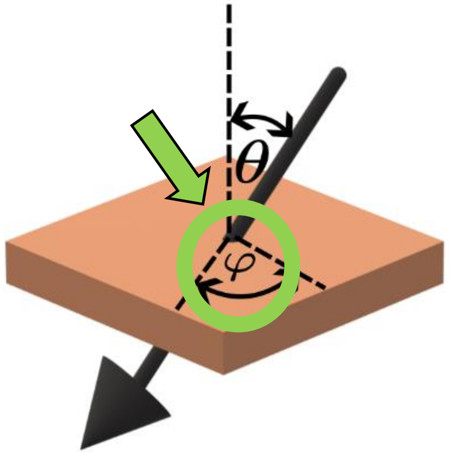

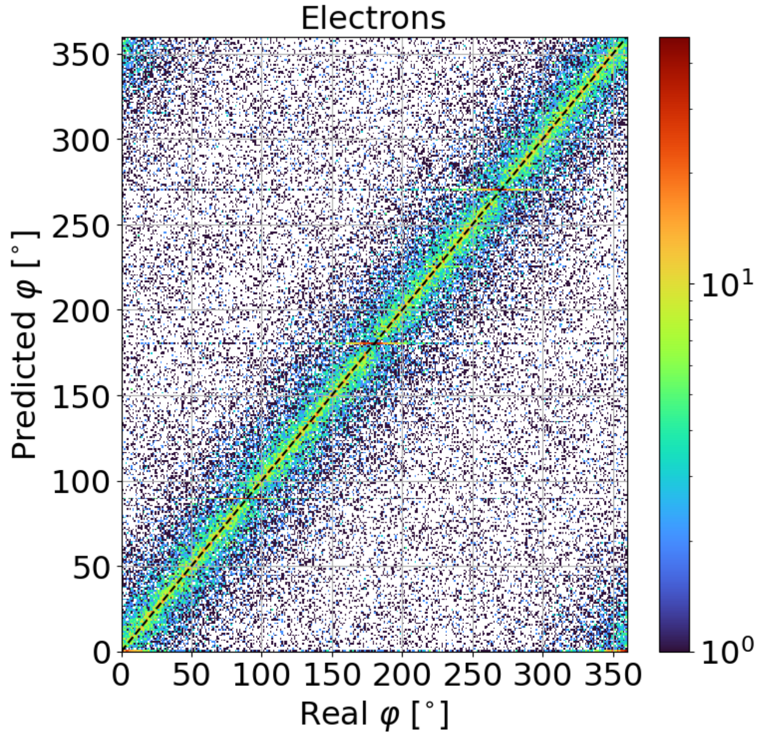

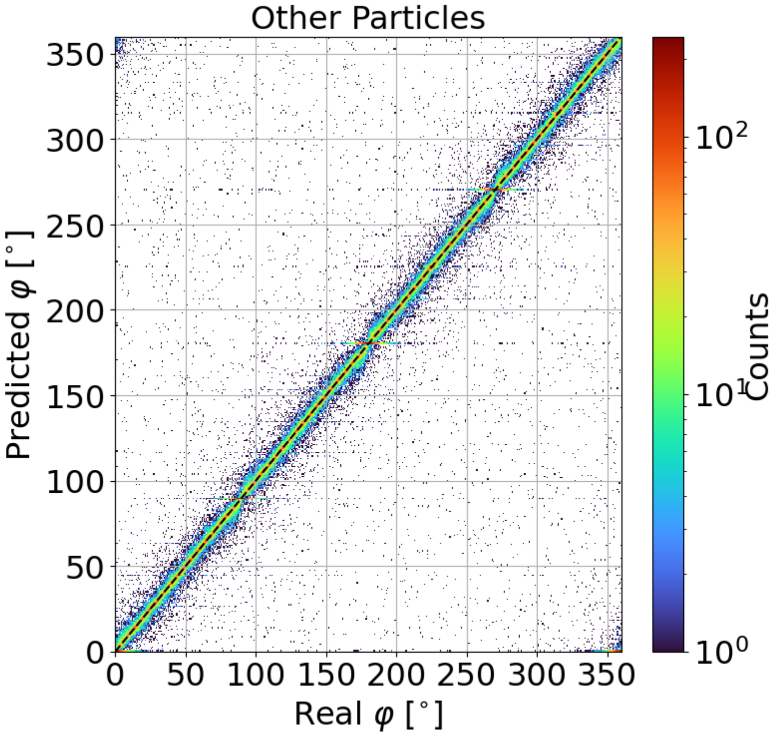

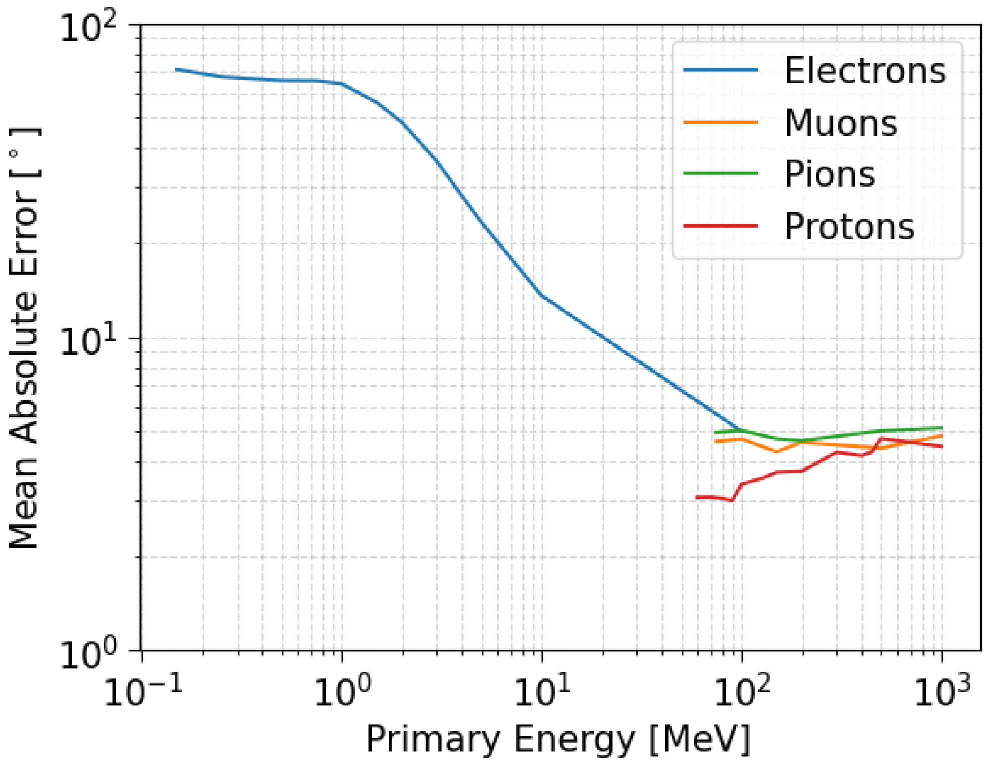

Rudimentary Classification

Particle tracks can be divided into two groups, with variable linearity and scattering:

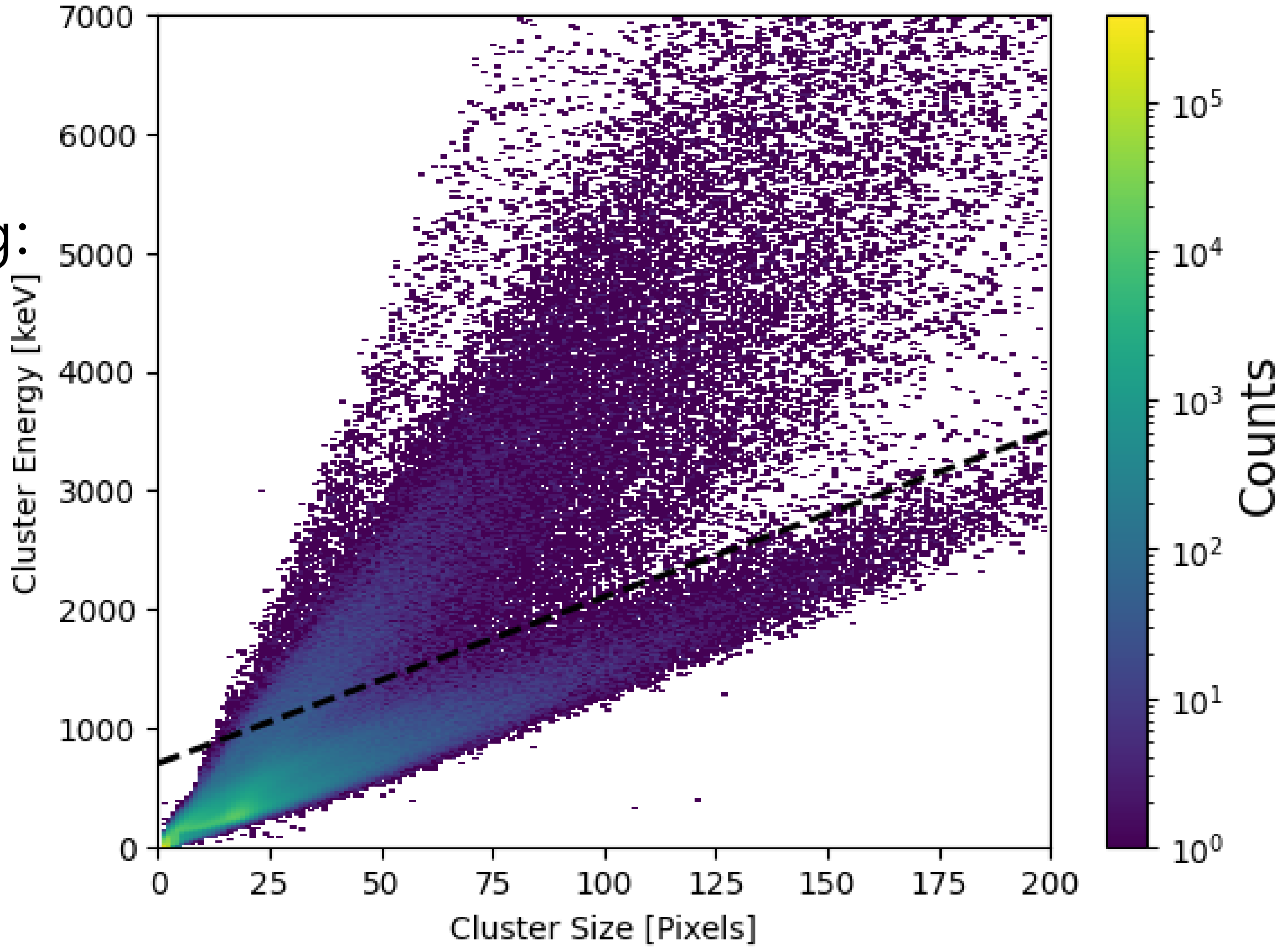

Rudimentary Classification

Particle tracks can be divided into two groups, with variable linearity and scattering:

1. **Lowly Ionising Particles (LIPs):**
   - ➪ Electrons
   - ➪ Photons
   - ➪ Relativistic singly charged particles

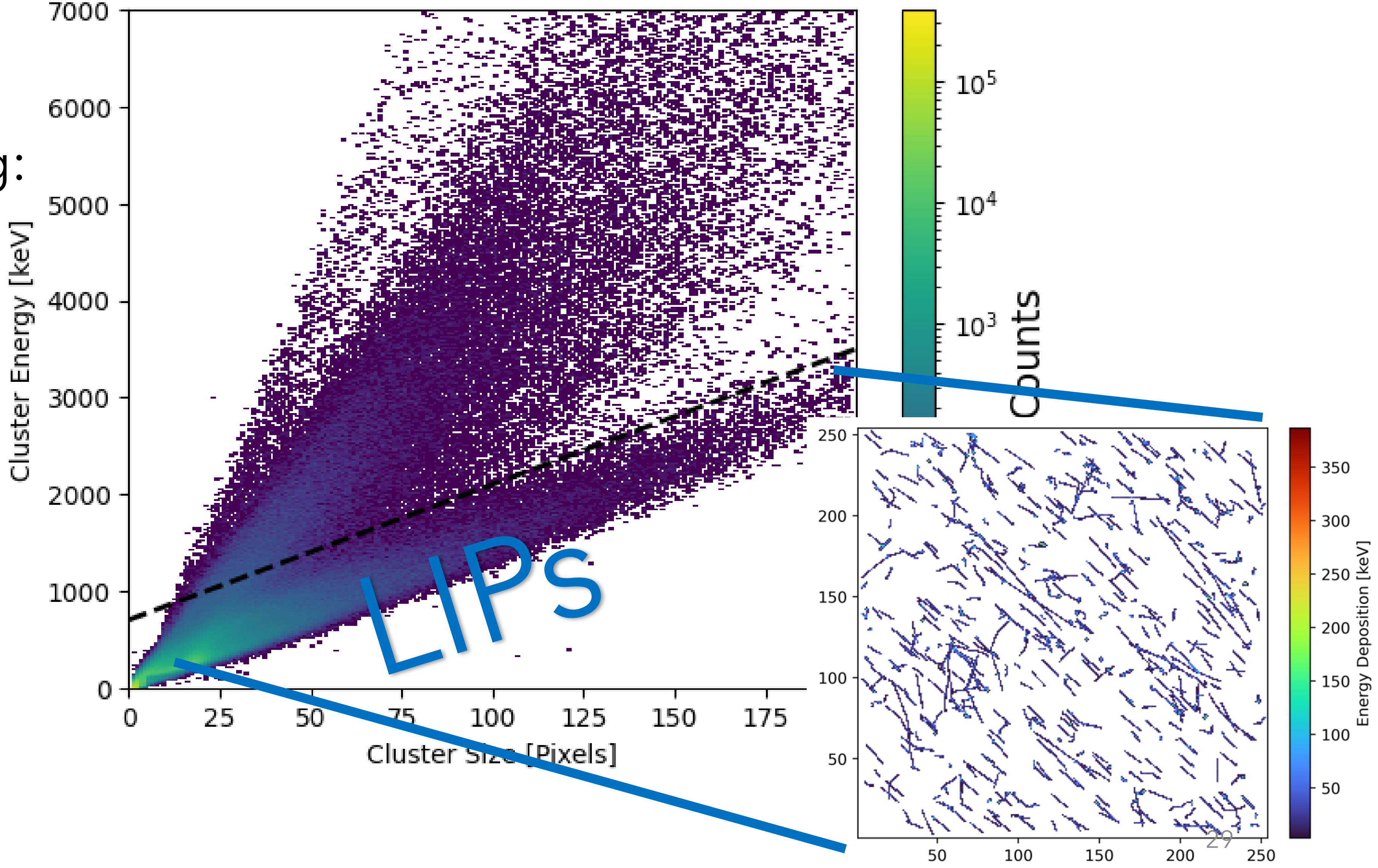

Rudimentary Classification

Particle tracks can be divided into two groups, with variable linearity and scattering:

1. **Lowly Ionising Particles (LIPs):**
   - ➩ Electrons
   - ➩ Photons
   - ➩ Relativistic singly charged particles
2. **Medium Ionising Particles (MeIPs):**
   - ➩ Protons <500 MeV
   - ➩ Pions <200 MeV
   - ➩ Muons <300 MeV
   - ➩ Z>1 particles

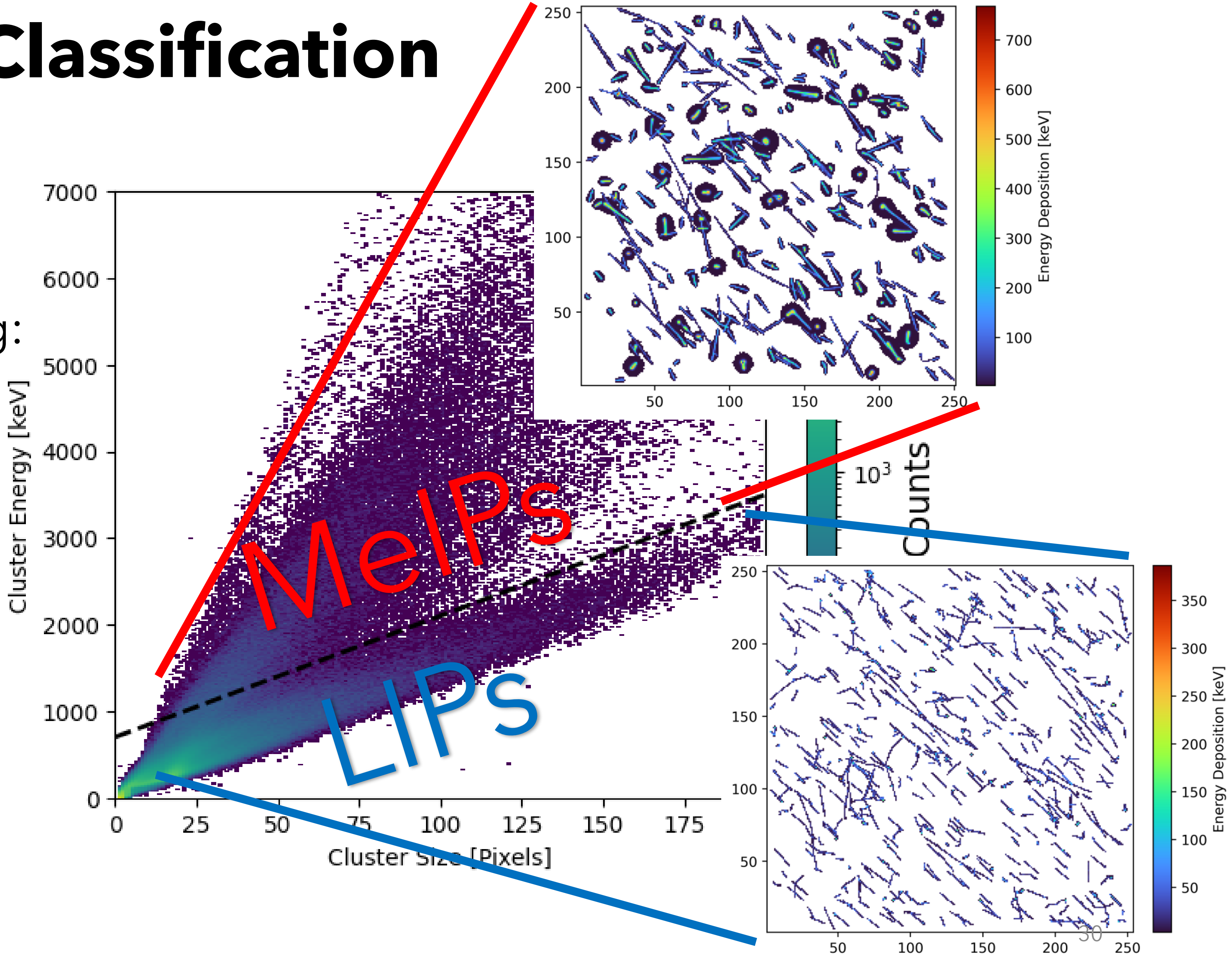

Field Directionality During Proton-Proton Collisions

E5 Detector

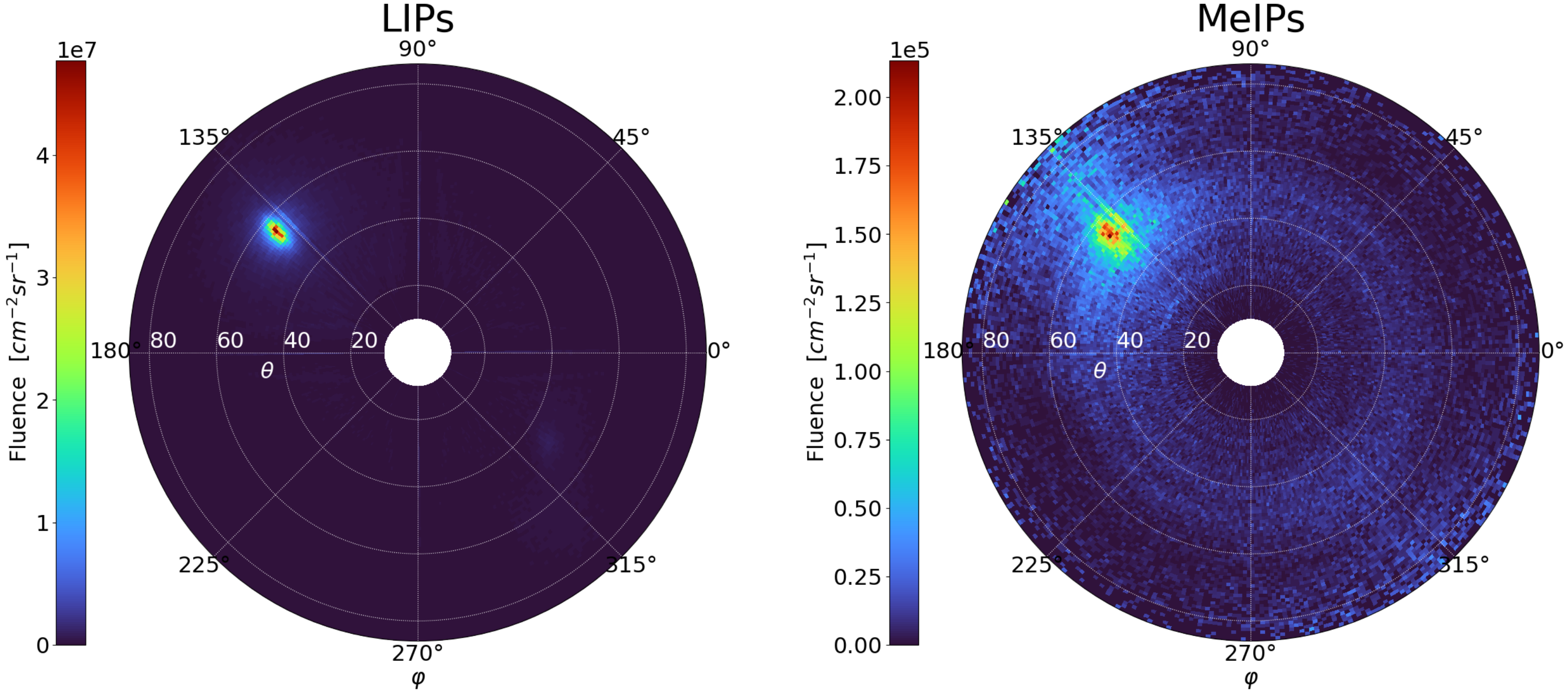

G4 Detector

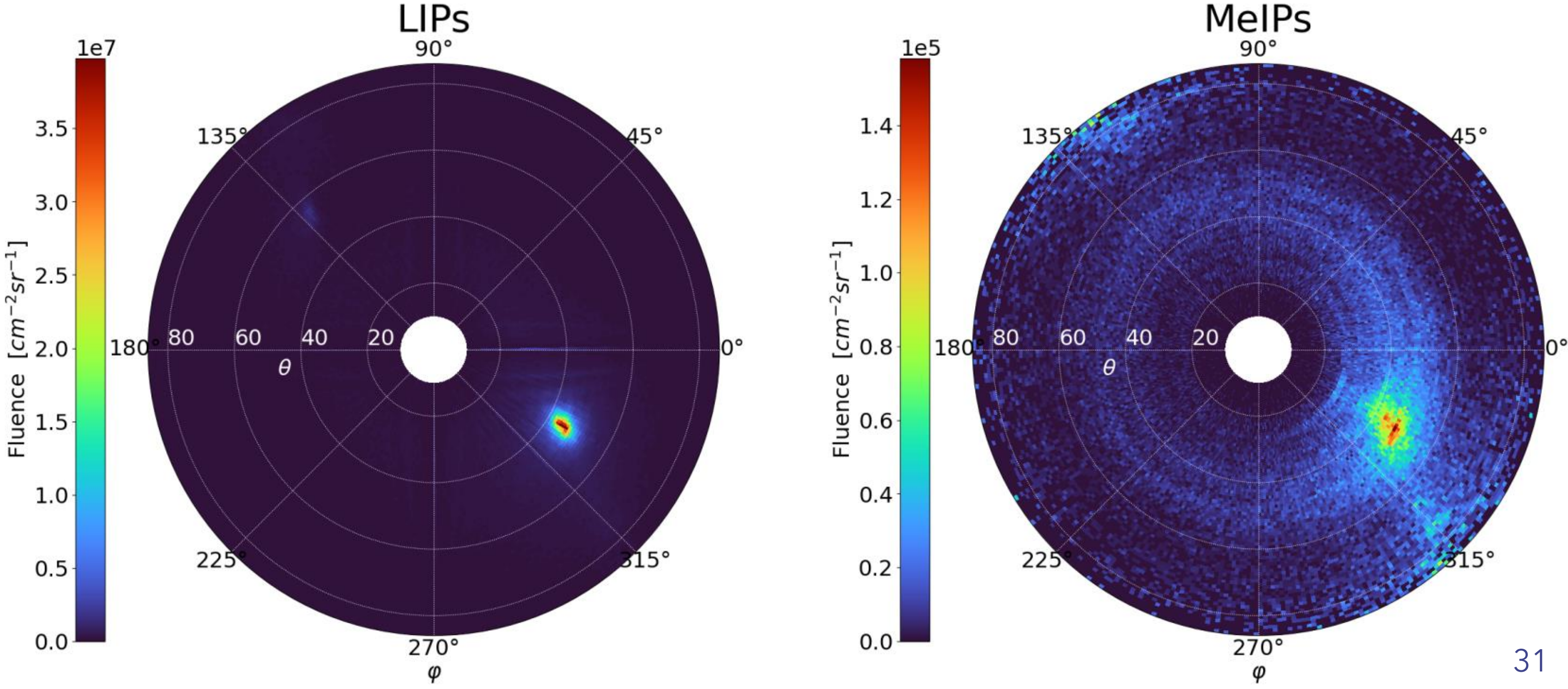

Field Directionality During Proton-Proton Collisions

E5 Detector

G4 Detector

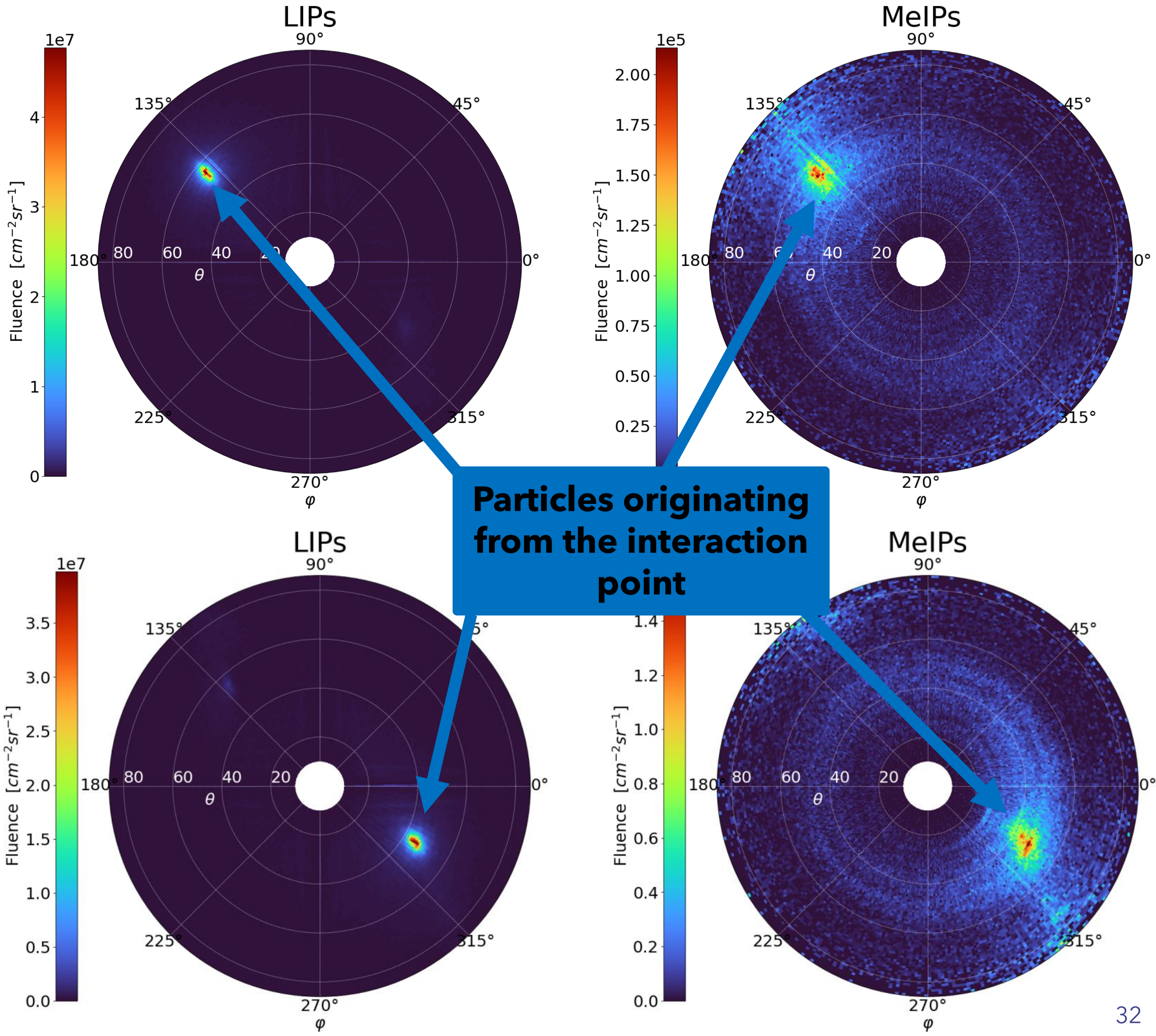

Field Directionality During Pb-Pb Collisions

E5 Detector

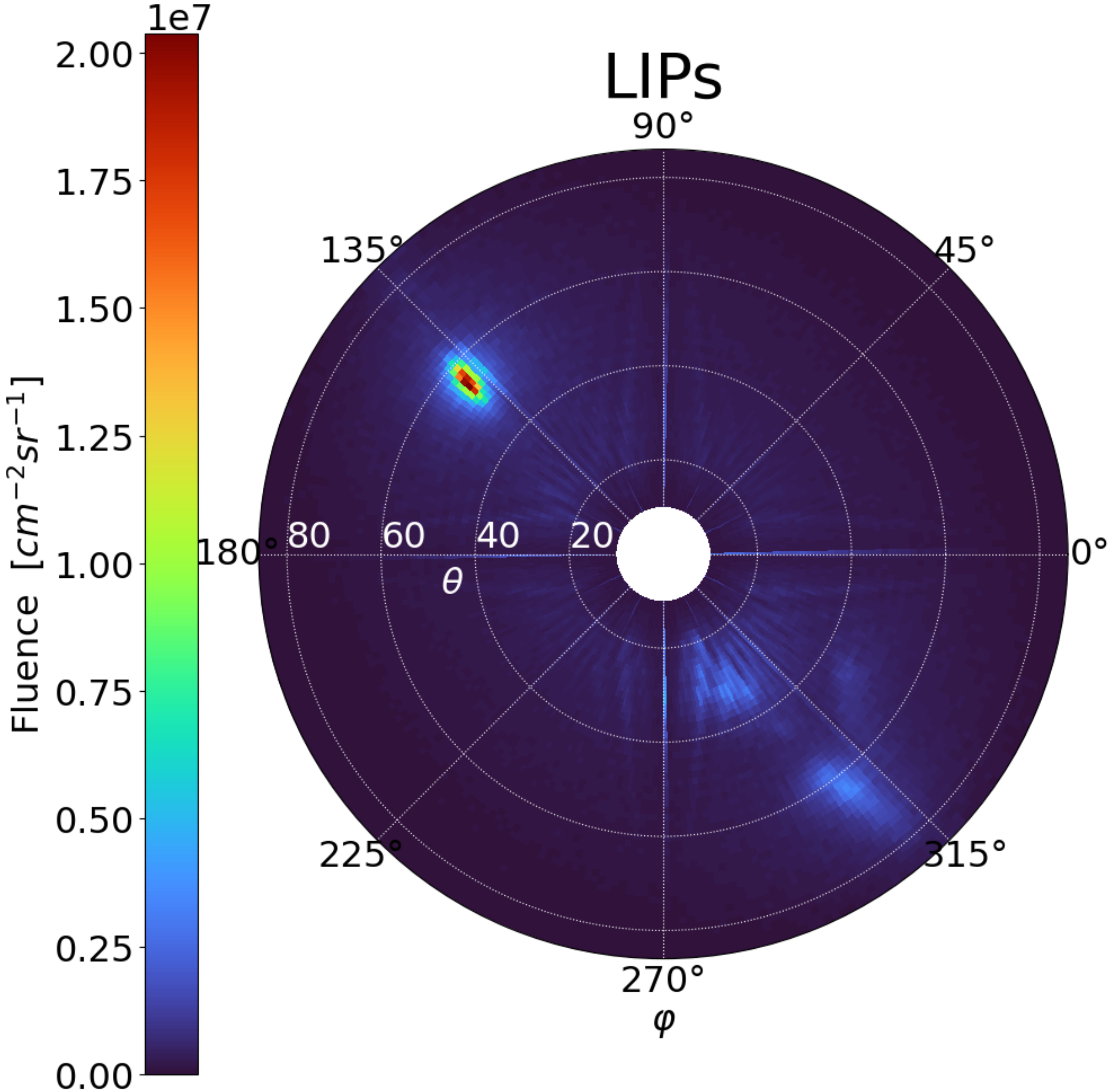

G4 Detector

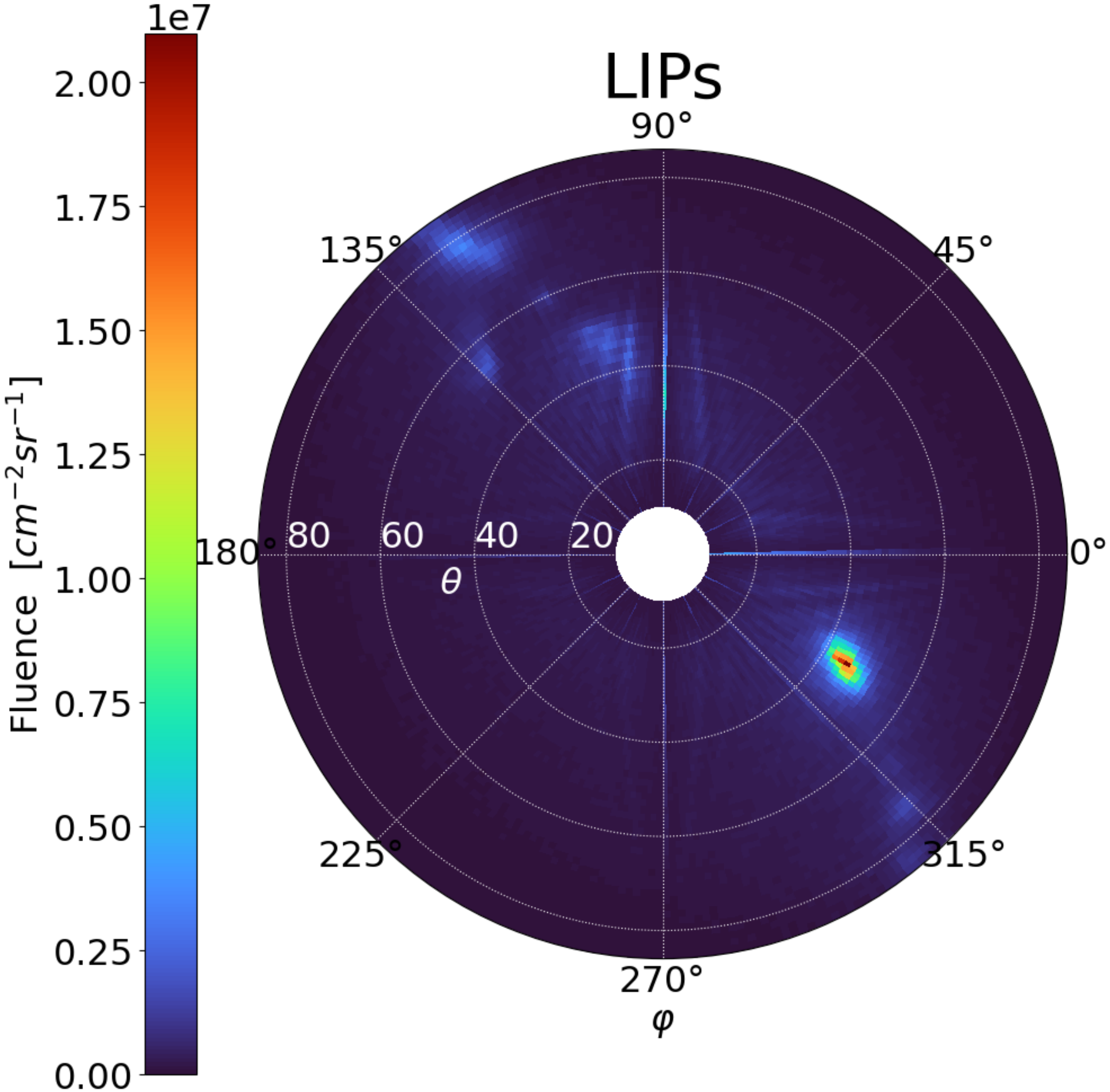

Field Directionality During Pb-Pb Collisions

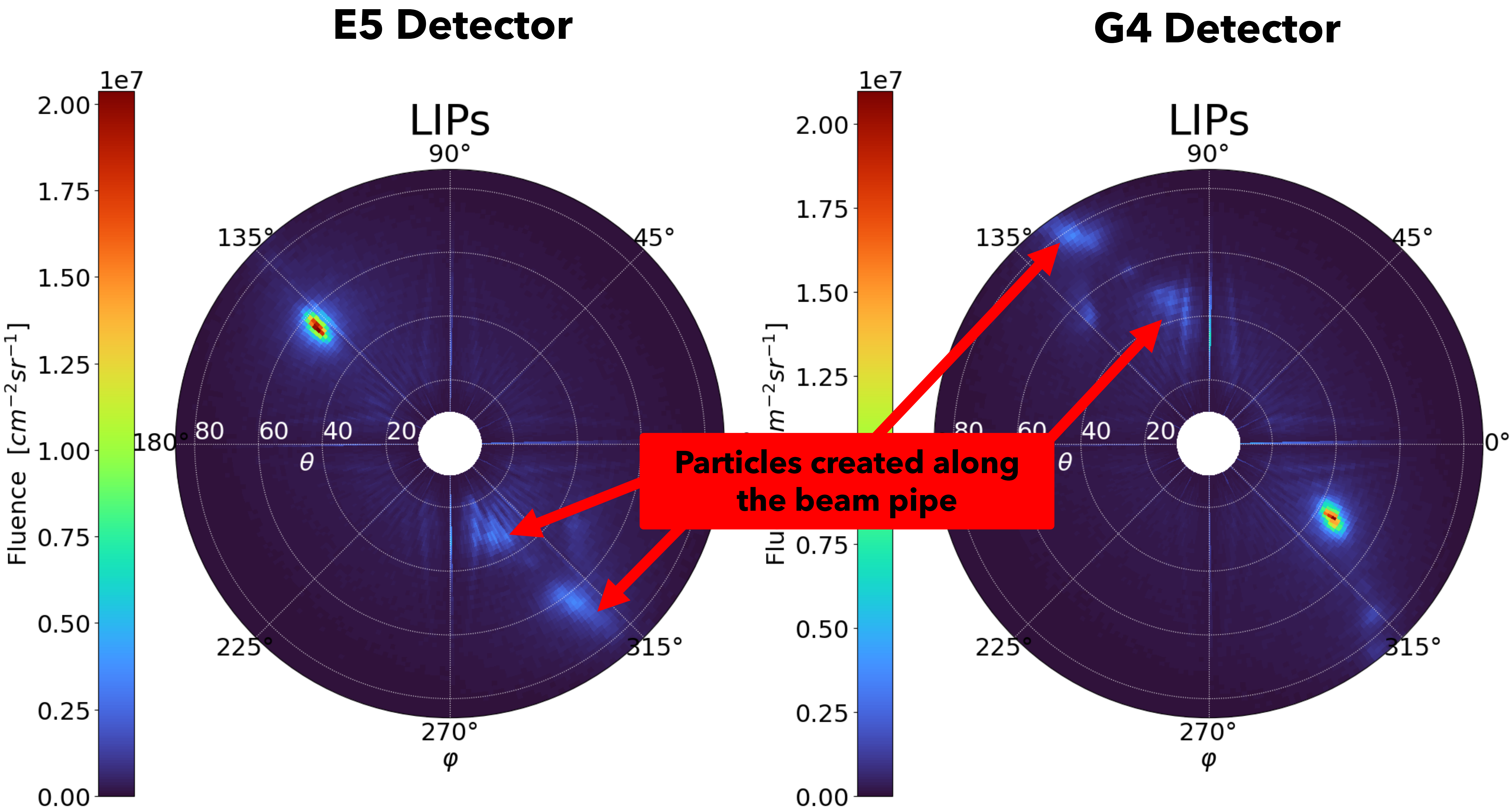

Time-Resolved Measurement of the Directionality Map Pb-Pb Collision Period

For increased accuracy only 5 minutes of data acquisition is need to produce reasonable statistics

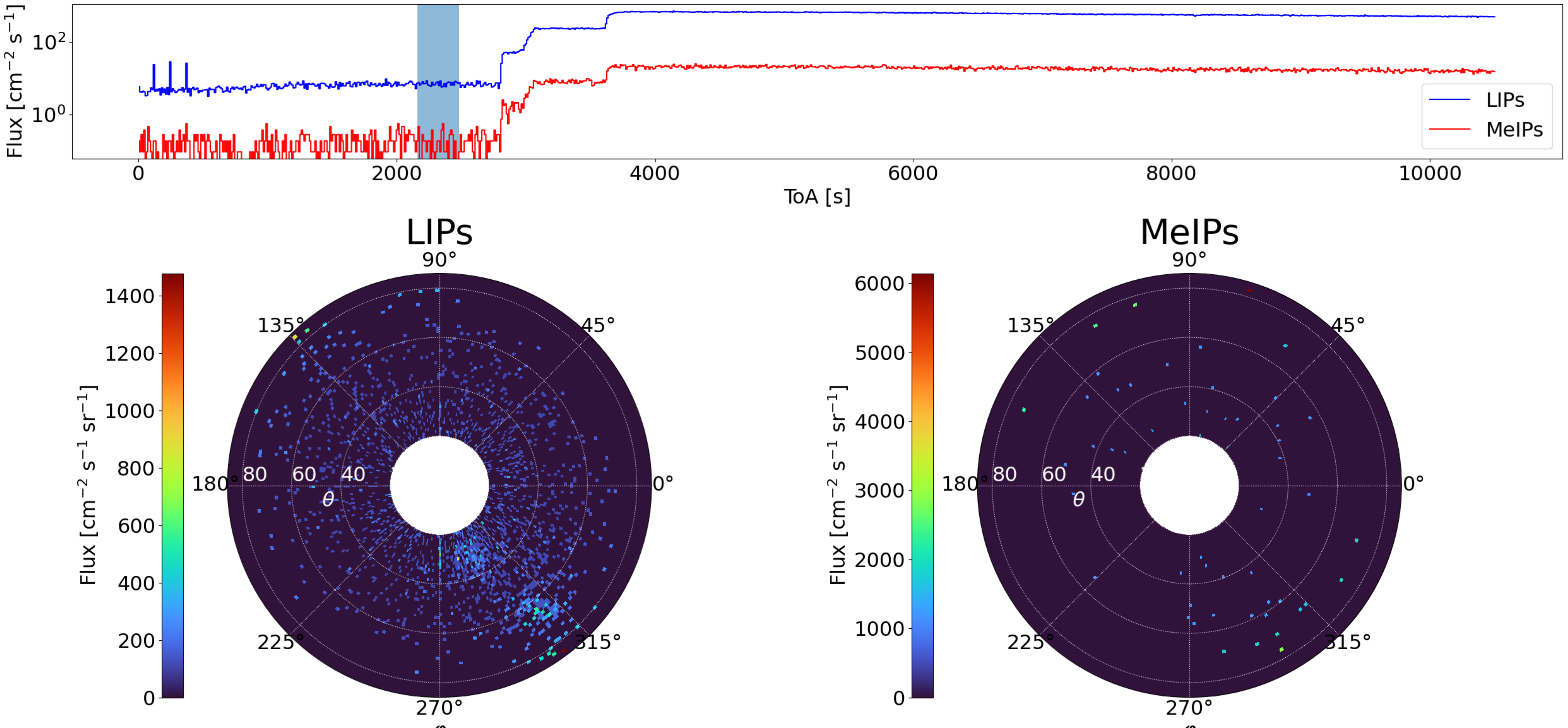

Time-Resolved Measurement of the Directionality Map Pb-Pb Collision Period

For increased accuracy only 5 minutes of data acquisition is need to produce reasonable statistics

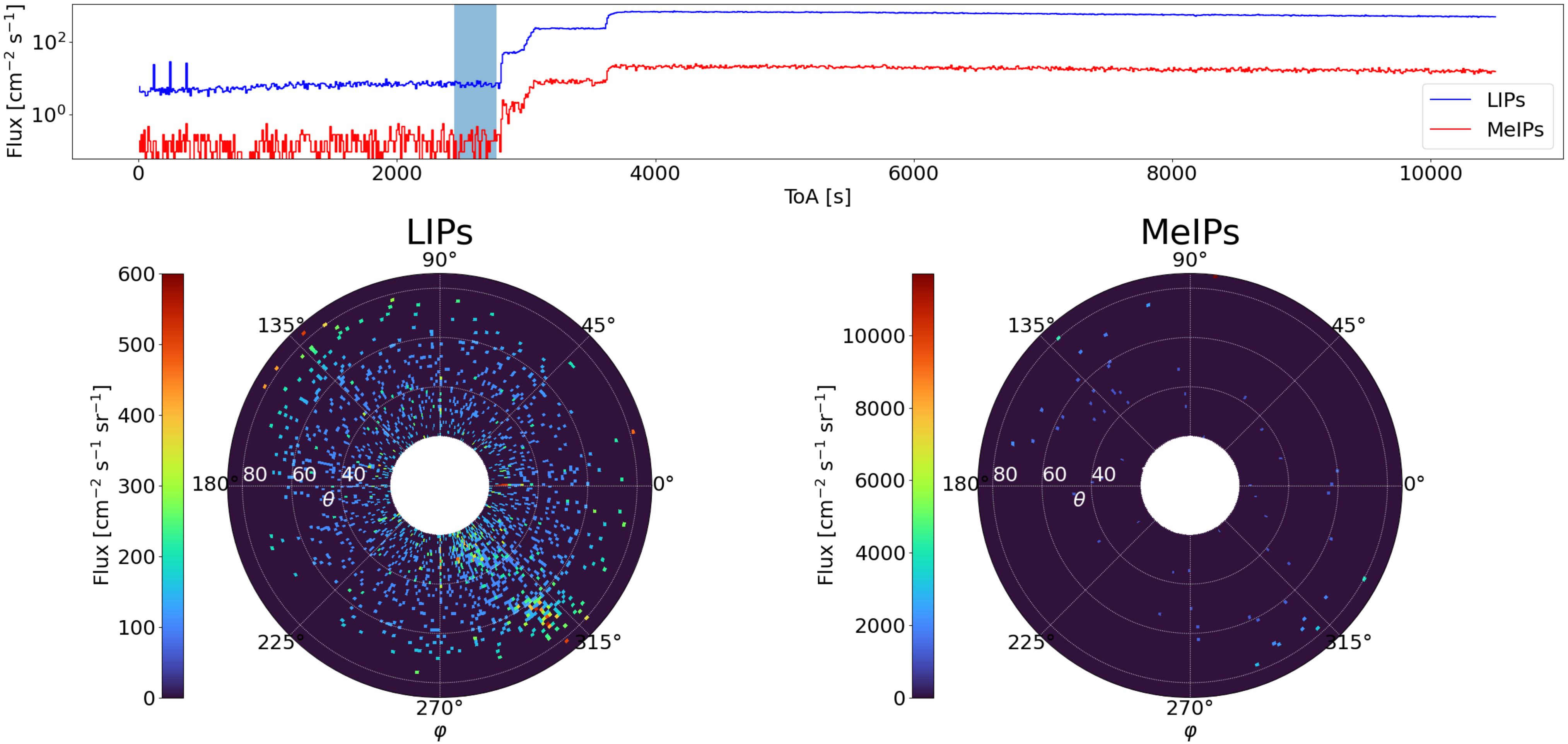

Time-Resolved Measurement of the Directionality Map Pb-Pb Collision Period

For increased accuracy only 5 minutes of data acquisition is need to produce reasonable statistics

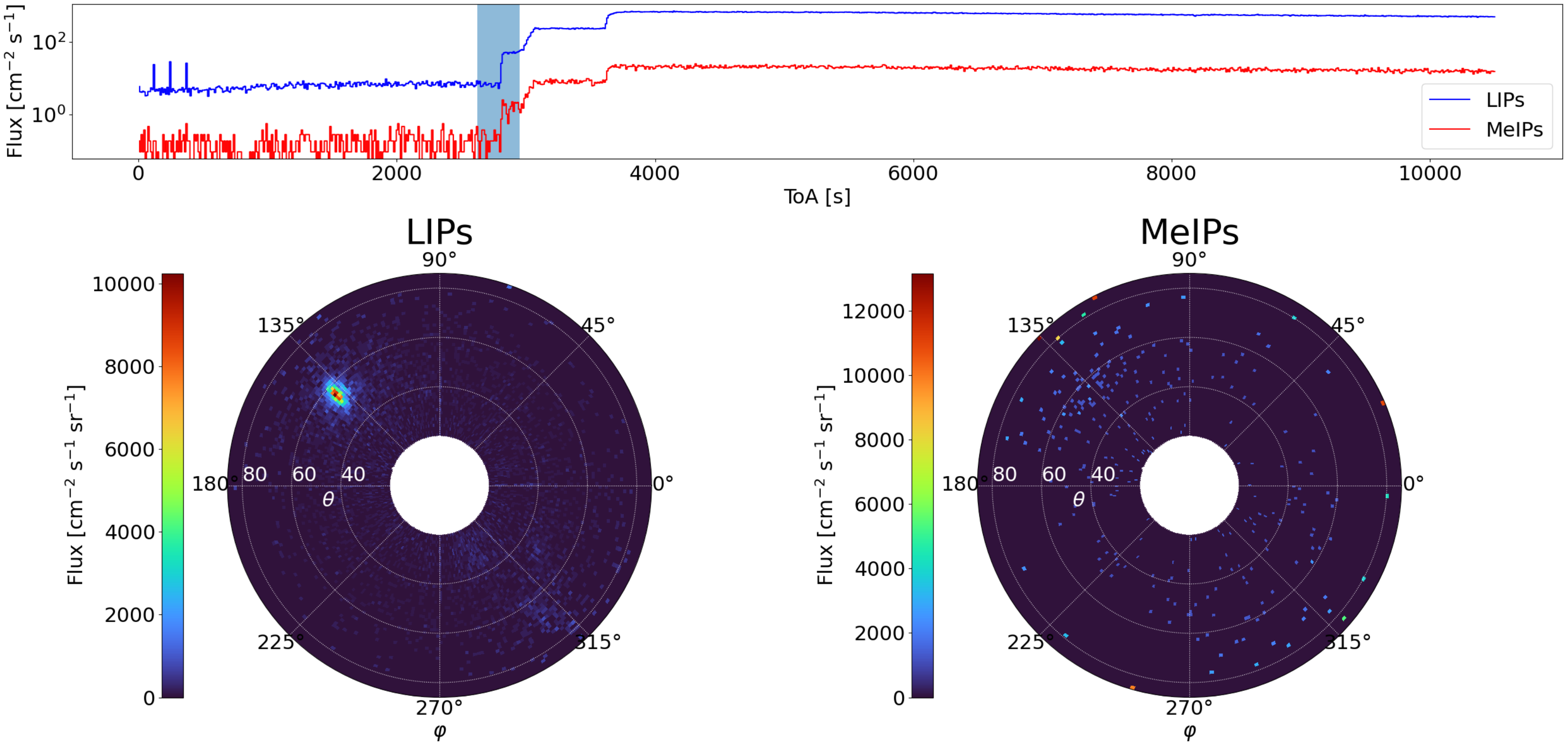

Time-Resolved Measurement of the Directionality Map Pb-Pb Collision Period

For increased accuracy only 5 minutes of data acquisition is need to produce reasonable statistics

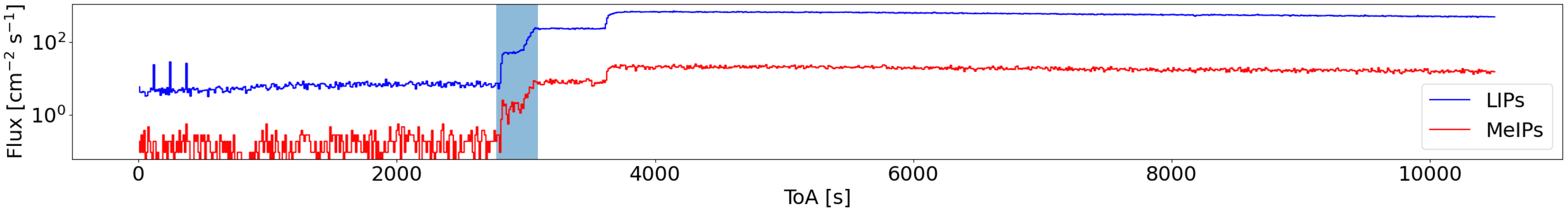

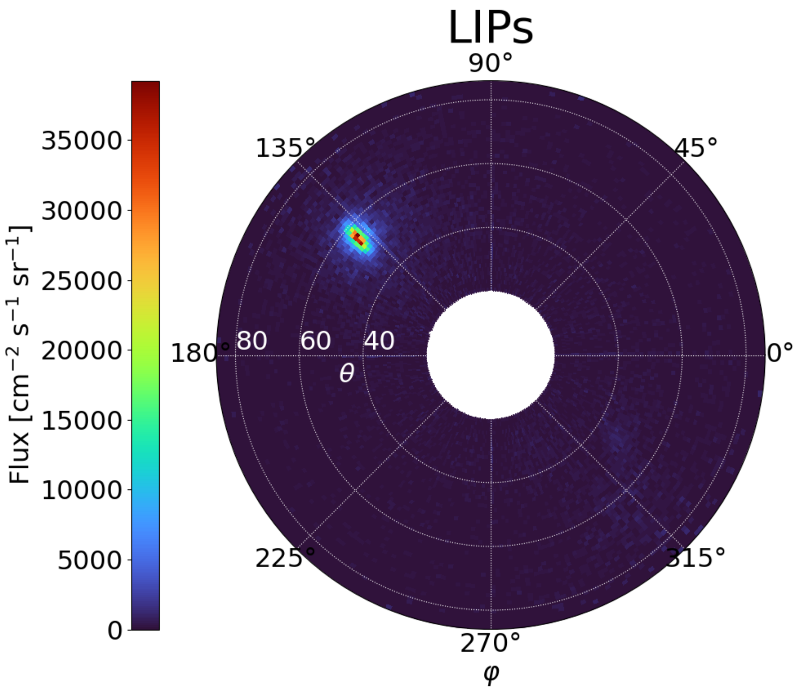

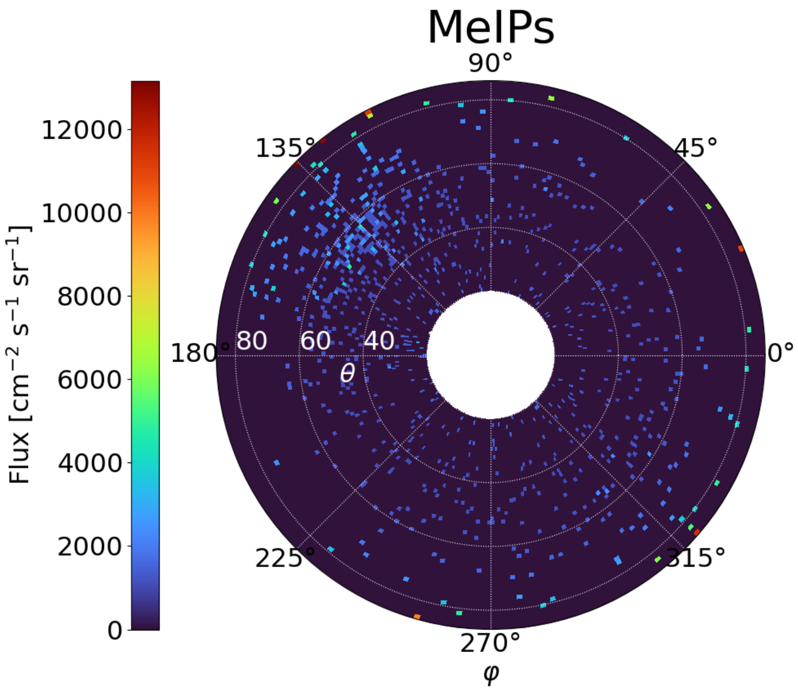

Time-Resolved Measurement of the Directionality Map Pb-Pb Collision Period

For increased accuracy only 5 minutes of data acquisition is need to produce reasonable statistics

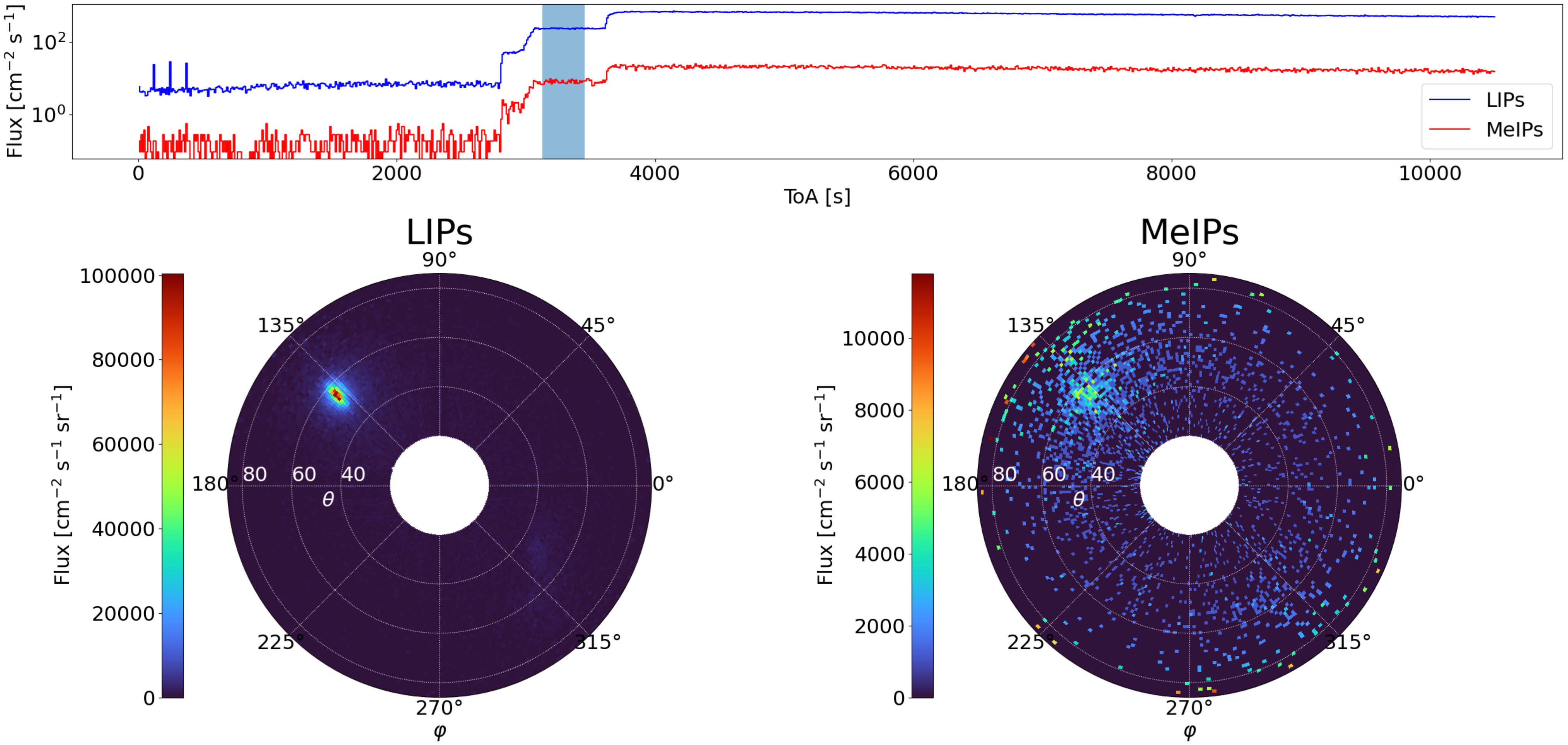

Time-Resolved Measurement of the Directionality Map Pb-Pb Collision Period

For increased accuracy only 5 minutes of data acquisition is need to produce reasonable statistics

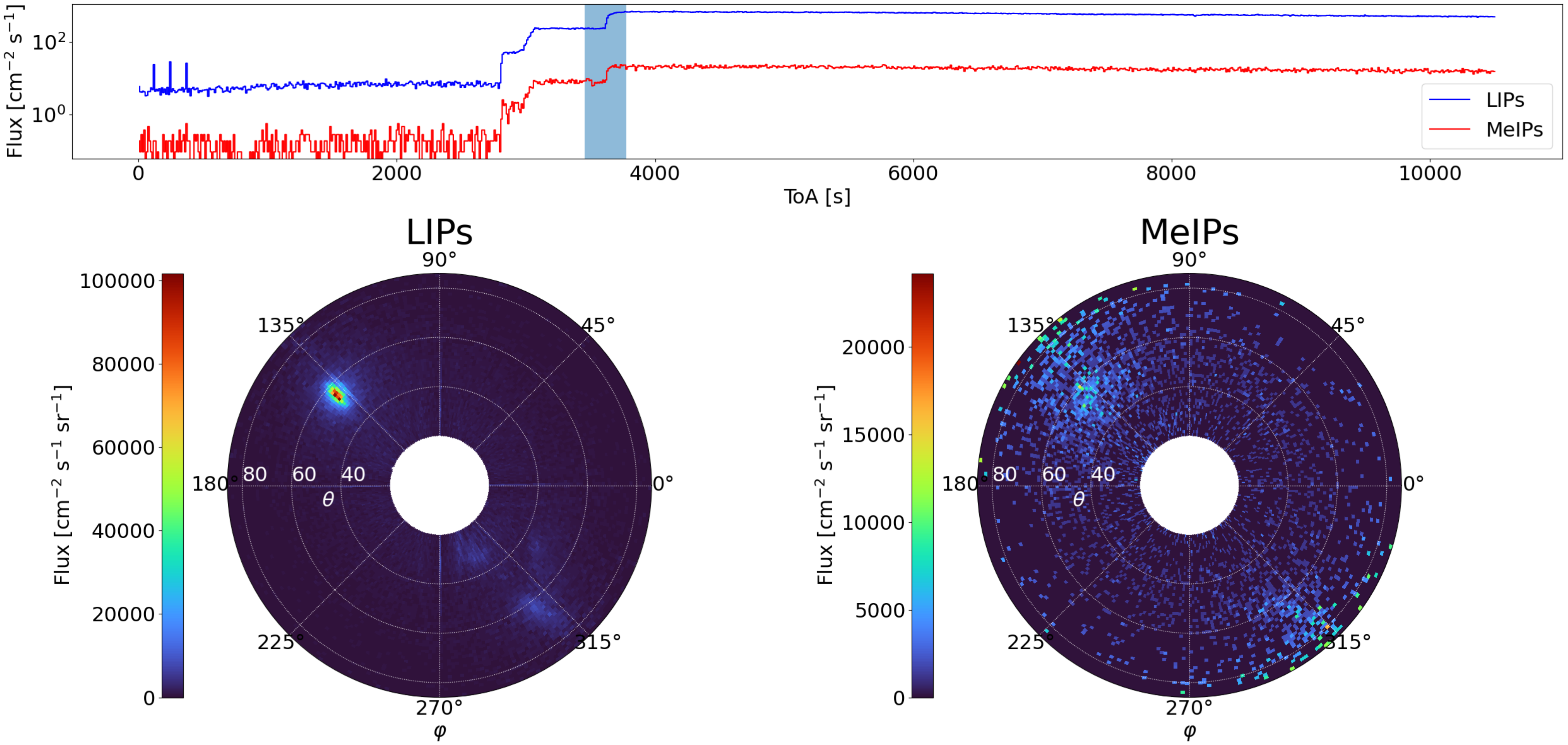

Time-Resolved Measurement of the Directionality Map Pb-Pb Collision Period

For increased accuracy only 5 minutes of data acquisition is need to produce reasonable statistics

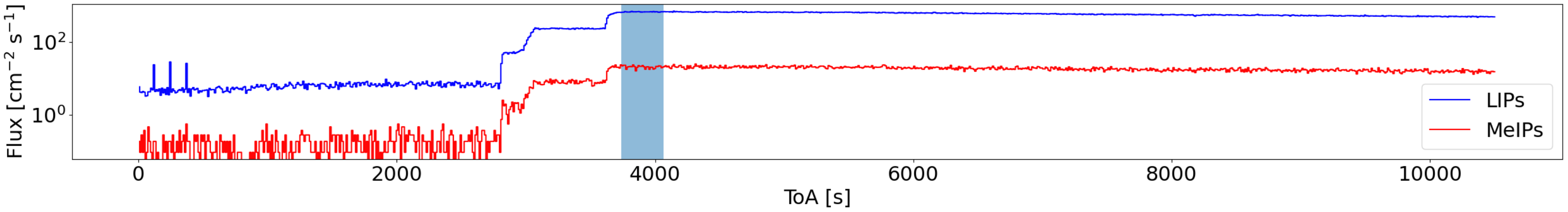

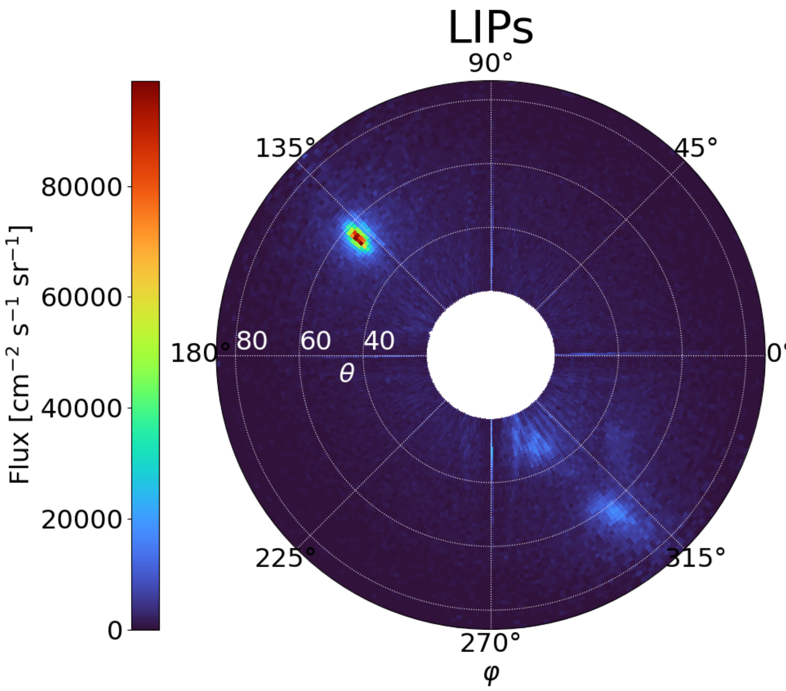

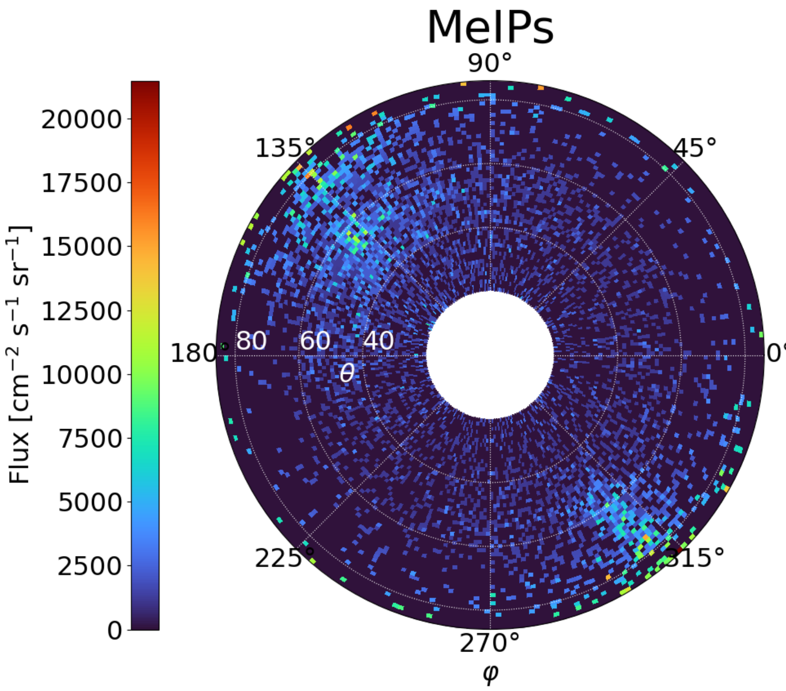

Radiation Field Decomposition According to Stopping Power

SATRAM And MOEDAL

A Brief Excursion:
Radiation Field Decomposition in Space

- Why the detour?
  - The mixed radiation field present in space has much lower complexity allowing us to more effectively develop and test algorithms for classification
- The data that will be used will come from the **S**pace **A**pplication **T**imepix **Ra**diation **M**onitor (**SATRAM**)
- The acquired knowledge can then be applied to the MoEDAL experiment

Space Application of Timepix Radiation Monitor (SATRAM)

- First Timepix in open space
- Power consumption of **2.5 W**
- Total mass **380 g** (107 x 70 x 55 mm)

Proba-V

- Minisatellite (158 kg)
- Altitude ~820 km (LEO)
- 101.21 minutes orbit duration
- Inclination 98.6°
- Sun-synchronous
- Launched 7th March 2013

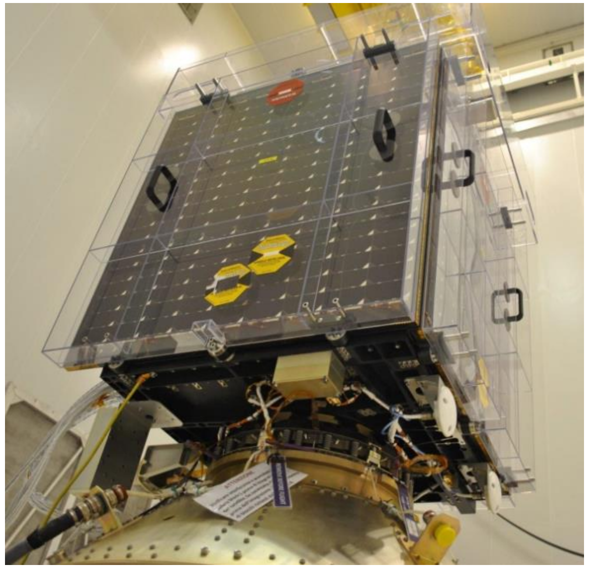

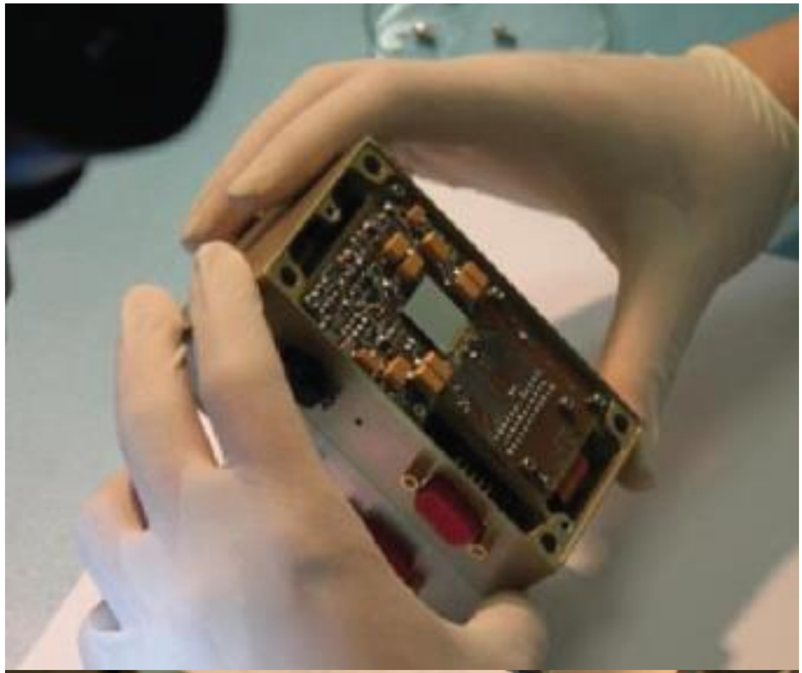

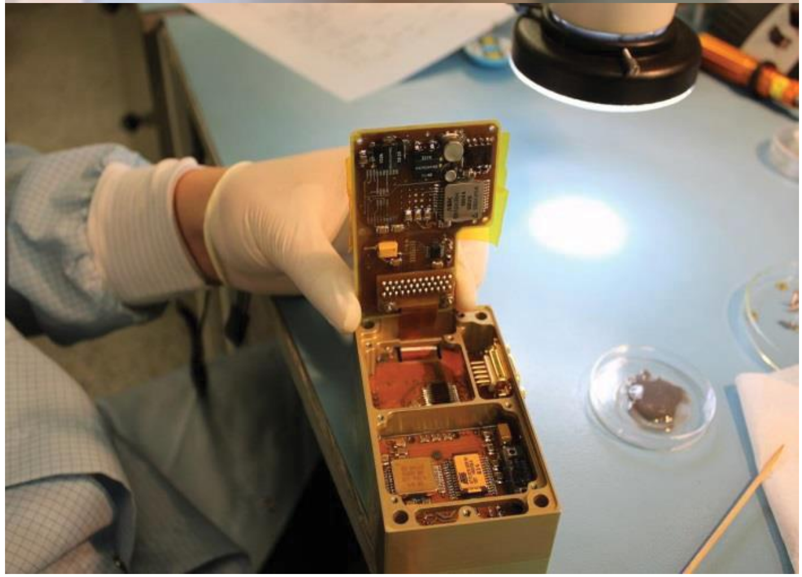

The Radiation Environment

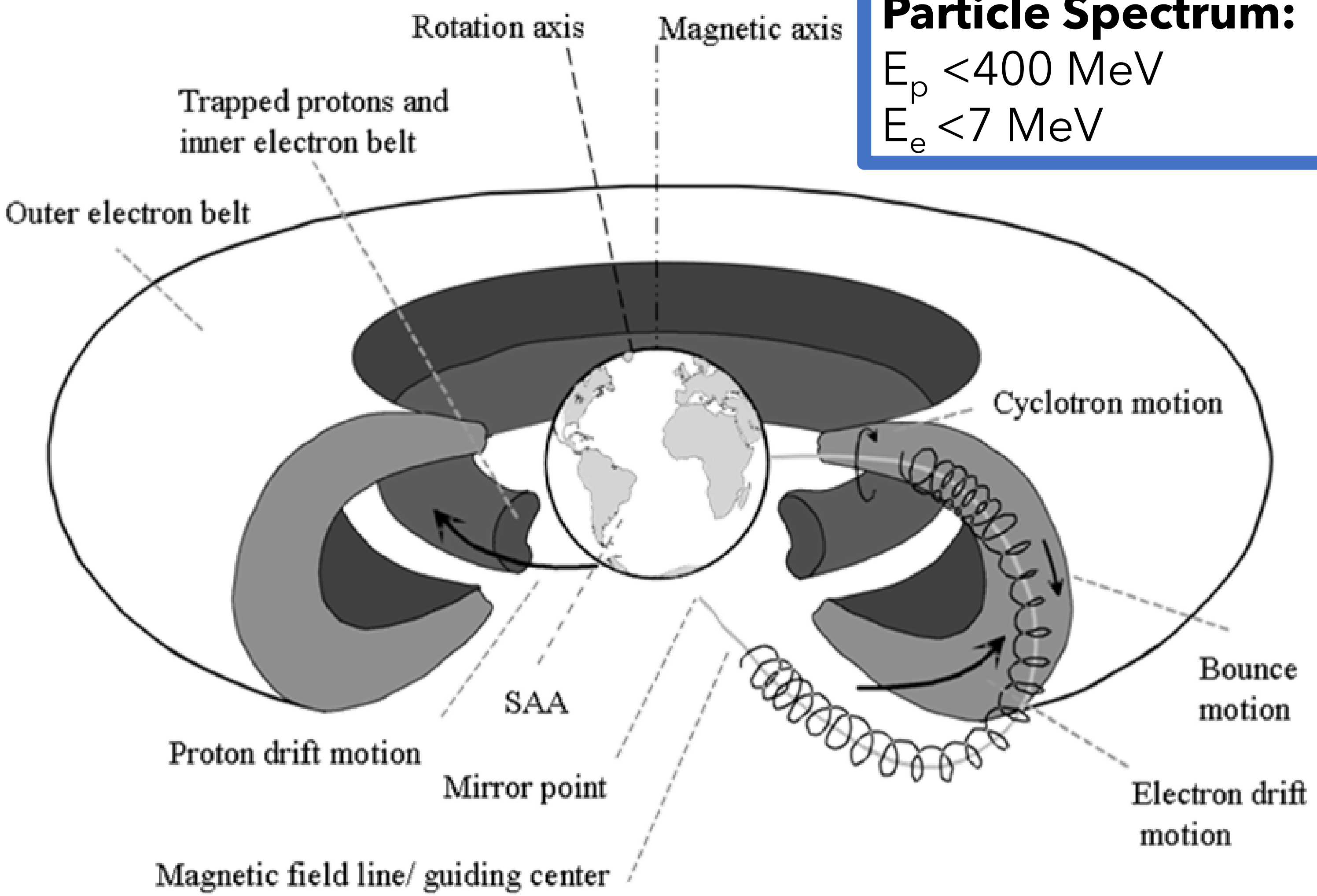

Particle Spectrum:
E_p <400 MeV
E_e <7 MeV

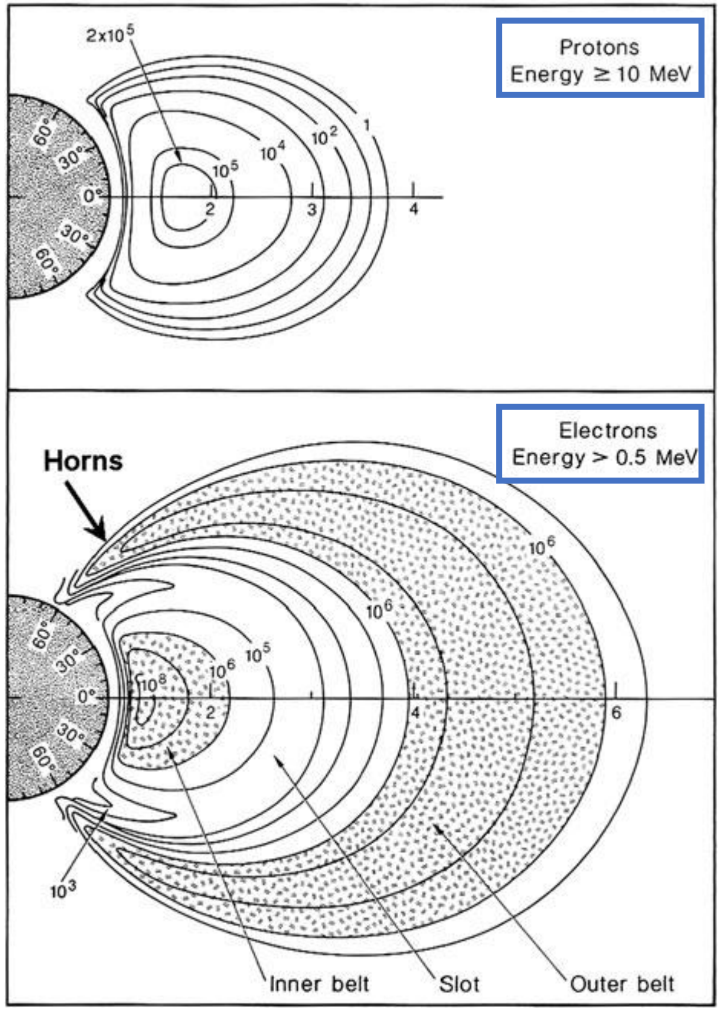

Mauk, B.H., Fox, N.J., Kanekal, S.G. et al. Space Sci Rev (2013) 179: 3.

The Radiation Environment

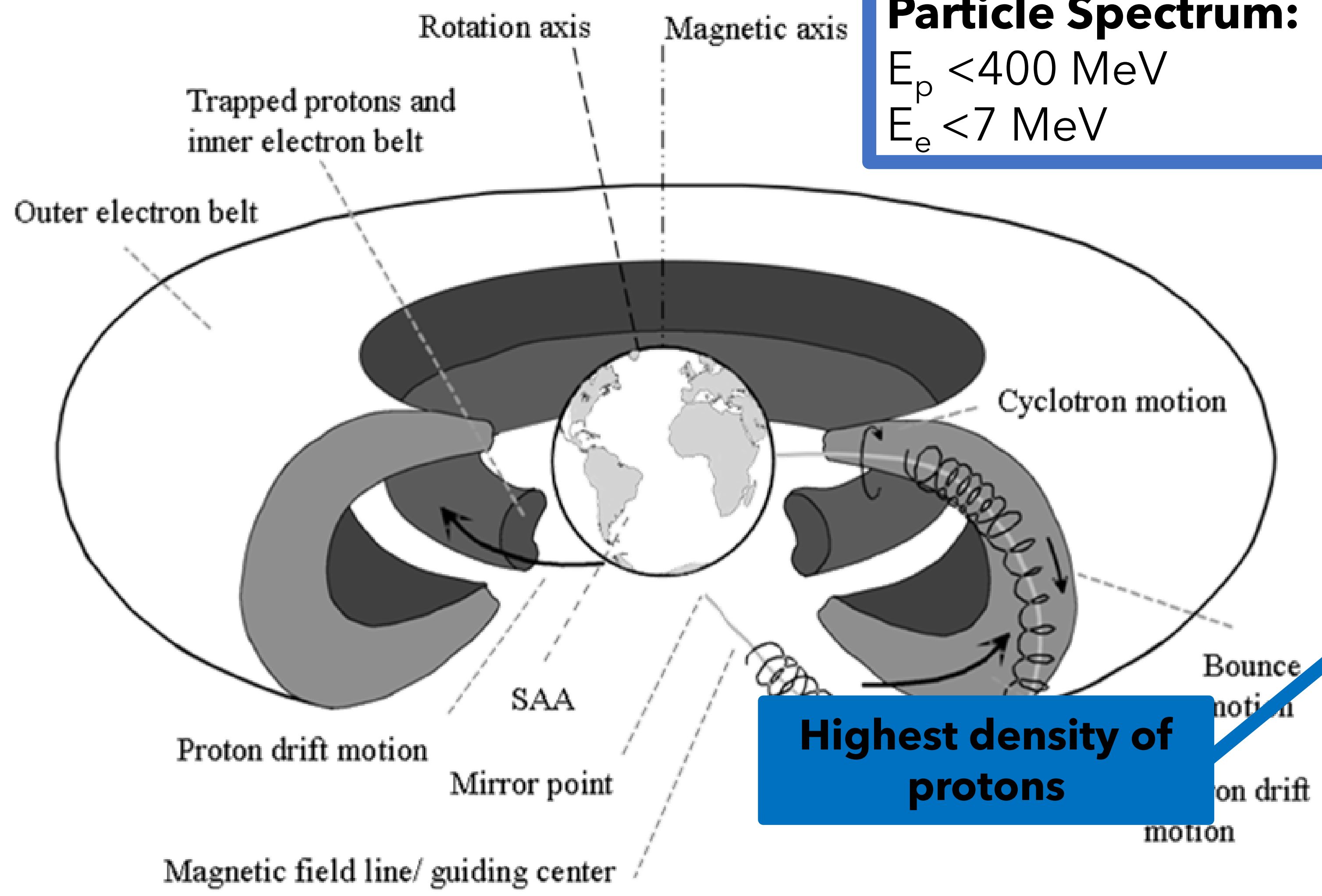

Particle Spectrum:
E_p <400 MeV
E_e <7 MeV

Highest density of protons

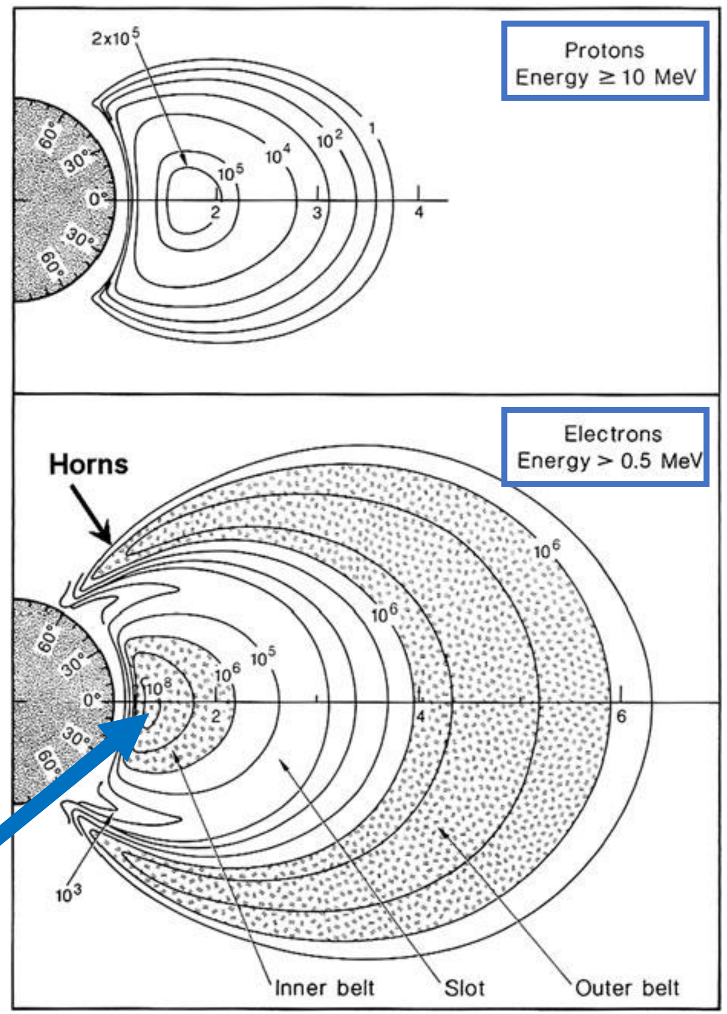

Mauk, B.H., Fox, N.J., Kanekal, S.G. et al. Space Sci Rev (2013) 179: 3.

https://satram.utef.cvut.cz/

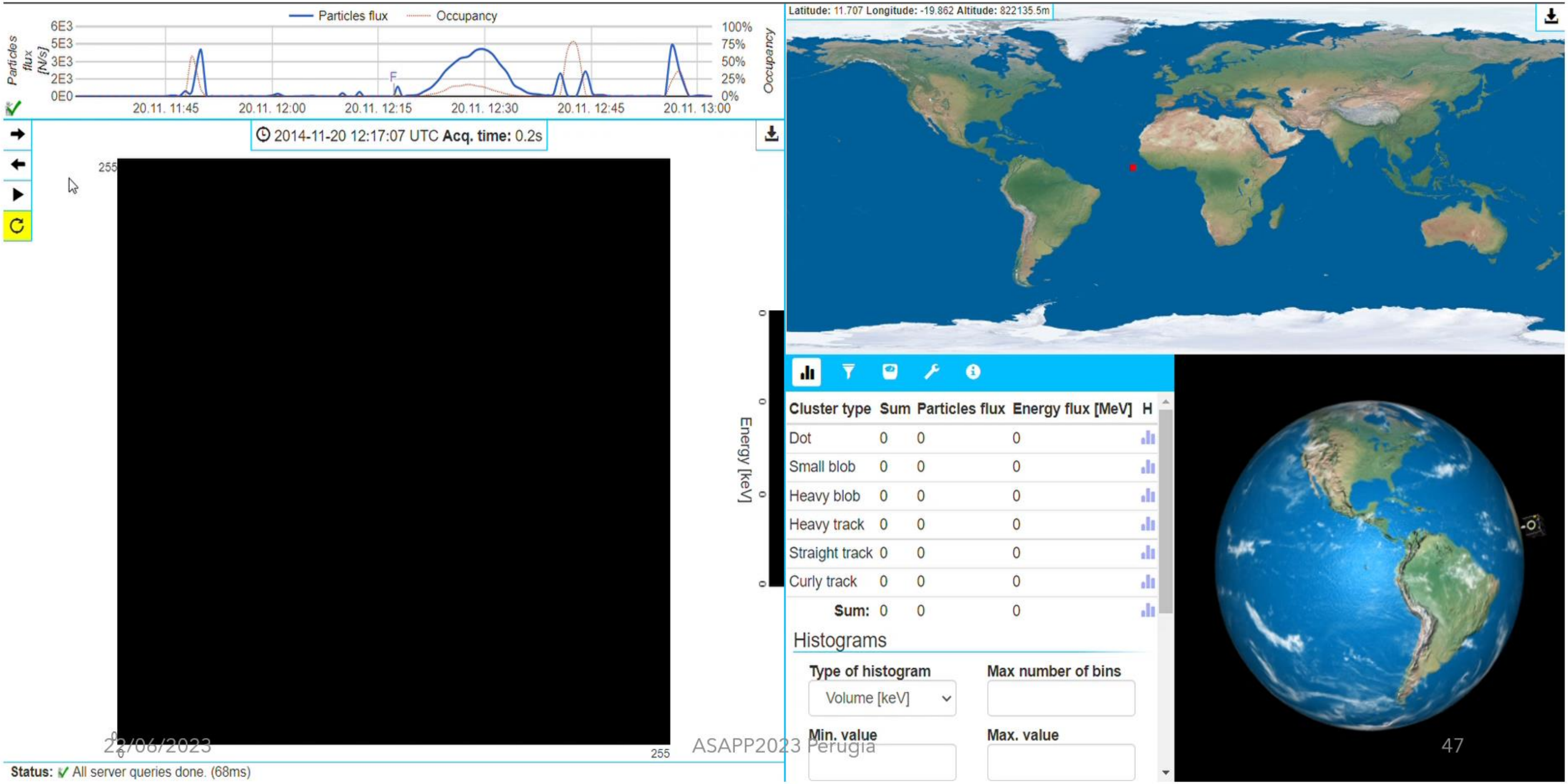

https://satram.utef.cvut.cz/

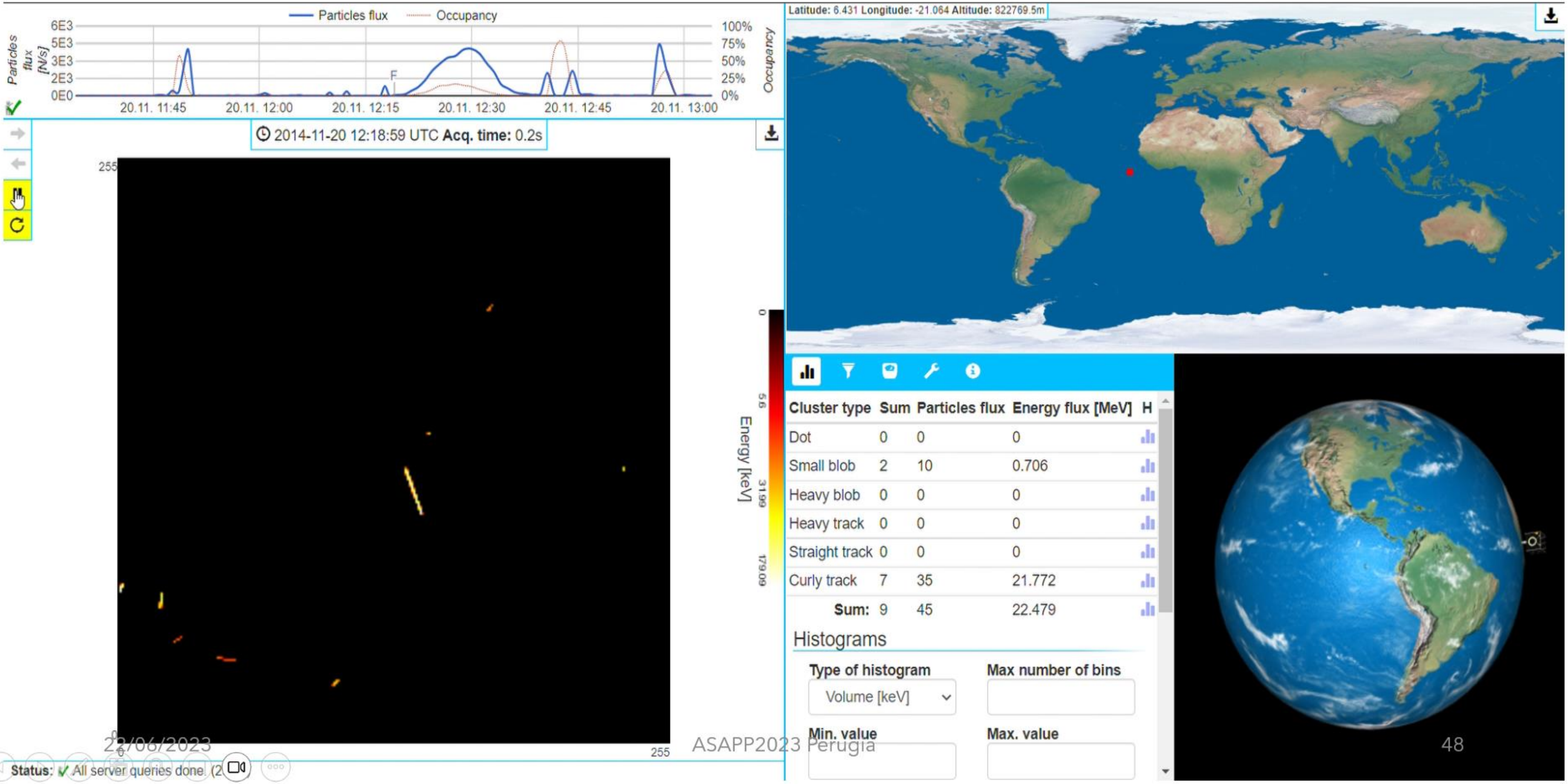

https://satram.utef.cvut.cz/

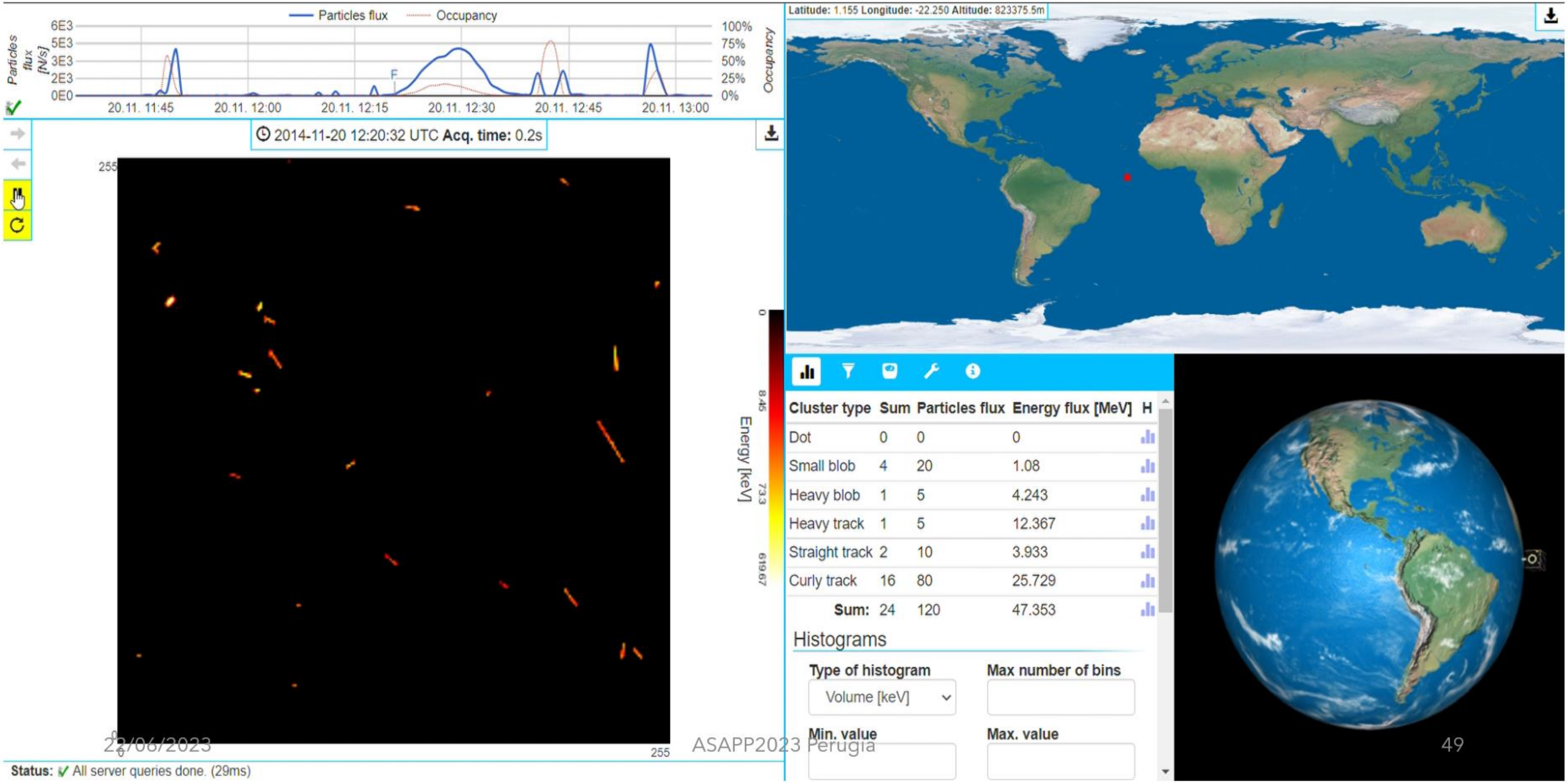

https://satram.utef.cvut.cz/

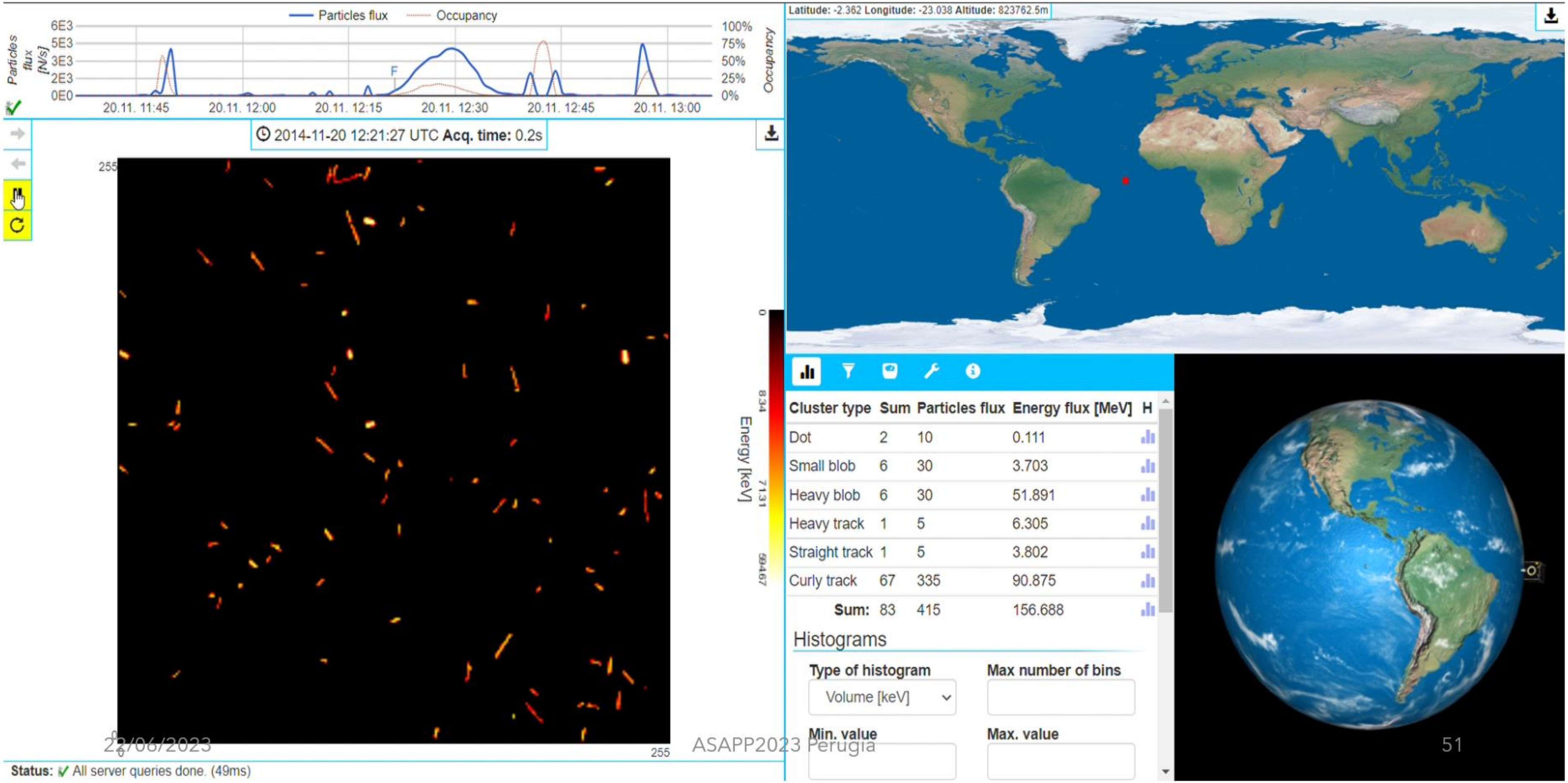

https://satram.utef.cvut.cz/

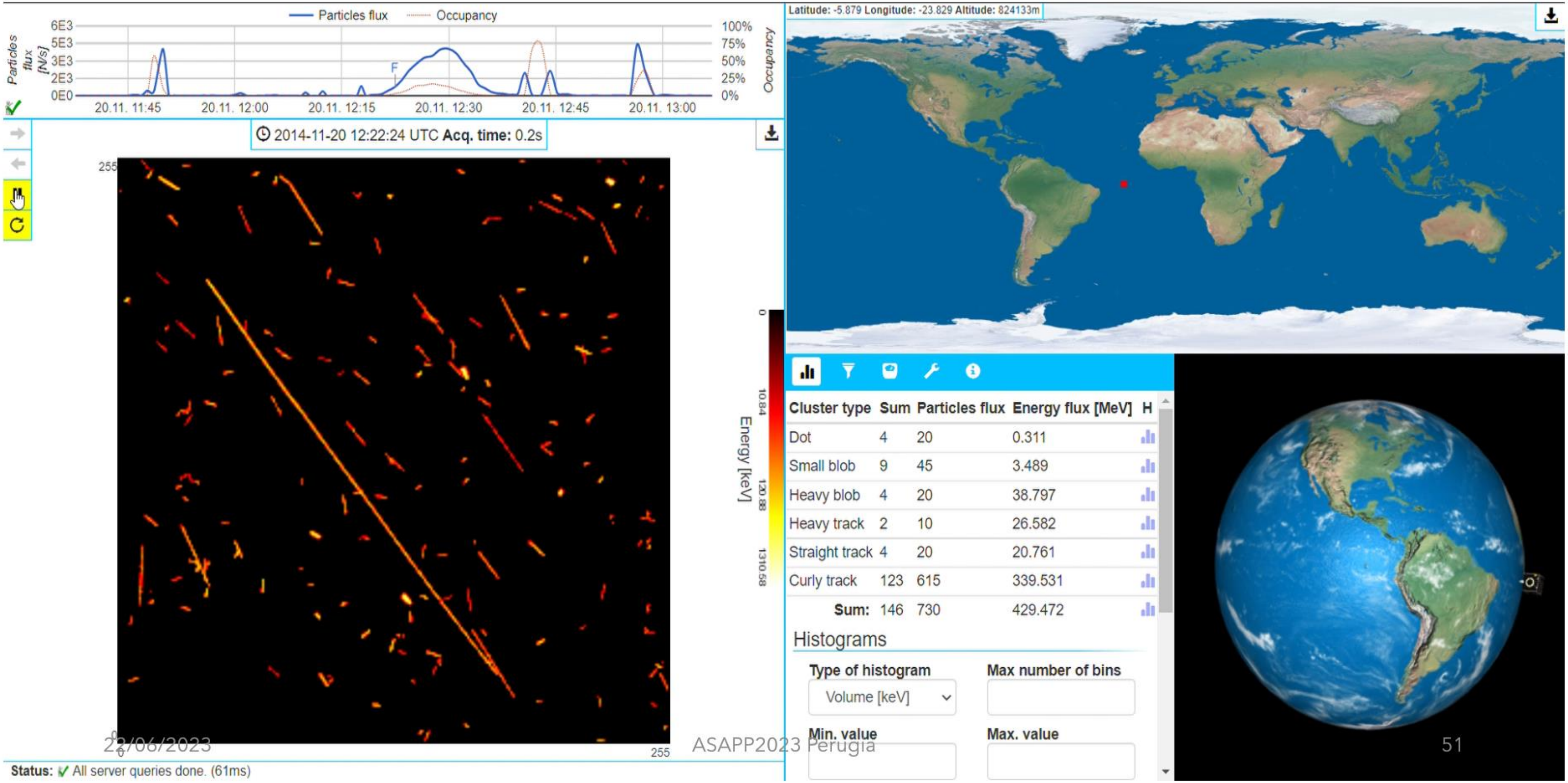

Cluster type	Sum	Particles flux	Energy flux [MeV]	H
Dot	4	20	0.311	
Small blob	9	45	3.489	
Heavy blob	4	20	38.797	
Heavy track	2	10	26.582	
Straight track	4	20	20.761	
Curly track	123	615	339.531	
Sum:	146	730	429.472	

https://satram.utef.cvut.cz/

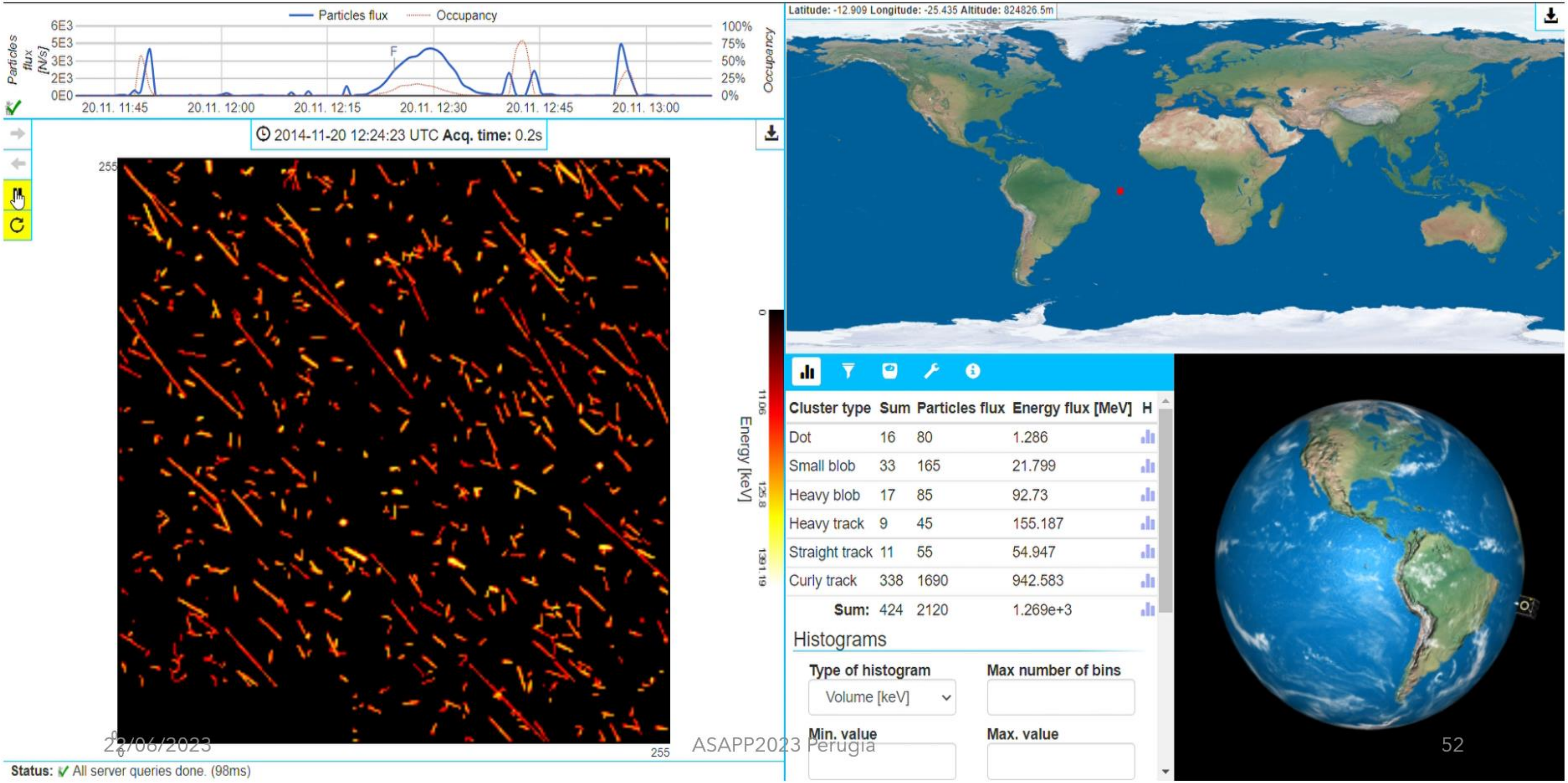

https://satram.utef.cvut.cz/

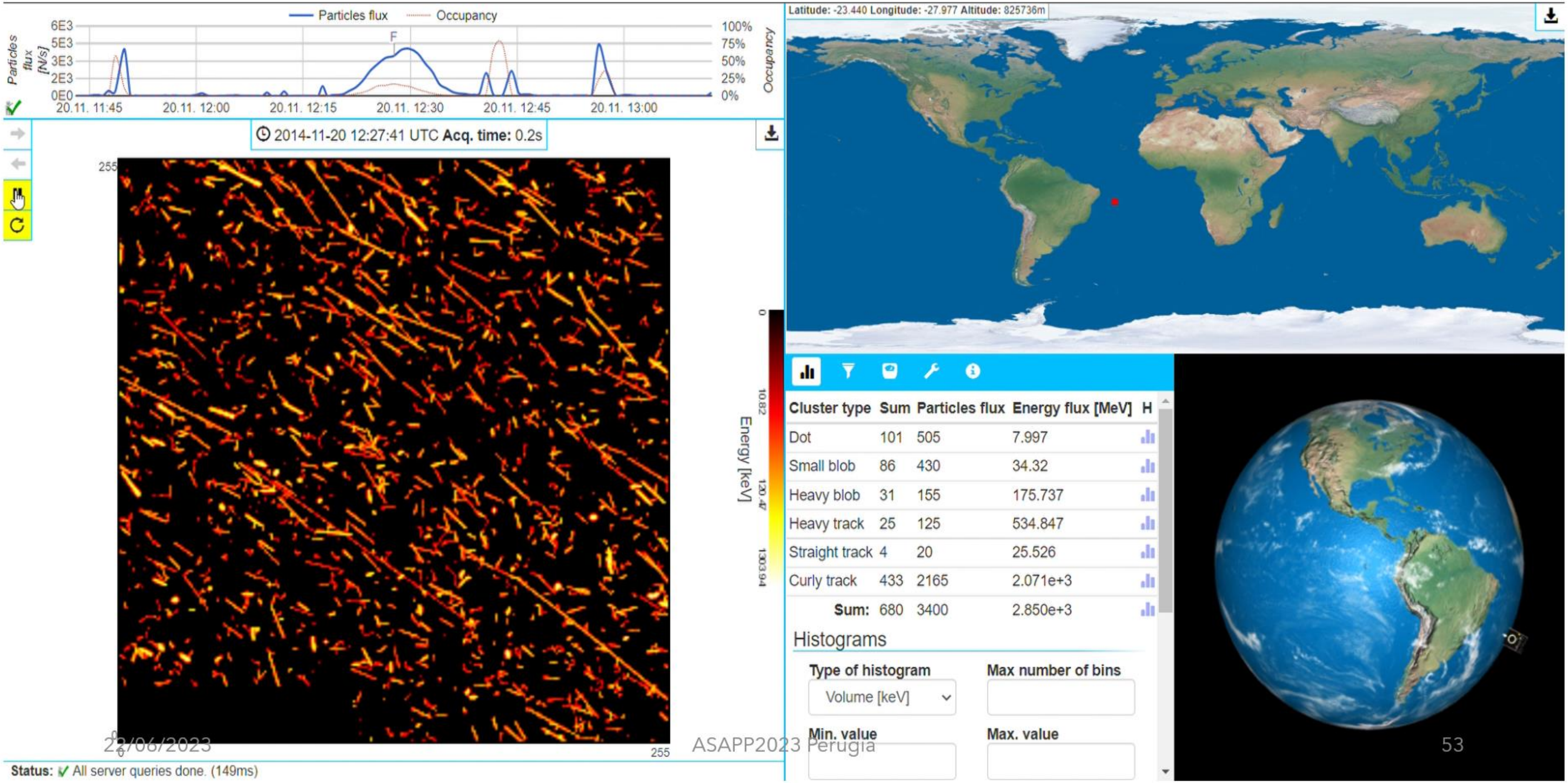

https://satram.utef.cvut.cz/

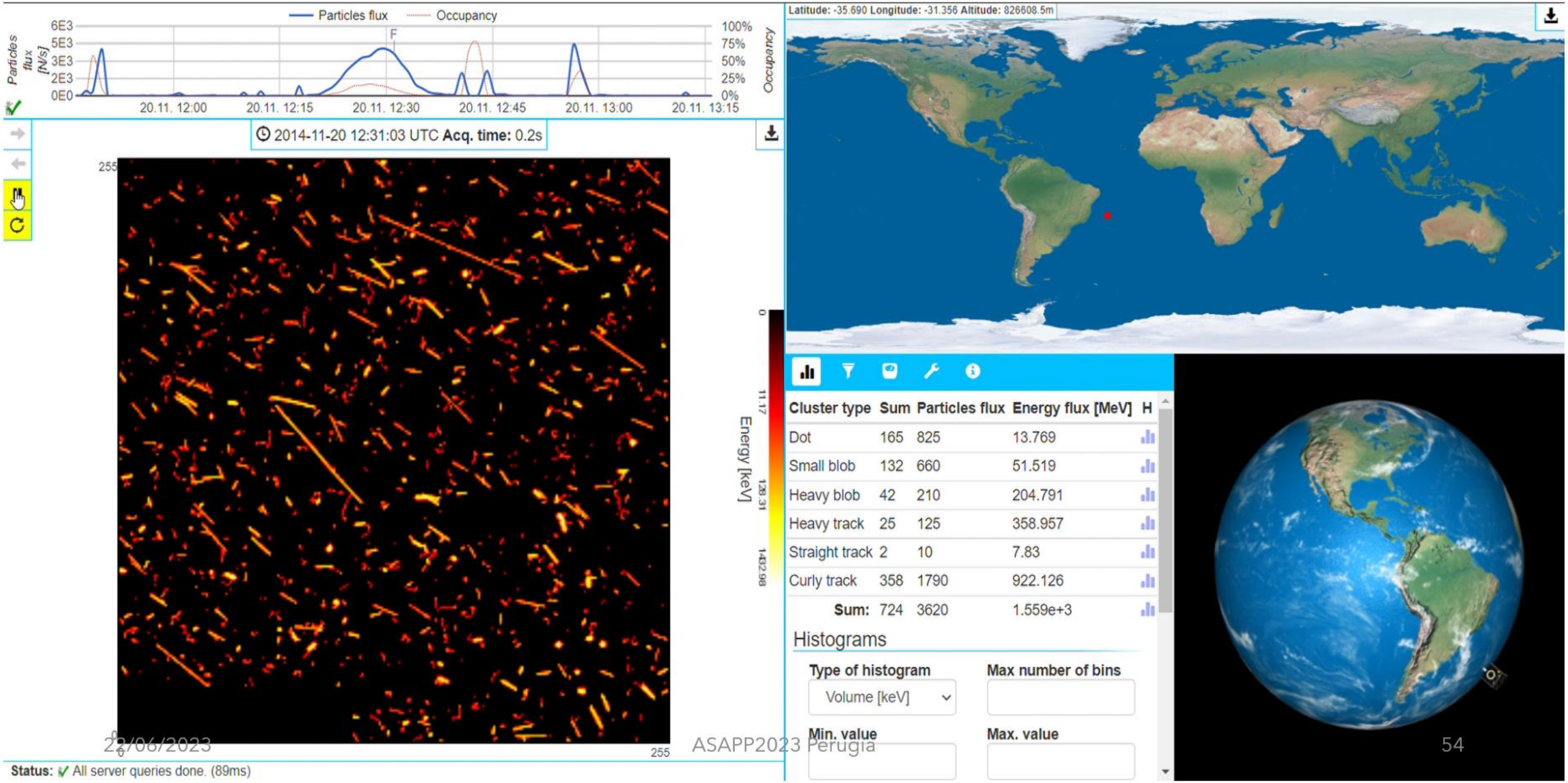

https://satram.utef.cvut.cz/

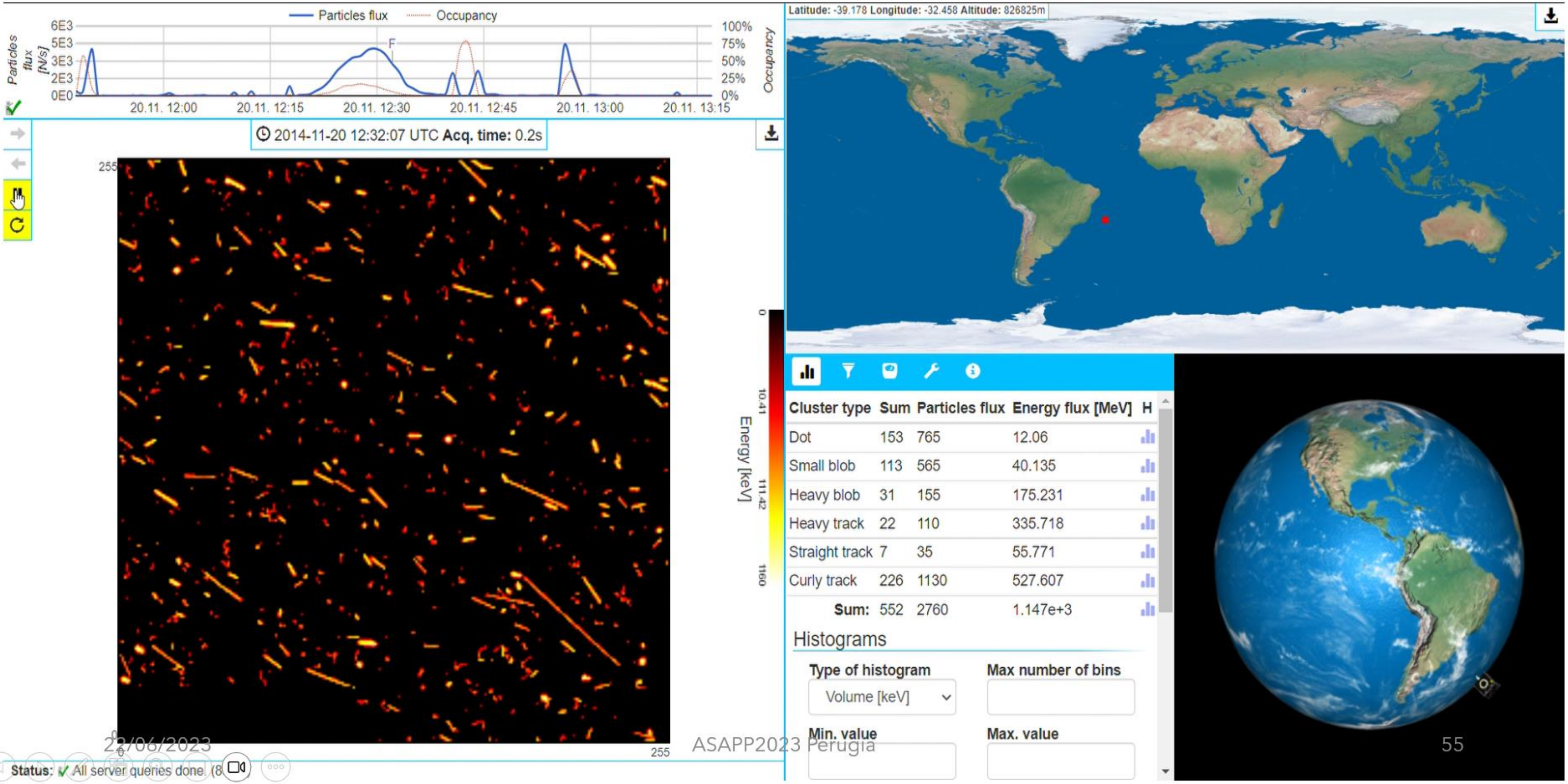

https://satram.utef.cvut.cz/

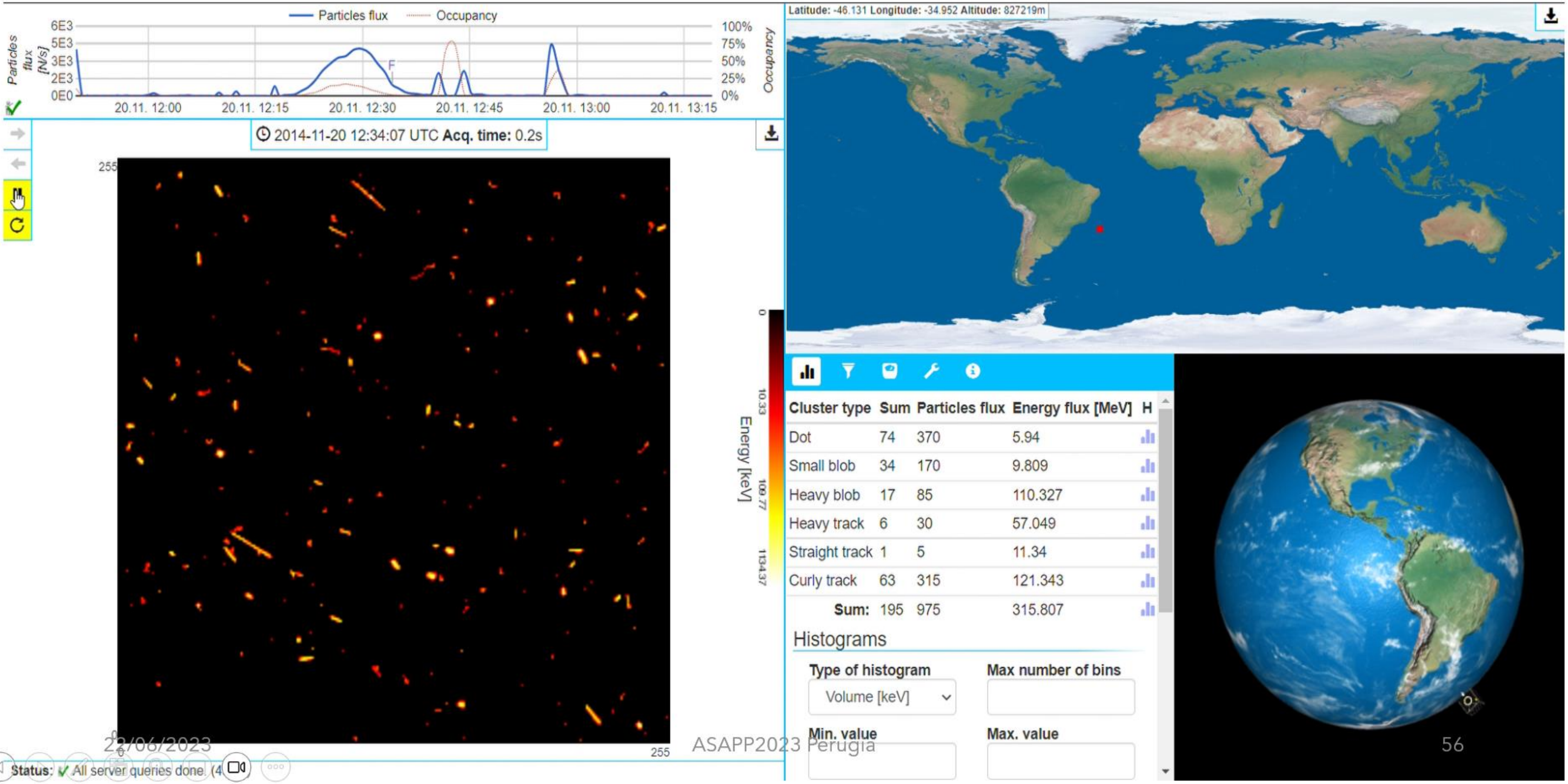

https://satram.utef.cvut.cz/

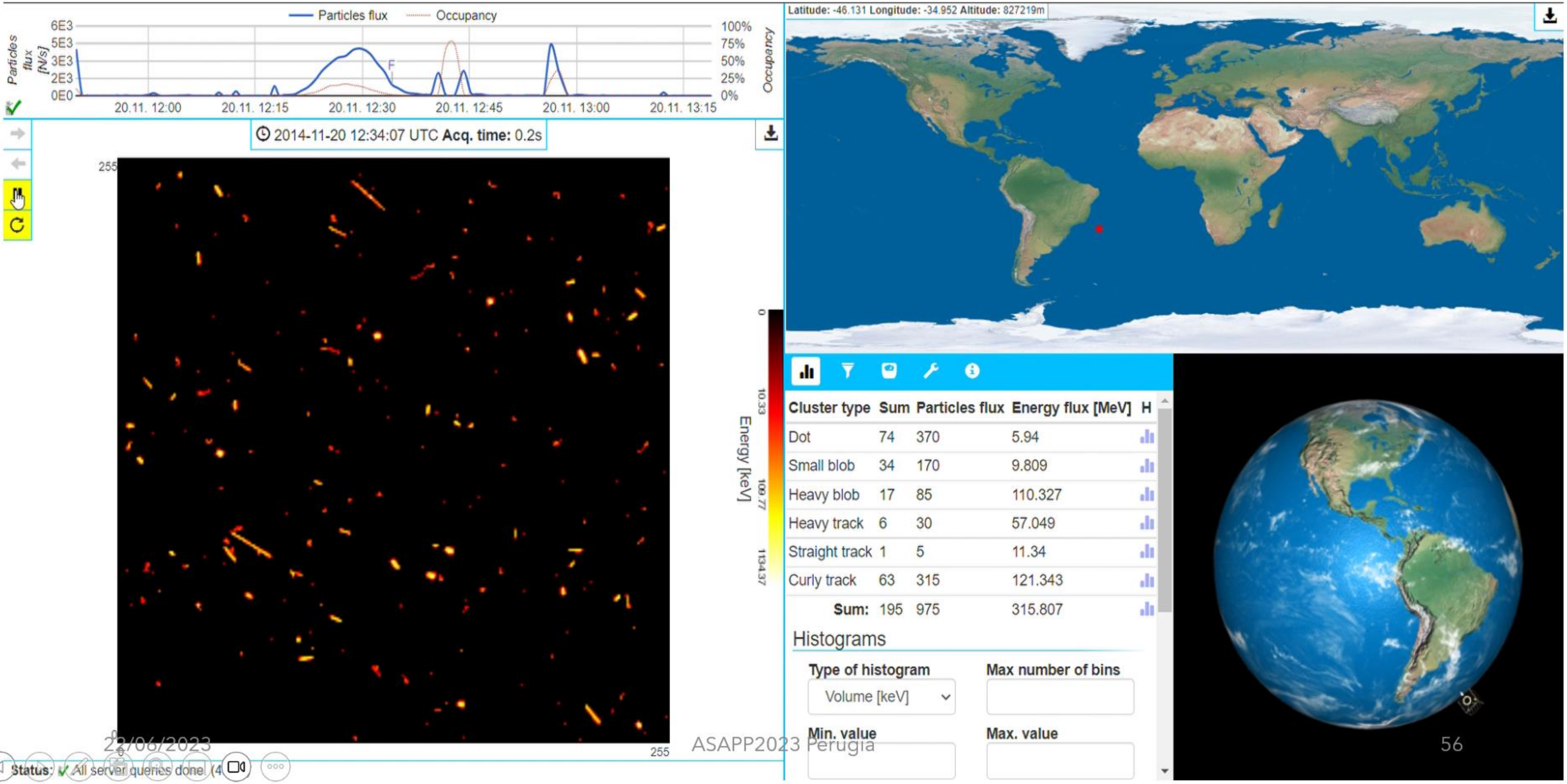

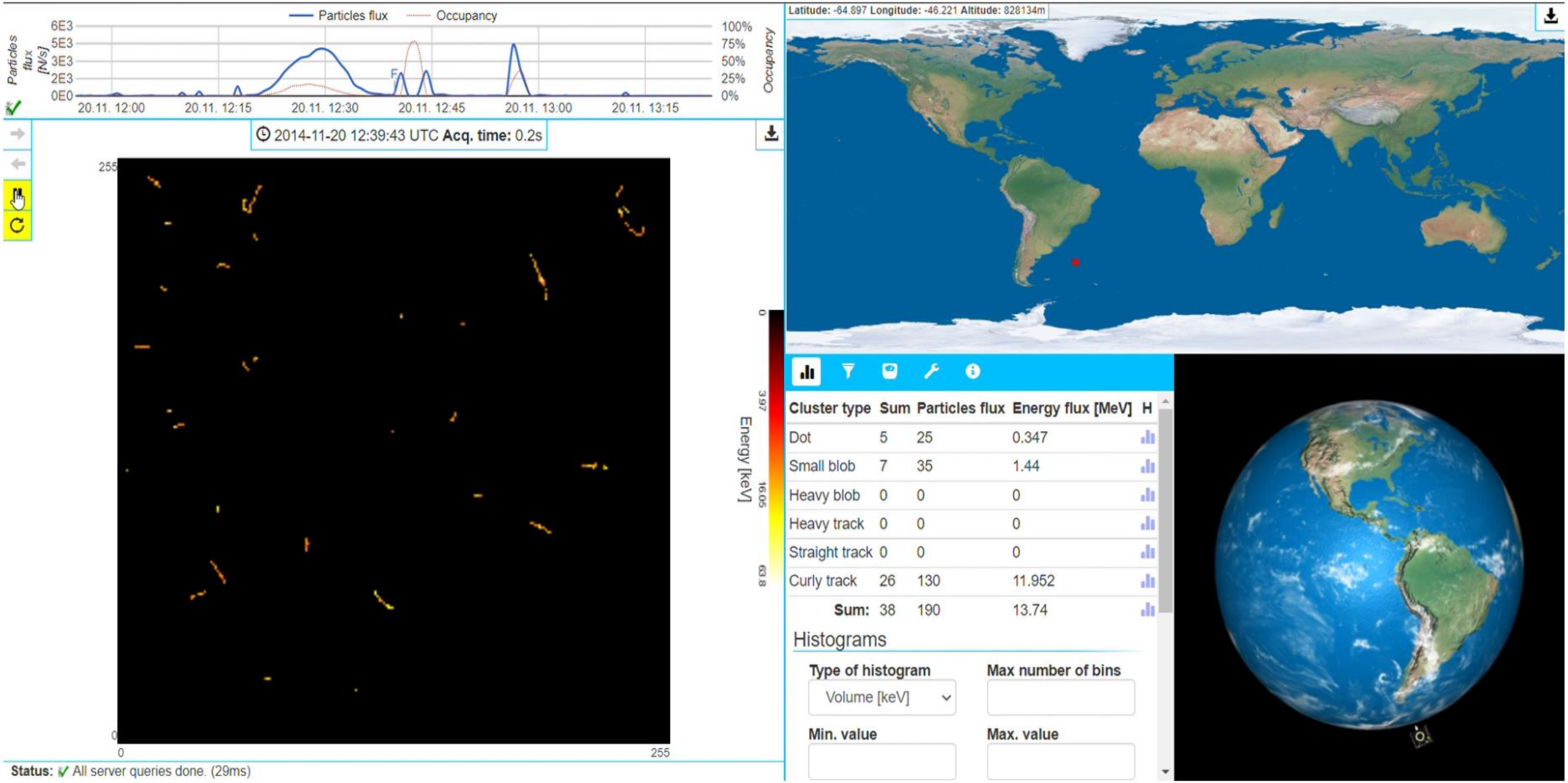

Cluster type	Sum	Particles flux	Energy flux [MeV]	H
Dot	5	25	0.347	
Small blob	7	35	1.44	
Heavy blob	0	0	0	
Heavy track	0	0	0	
Straight track	0	0	0	
Curly track	26	130	11.952	
Sum:	38	190	13.74	

Particle Classification – Bayesian Deconvolution

This method works by decomposing the stopping power "signal" of the field into its contributing particle signals, from which the particle's distributions can be inferred

Response Matrix

$$n(E) = R\,\phi(C)$$

Measured dE/dx Spectrum

Particle Spectrum

$$R^T =$$

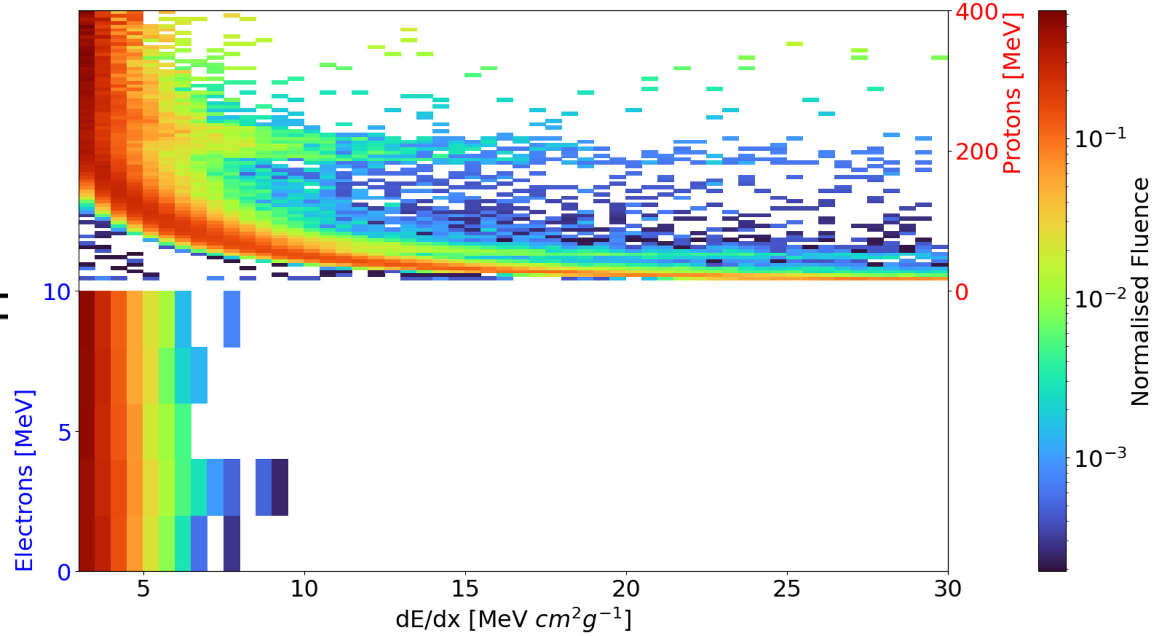

G. D'Agostini. Improved iterative Bayesian unfolding. 2010.
https://doi.org/10.48550/arXiv.1010.0632

dE/dX and Particle Classification

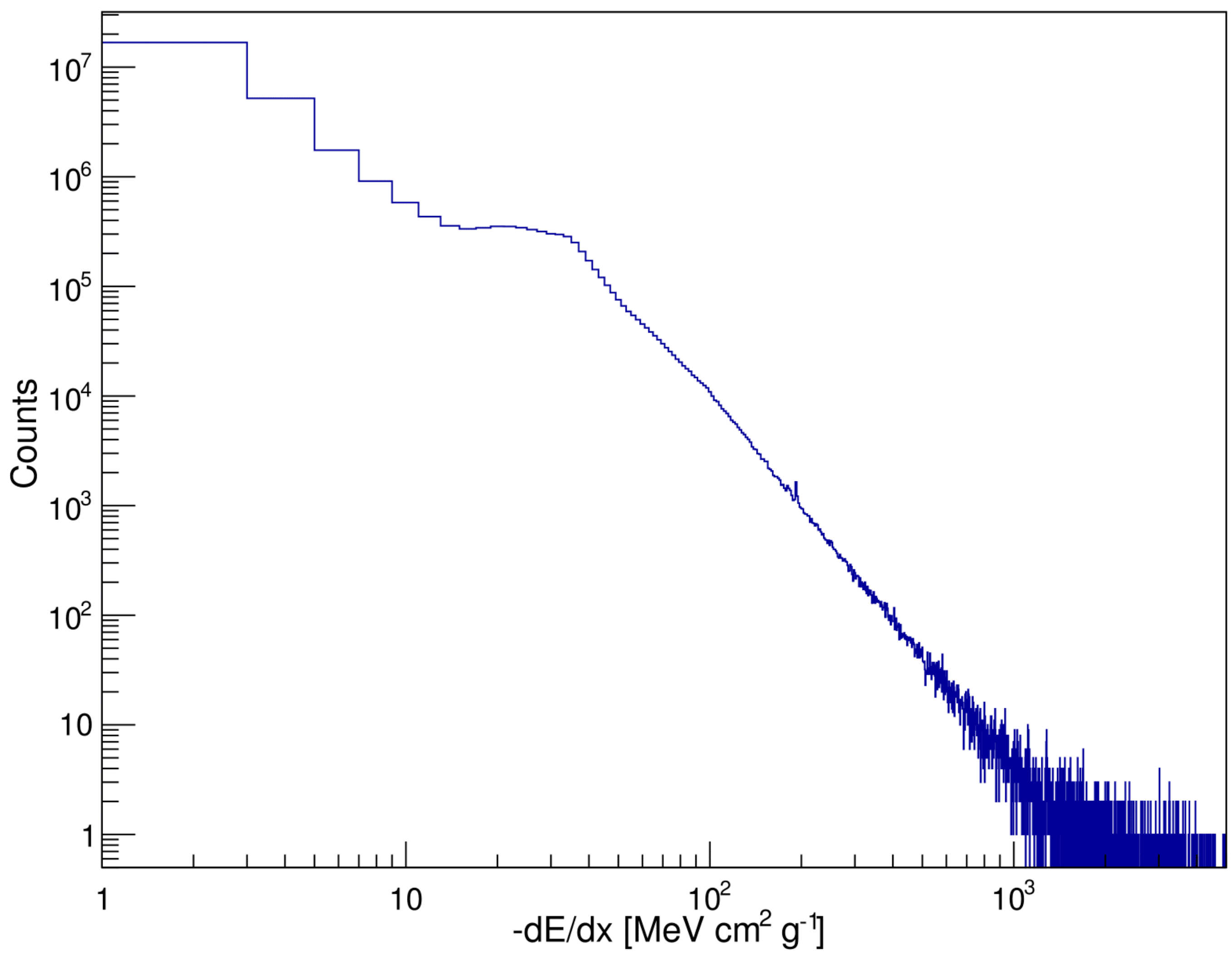

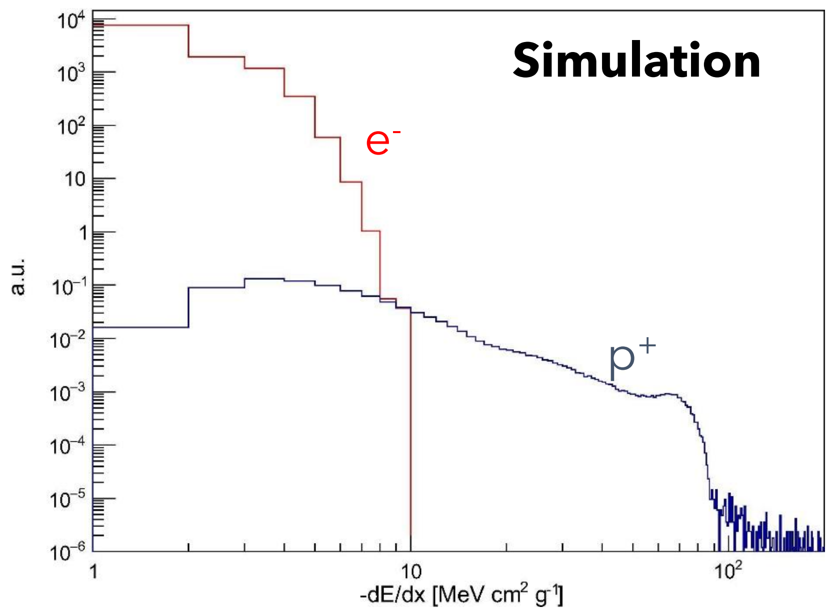

*St. Gohl et al., "Study of the radiation fields in LEO with the Space Application of Timepix Radiation Monitor (SATRAM)", Advances in Space Research **63**, Issue 5, pp. 1646-1660, (2019).*

dE/dX and Particle Classification

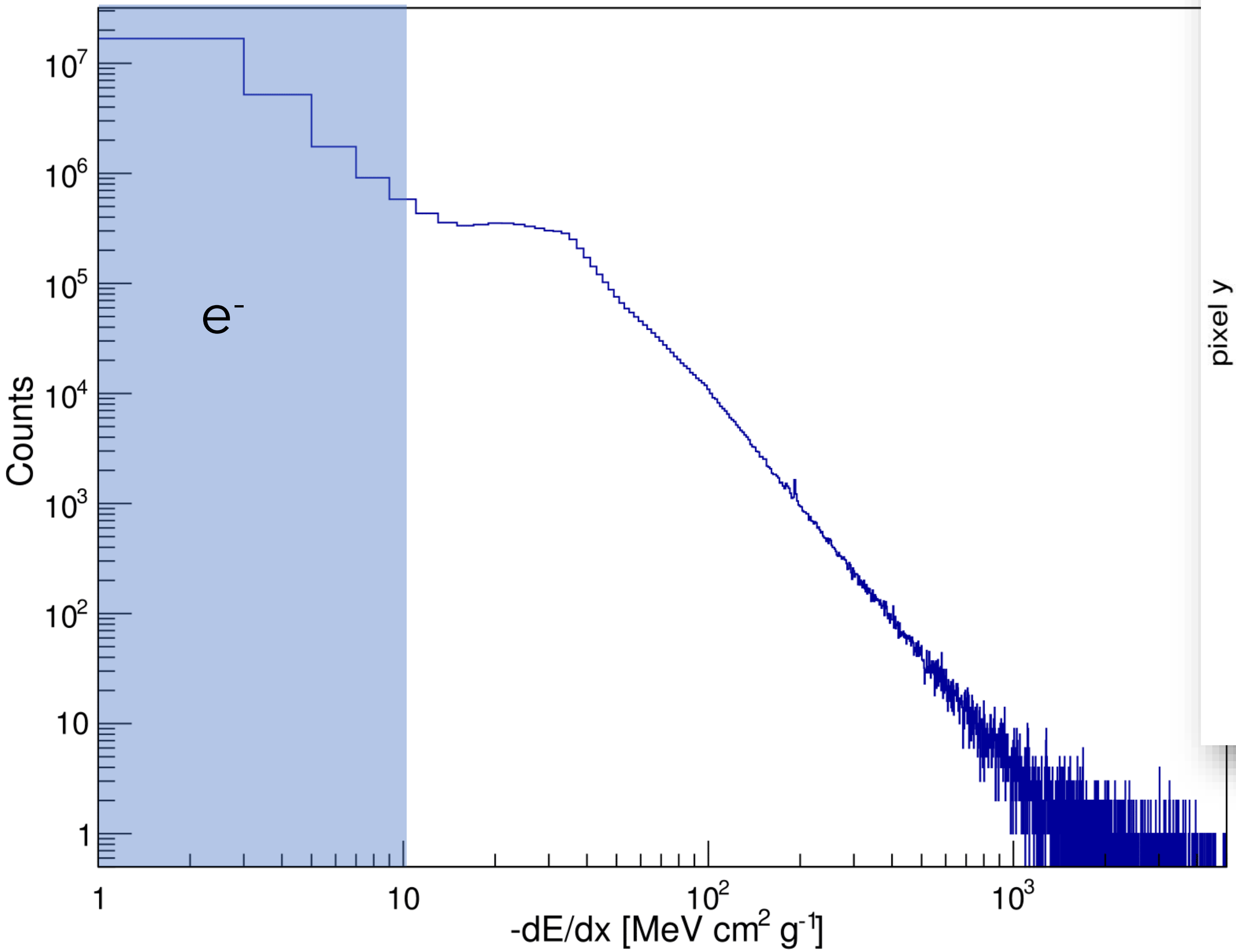

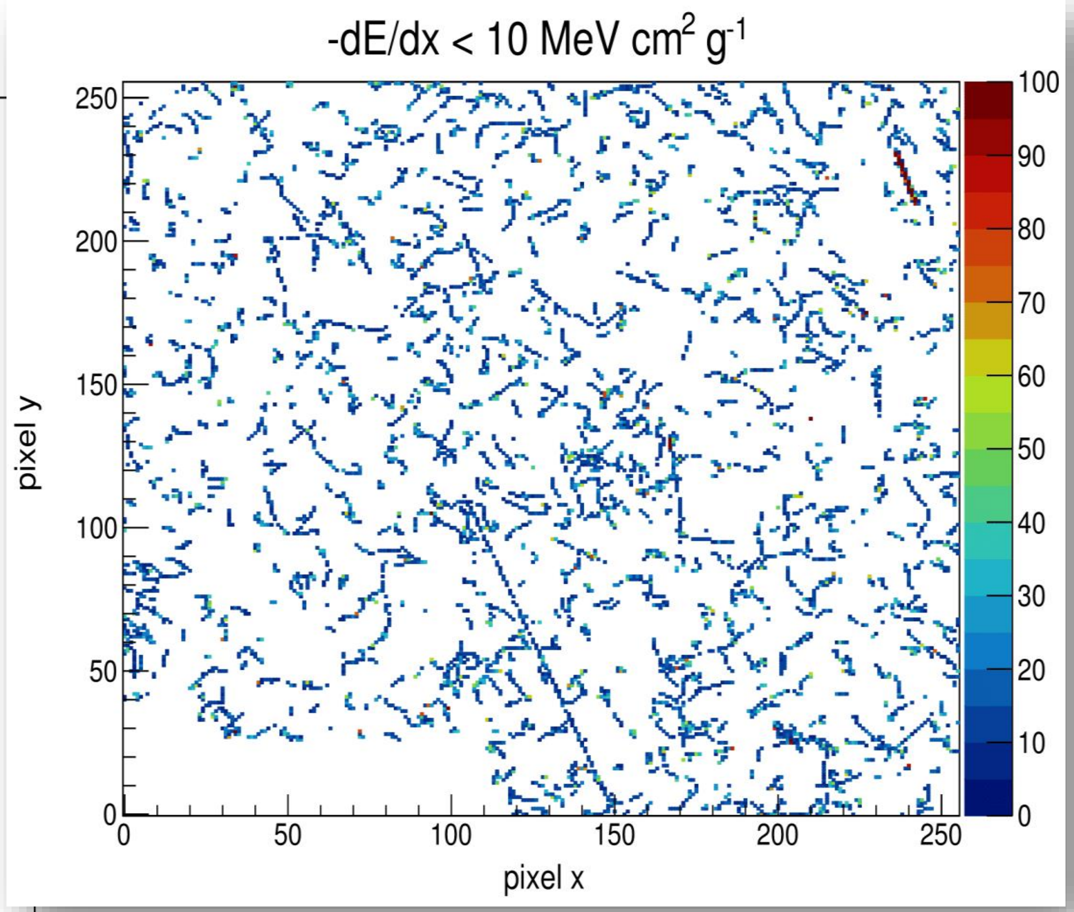

*St. Gohl et al., "Study of the radiation fields in LEO with the Space Application of Timepix Radiation Monitor (SATRAM)", Advances in Space Research **63**, Issue 5, pp. 1646-1660, (2019).*

dE/dX and Particle Classification

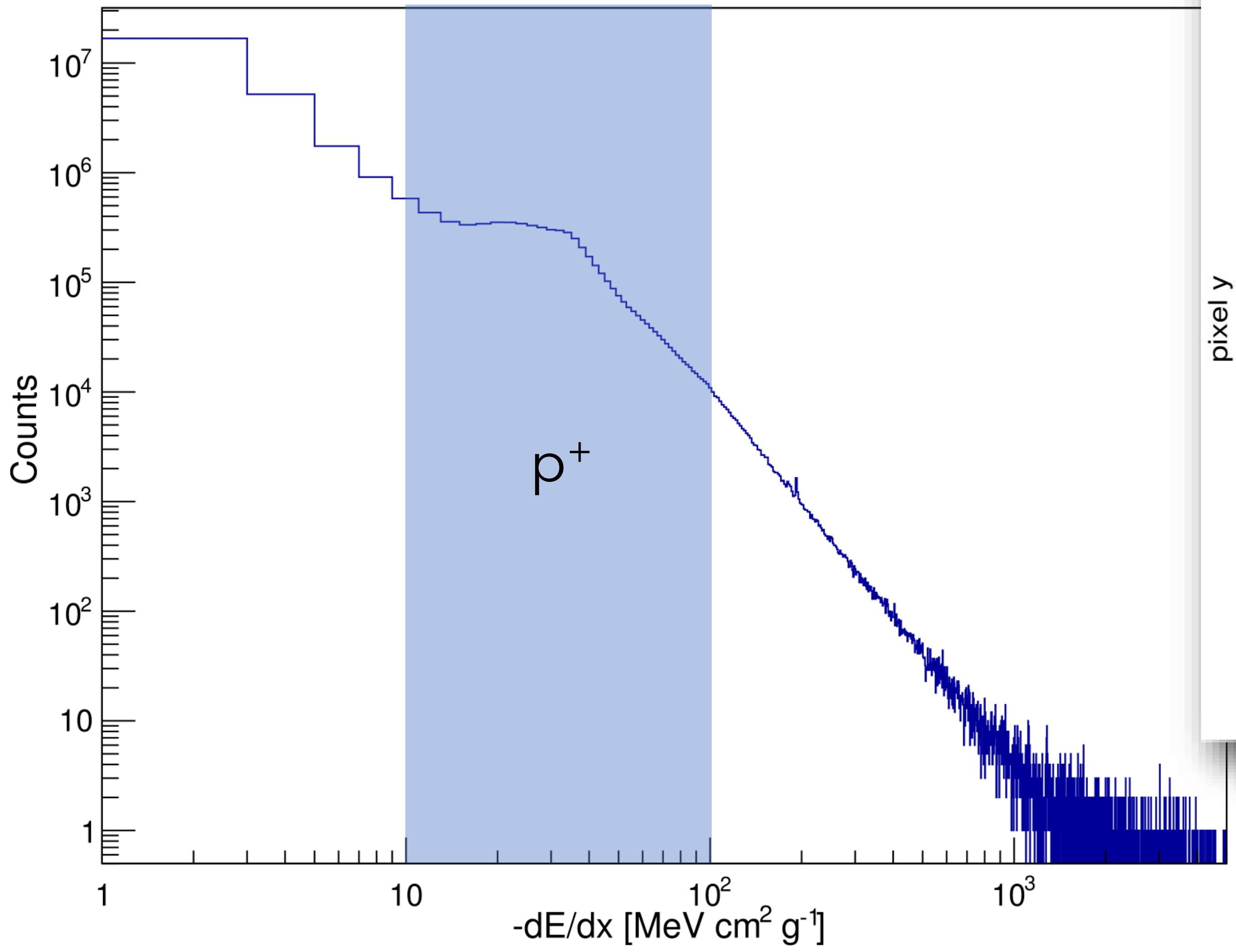

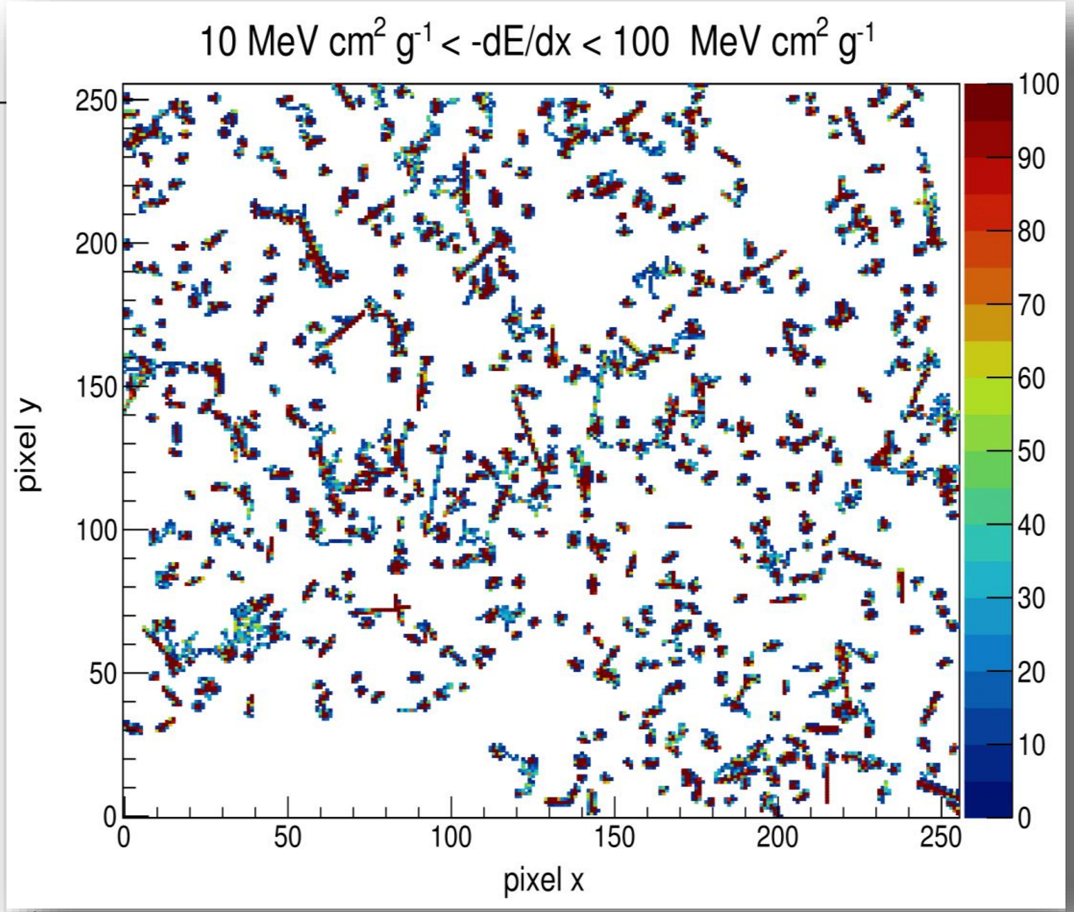

St. Gohl et al., "Study of the radiation fields in LEO with the Space Application of Timepix Radiation Monitor (SATRAM)", Advances in Space Research ***63****, Issue 5, pp. 1646-1660, (2019).*

dE/dX and Particle Classification

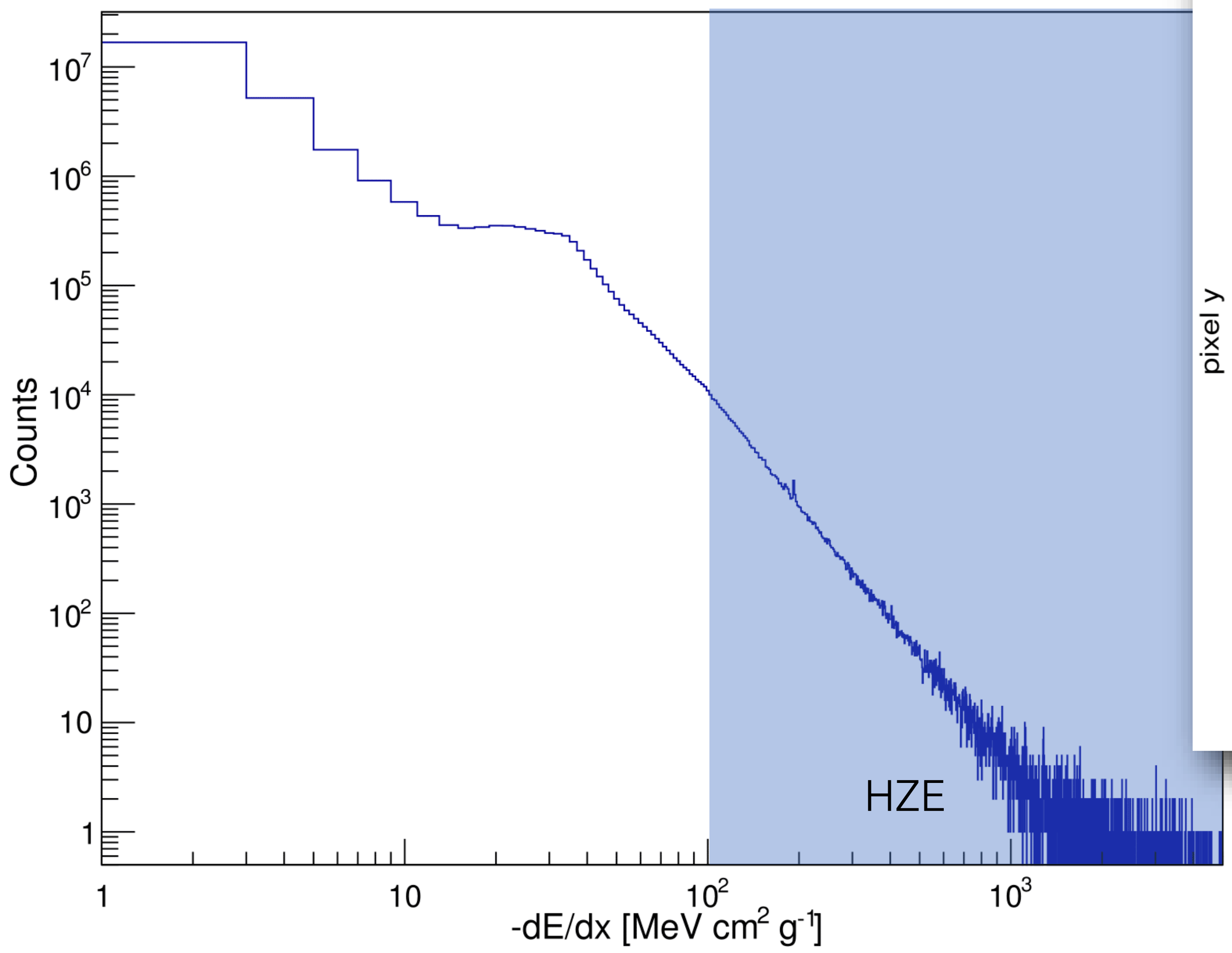

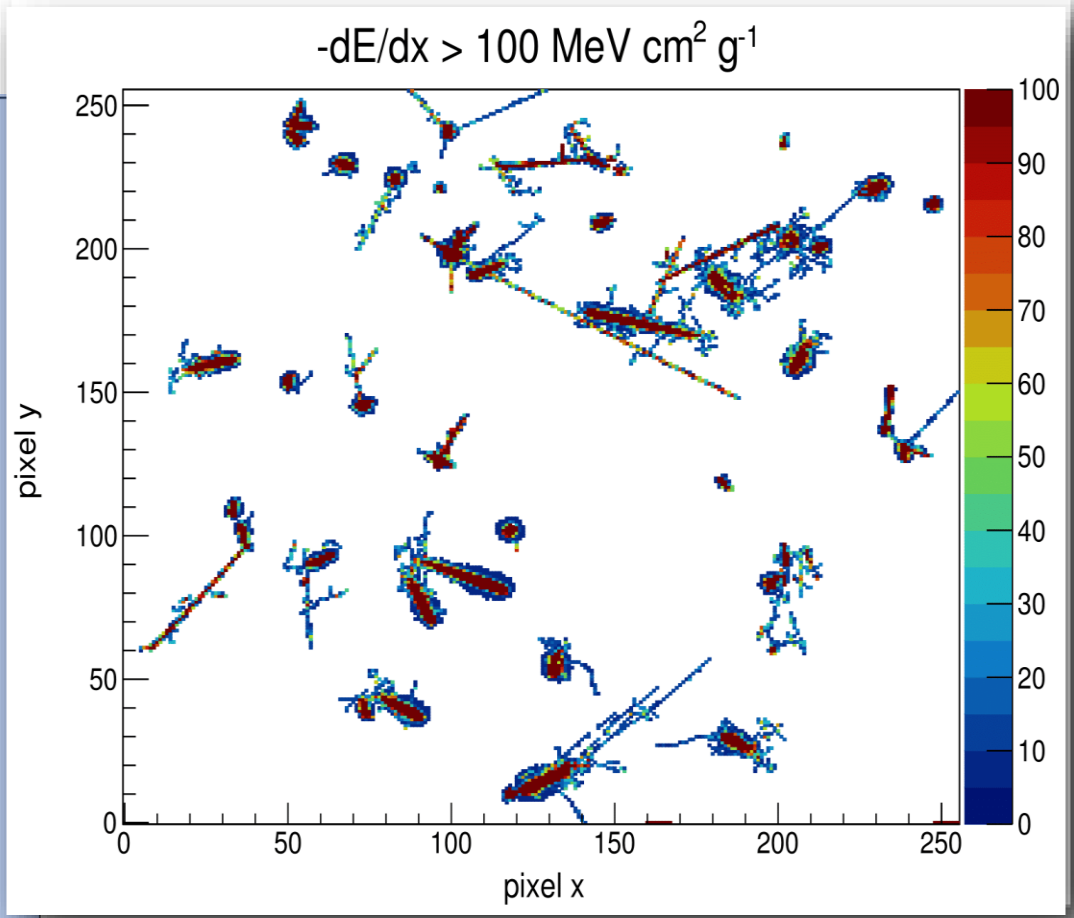

St. Gohl et al., "Study of the radiation fields in LEO with the Space Application of Timepix Radiation Monitor (SATRAM)", Advances in Space Research ***63****, Issue 5, pp. 1646-1660, (2019).*

Electron and Proton Flux Maps

e^- fluxes 3 orders of magnitude larger than p^+ fluxes

➪ Even small e^- misclassification distorts p^+ flux measurement

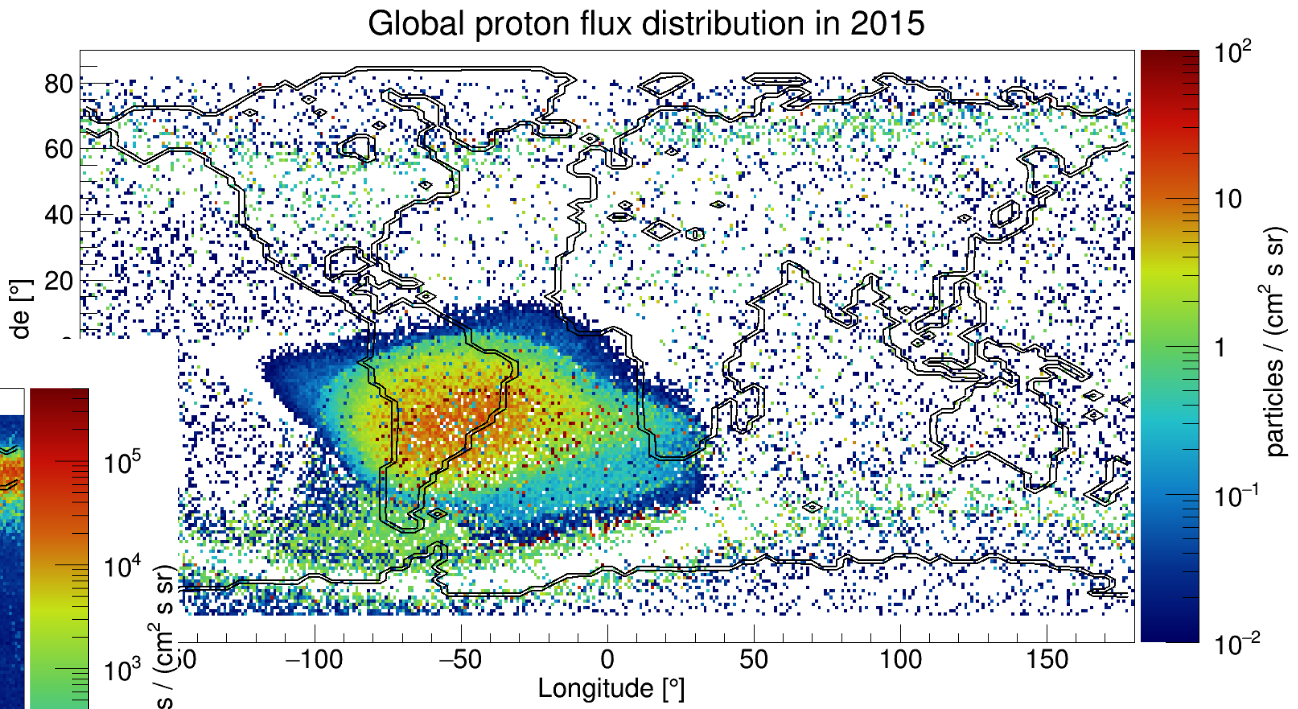

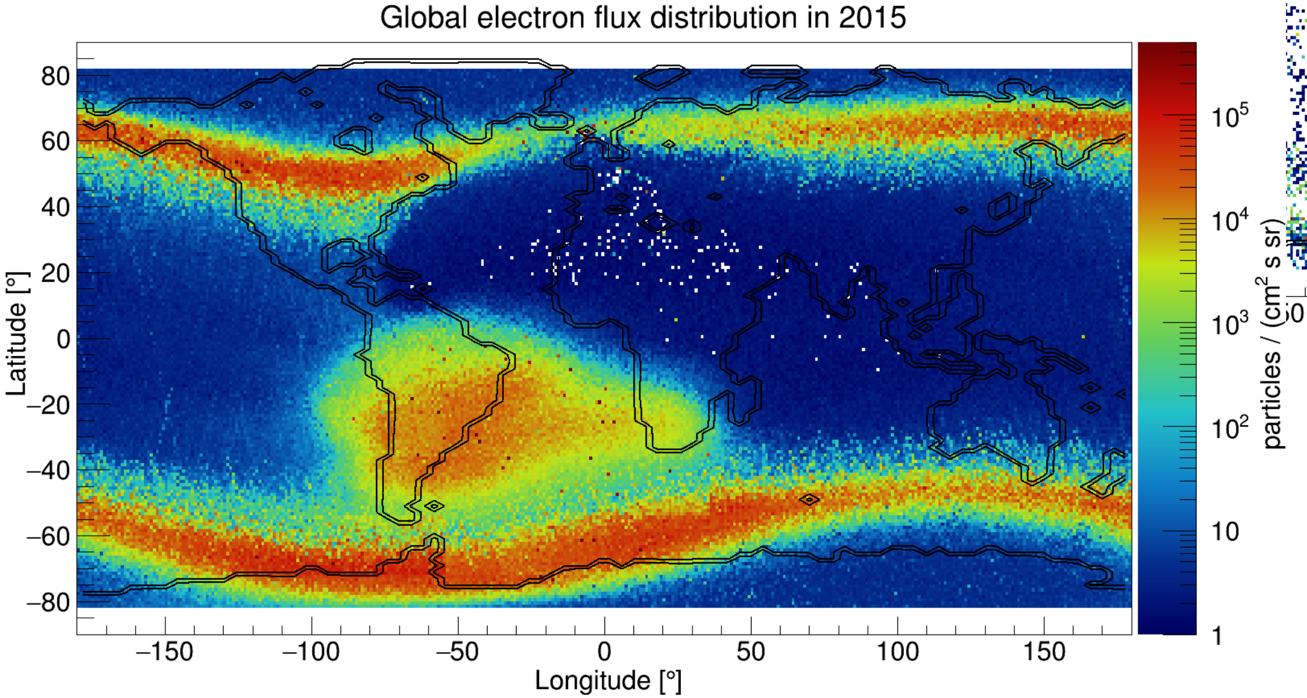

St. Gohl et al., "Study of the radiation fields in LEO with the Space Application of Timepix Radiation Monitor (SATRAM)", Advances in Space Research ***63****, Issue 5, pp. 1646-1660 (2019).*

First Measurement of the Trapped Proton Energy Spectrum with a Single-Layer Detector

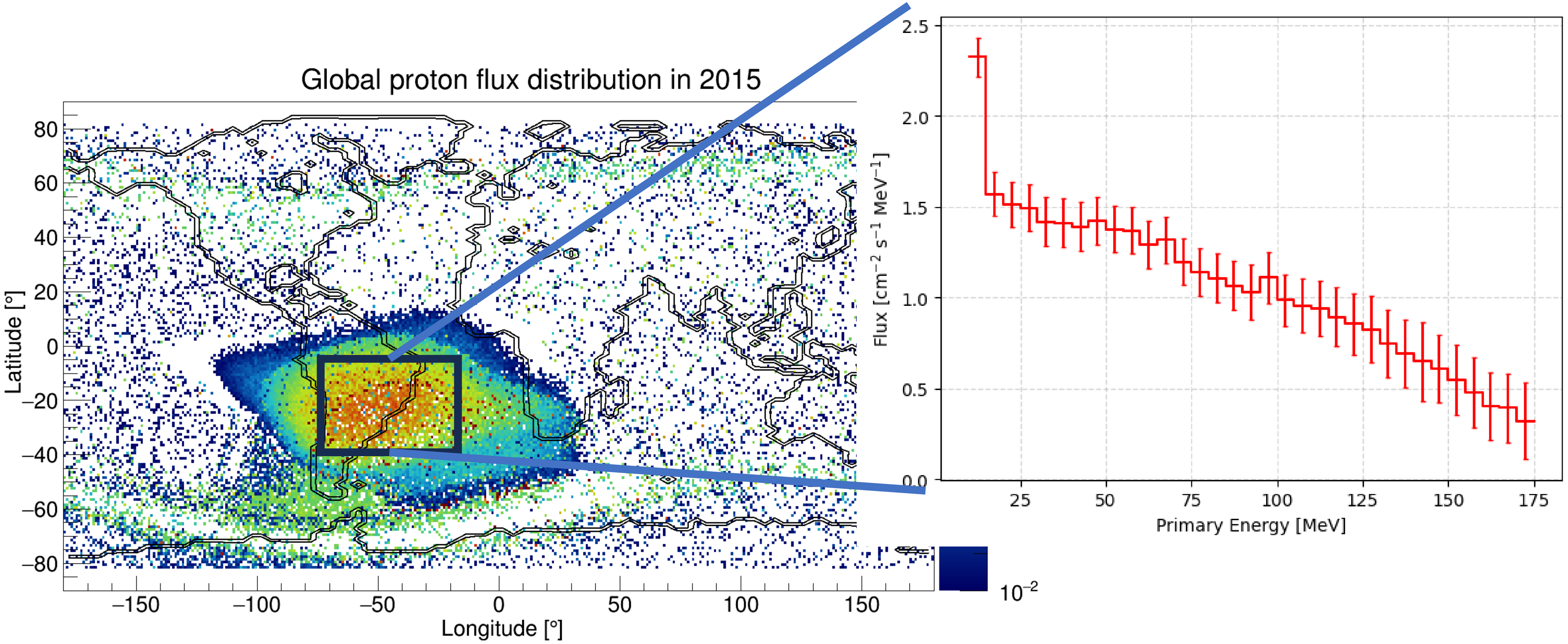

Stopping Power Classification at MoEDAL

A Closer look at Stopping Power

Region 1:

- ⇨Electrons
- ⇨Gammas
- ⇨Singly charged relativistic particles

Region 2:

- ⇨Protons <250 MeV
- ⇨Pions <15 MeV
- ⇨Muons <10 MeV

Regions 3:

- ⇨Fragmentations
- ⇨ Z>1 particles

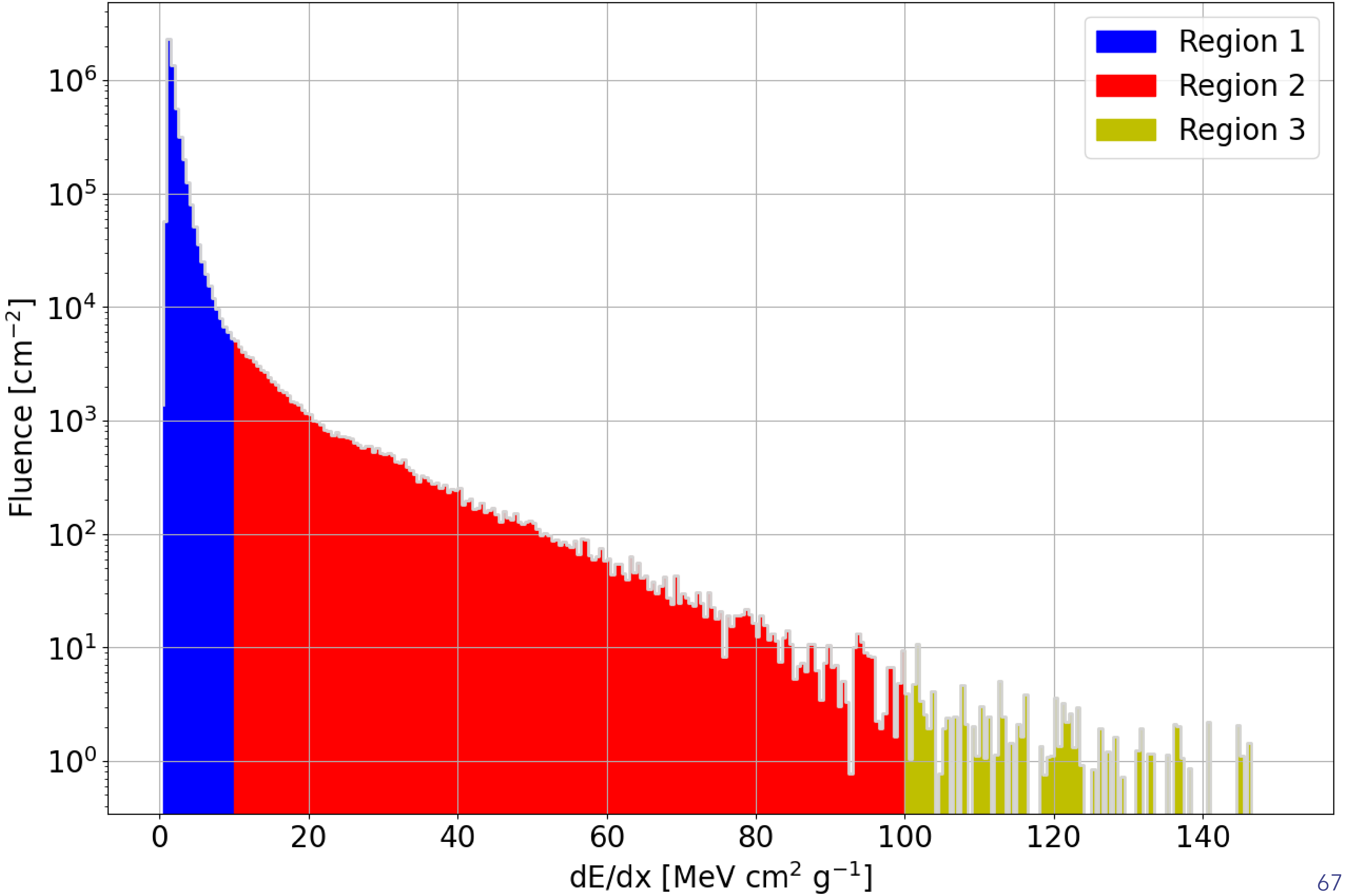

A Closer look at Stopping Power

Region 1:

- Electrons
- Gammas
- Singly charged relativistic particles

Region 2:

- Protons <250 MeV
- Pions <15 MeV
- Muons <10 MeV

Regions 3:

- Fragmentations
- Z>1 particles

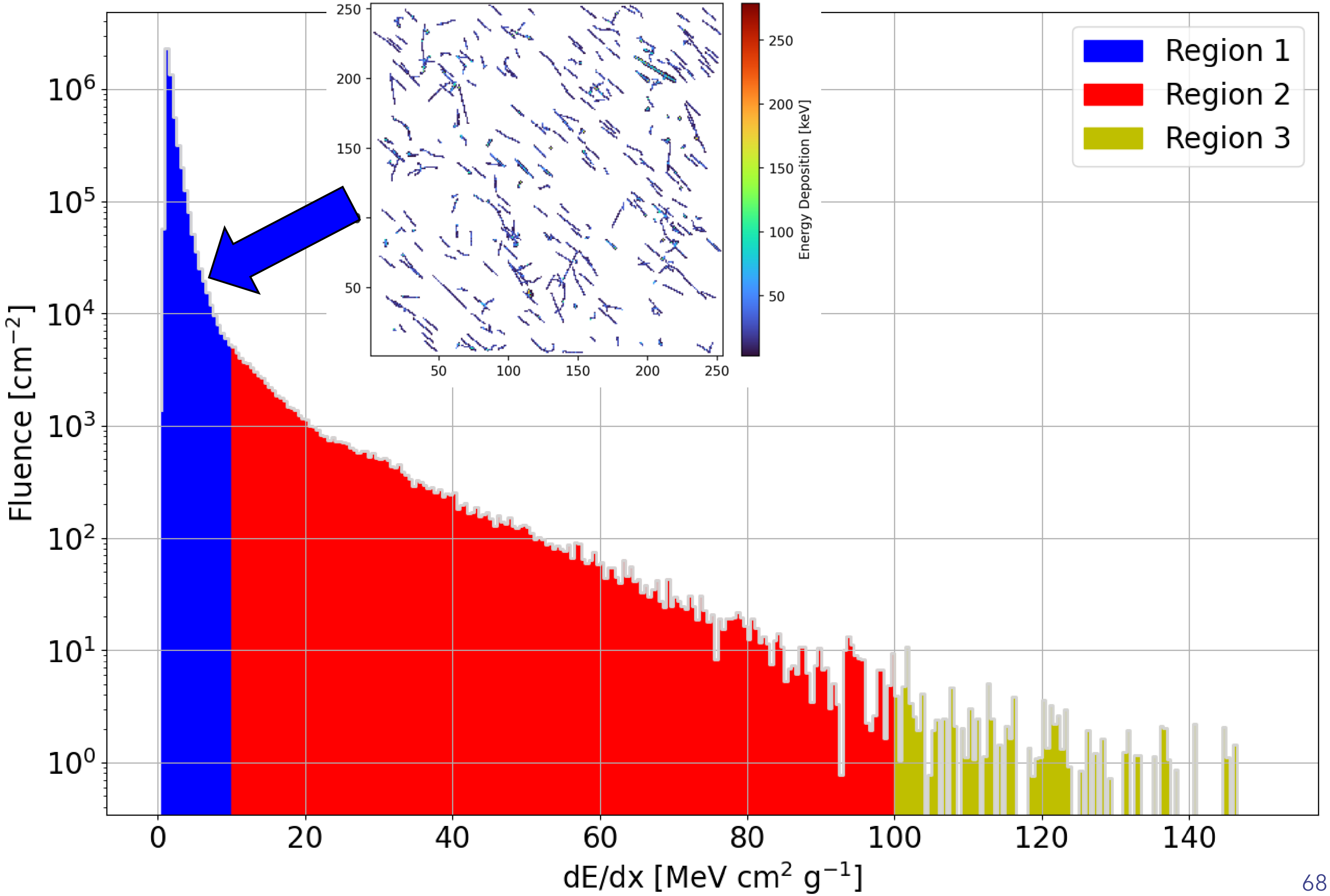

A Closer look at Stopping Power

Region 1:
- ⇨Electrons
- ⇨Gammas
- ⇨Singly charged relativistic particles

Region 2:
- ⇨Protons <250 MeV
- ⇨Pions <15 MeV
- ⇨Muons <10 MeV

Regions 3:
- ⇨Fragmentations
- ⇨ Z>1 particles

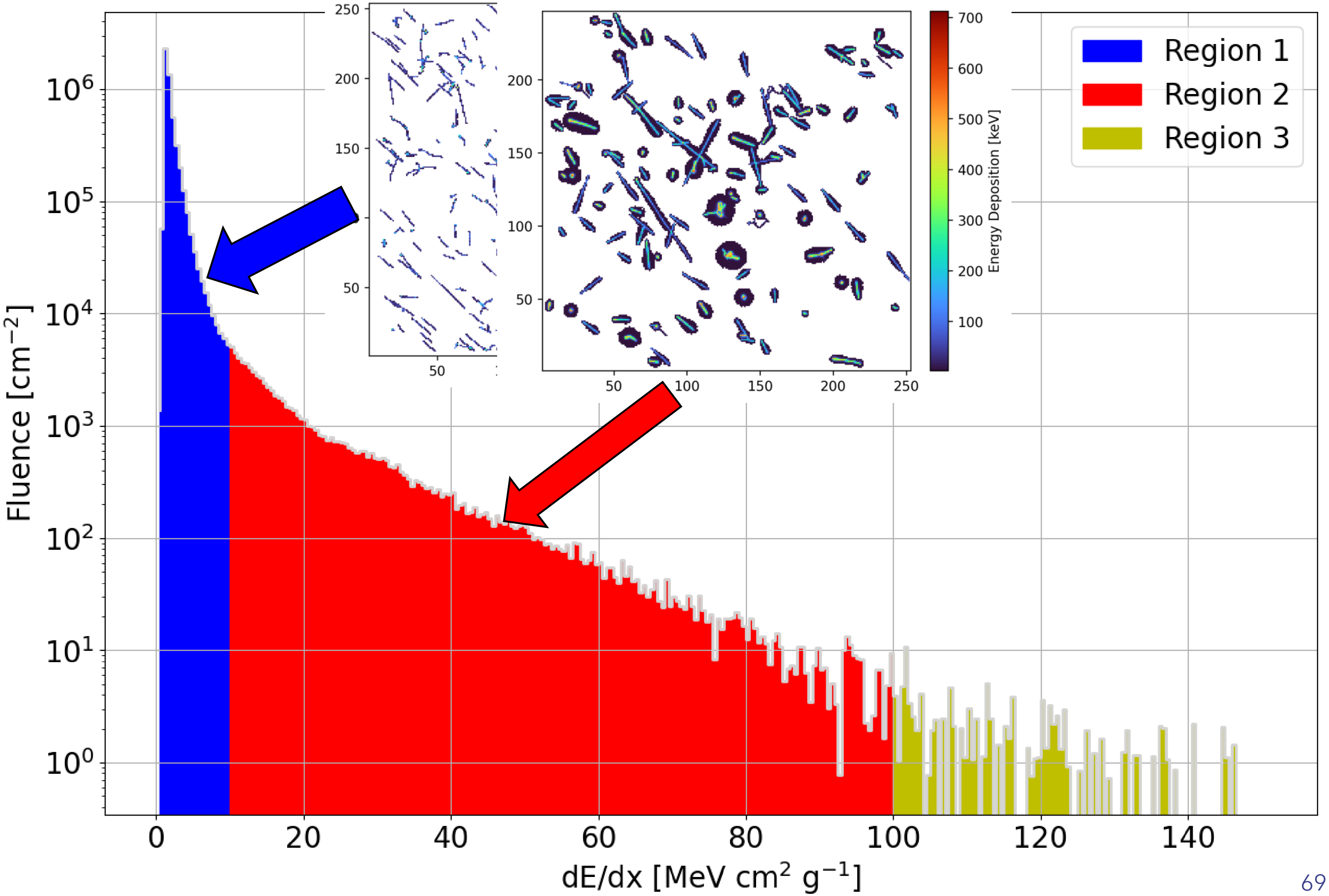

A Closer look at Stopping Power

Region 1:
- ⇨Electrons
- ⇨Gammas
- ⇨Singly charged relativistic particles

Region 2:
- ⇨Protons <250 MeV
- ⇨Pions <15 MeV
- ⇨Muons <10 MeV

Regions 3:
- ⇨Fragmentations
- ⇨ Z>1 particles

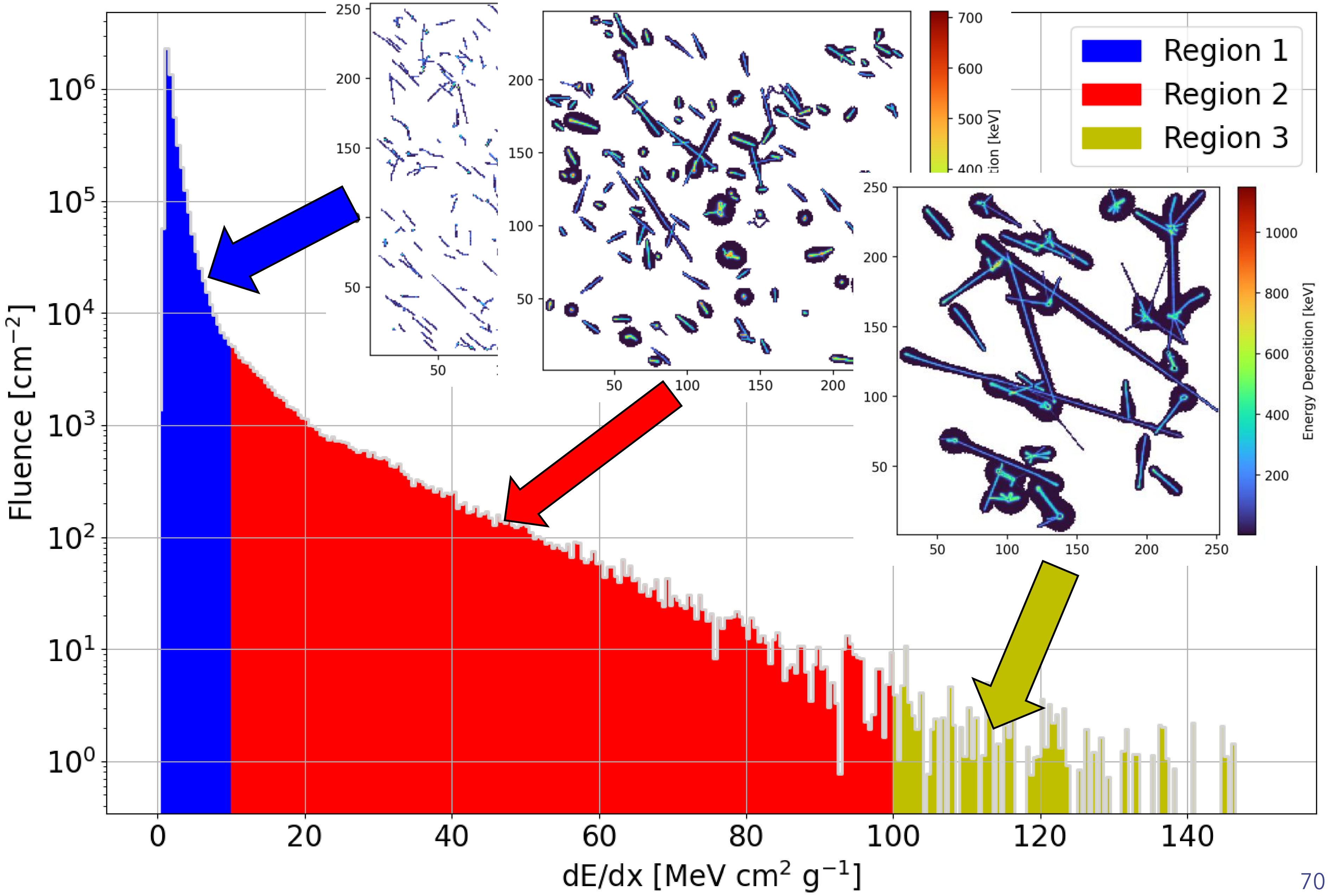

Conclusions

- 3D tracking
  - ➡The capabilities of reconstructing particle trajectories from IP8 in real time and with single layer Timepix3 detectors have been demonstrated
- Stopping power and radiation field decomposition
  - ➡The current are state-of-the-art algorithms in particle classification were shown and validated in the environment found in low earth orbit
  - ➡Future work will be to improve particle classification by using advanced machine learning algorithms

Can we use Timepix3 in Search for the Avatars of New Physics?

$$\left\langle -\frac{dE}{dx} \right\rangle = Kz^2 \frac{Z}{A} \frac{1}{\beta^2} \left[\frac{1}{2} \ln \frac{2m_e c^2 \beta^2 \gamma^2 W_{max}}{I^2} - \beta^2 - \frac{\delta(\beta\gamma)}{2} \right]$$

Highly charged energetic particles are known to produce distinct cluster pattern within Timepix3

Associated with:

- High Stopping Power
- Large number of delta rays

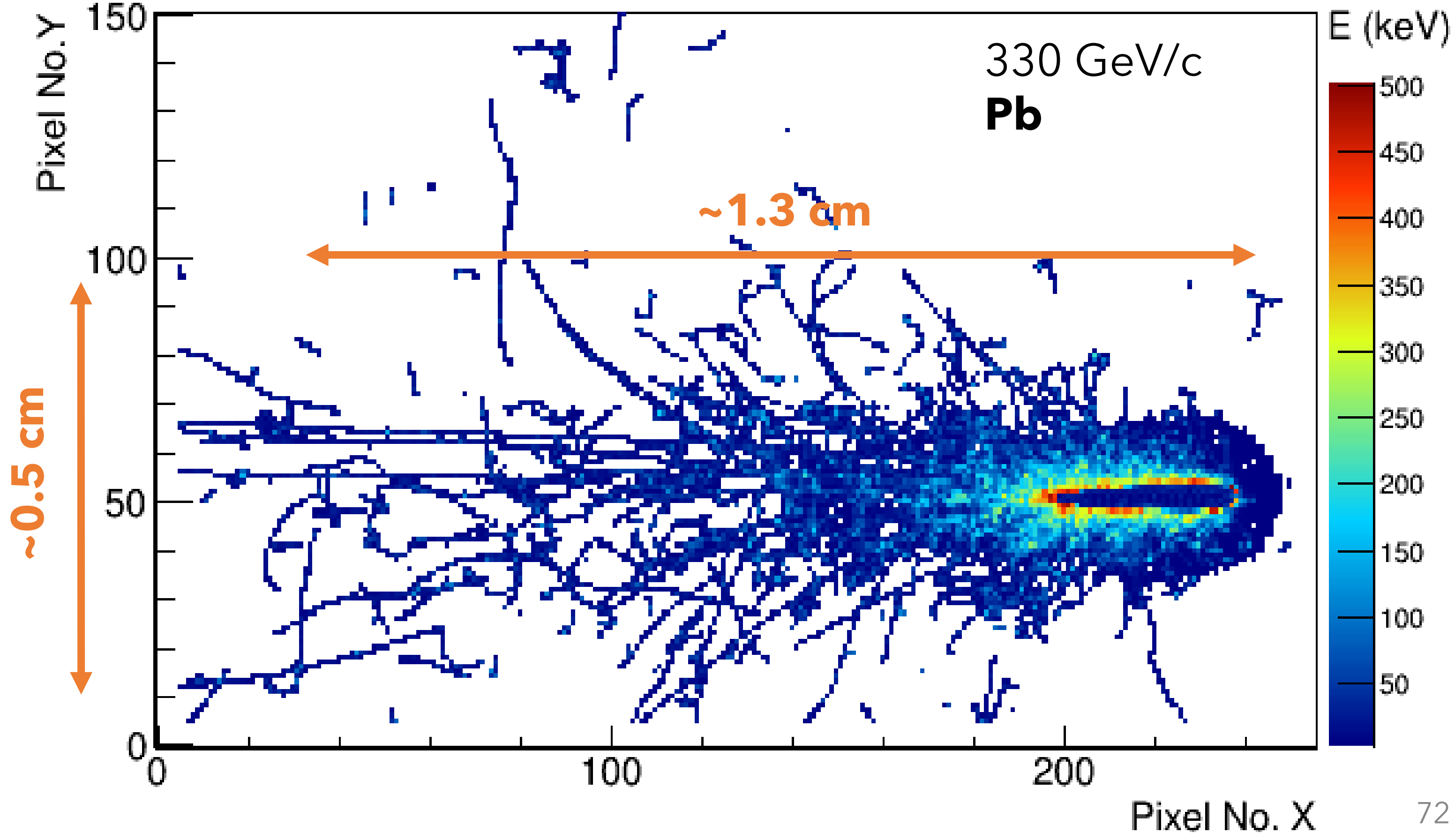

Thank you for your attention

This research was funded by the Czech Science Foundation grant number GM23-04869M.

Instruments for measurements in LEO

Next Generation Radiation Monitor (NGRM)

- Mass ~ 1 kg
- Consumption ~1-2 W

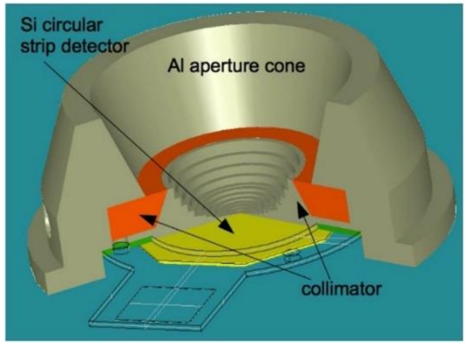

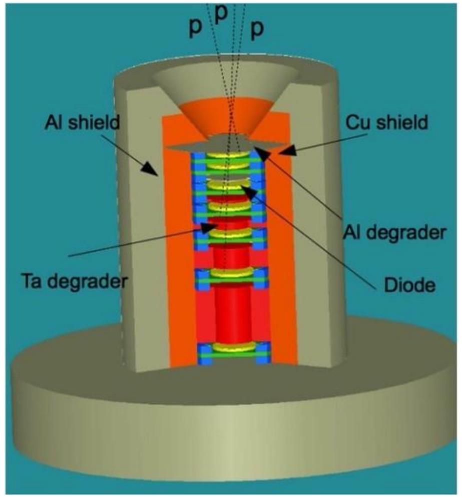

EPT (Energetic Particle Telescope)

- Mass: **4.6 kg**
- Consumption: 5.6 W

ICARE-NG:

- Mass: **2.4 kg**
- Consumption: 3 W

Particle Fluence

The formula was derived analytically to account for the removal of edge clusters

$$F = \sum_{i \in \{particles\}} \frac{d/cos(\theta_i)}{l \cdot d \cdot (l - d \cdot tan(\theta_i))}$$

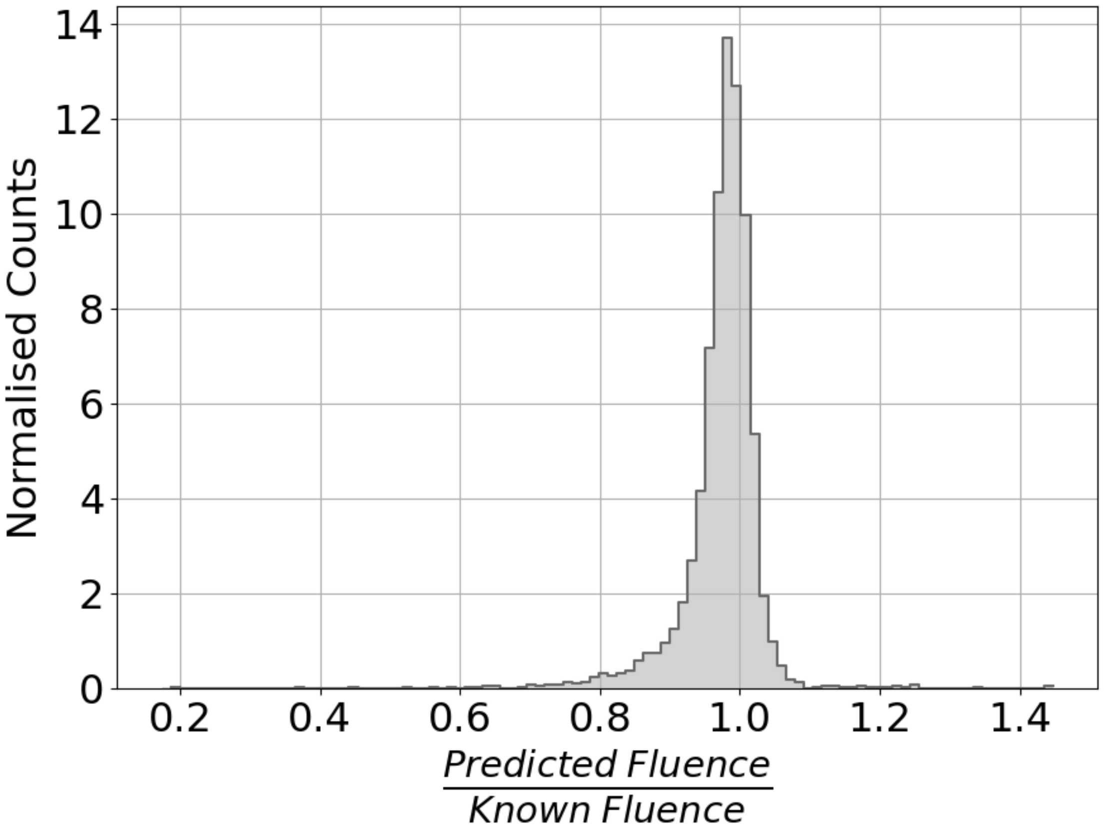

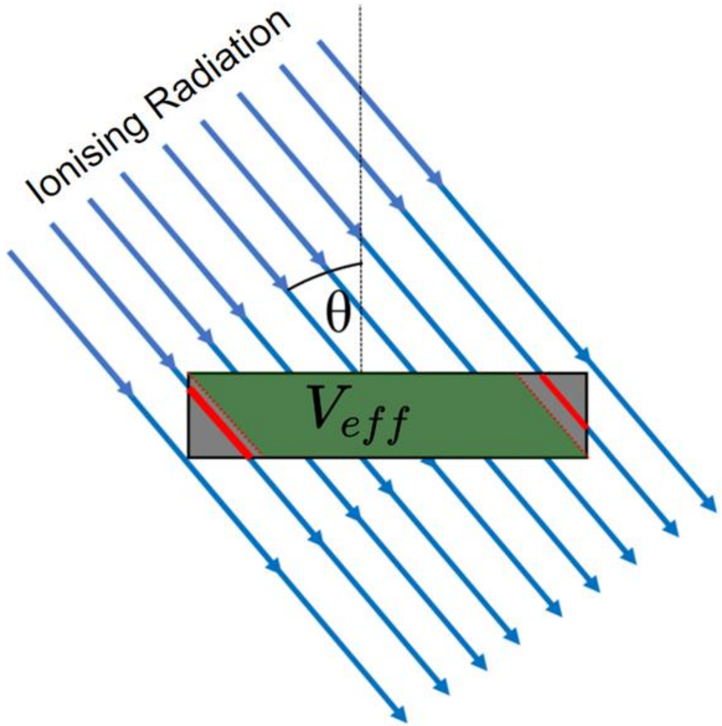

The new algorithm was tested in a Geant4 omnidirectional field simulation.

Testing Accuracy: 97%

Second Peak Localisation

- Follow correct alignment of the interaction of point
- It becomes possible to project the second peak in 3D space to determine its origin
- Projection shows the origin along the beam line further the theory of scattering beam due to wider beam

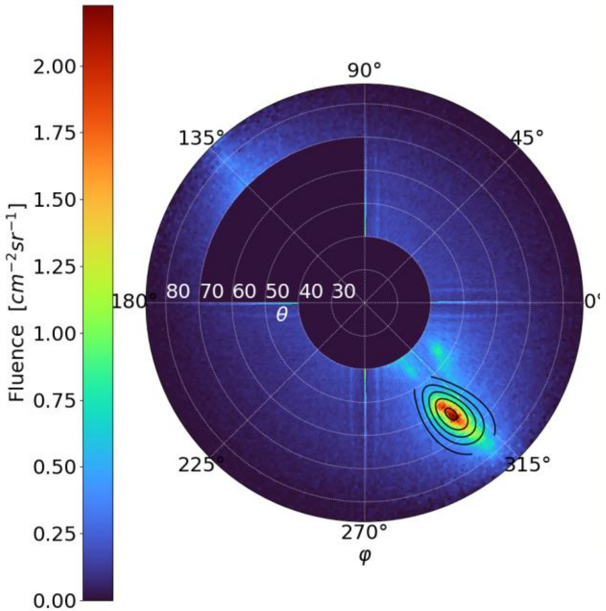

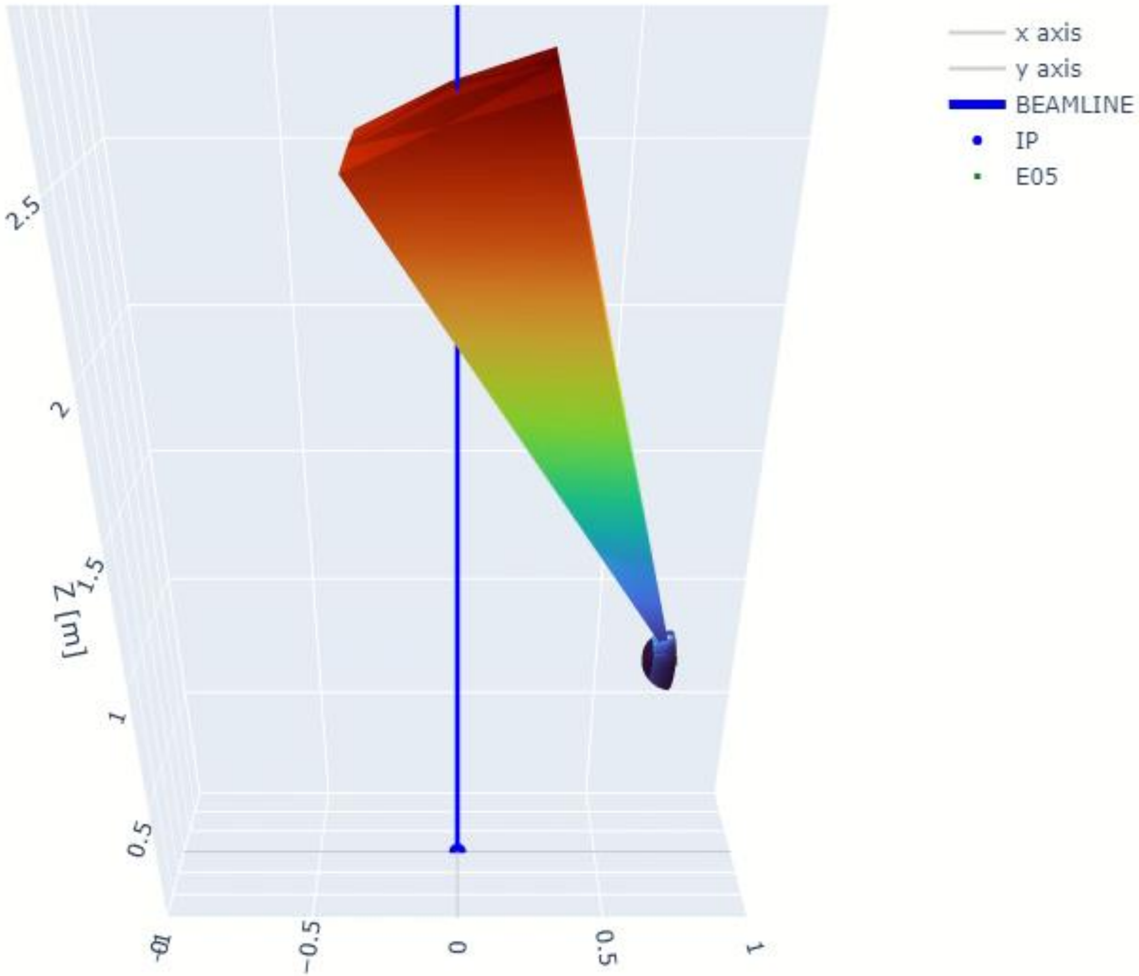

Bayesian Deconvolution Mathematical Background

Response Matrix

$$n(E) = R\,\phi(C)$$

Particle Spectrum

Measured dE/dx Spectrum

$$M \approx R^{-1} \Rightarrow \phi(C) = M\,n(E)$$

Bayesian Formula $\Rightarrow$

$$P(C_\mu|E_j) = \frac{P(E_j|C_\mu)\,P(C_\mu)}{\sum_\nu^{n_C} P(E_j|C_\nu)\,P(C_\nu)}$$

Probability of a cause (particle class present) given an effect (measurement)

$$\Rightarrow \phi(C_\mu) = \sum_{i=1}^{n_E} P(C_\mu|E_i)n(E_i)$$